CANADIAN THESES ON MICROFICHE

I.S.B.N.

THESES CANADIENNES SUR MICROFICHE

National Library of Canada
Collections Development Branch

Canadian Theses on
Microfiche Service

Ottawa, Canada
K1A 0N4

Bibliothèque nationale du Canada
Direction du développement des collections

Service des thèses canadiennes
sur microfiche

NOTICE

The quality of this microfiche is heavily dependent upon the quality of the original thesis submitted for microfilming. Every effort has been made to ensure the highest quality of reproduction possible.

If pages are missing, contact the university which granted the degree.

Some pages may have indistinct print especially if the original pages were typed with a poor typewriter ribbon or if the university sent us a poor photocopy.

Previously copyrighted materials (journal articles, published tests, etc.) are not filmed.

Reproduction in full or in part of this film is governed by the Canadian Copyright Act, R.S.C. 1970, c. C-30. Please read the authorization forms which accompany this thesis.

THIS DISSERTATION
HAS BEEN MICROFILMED
EXACTLY AS RECEIVED

AVIS

La qualité de cette microfiche dépend grandement de la qualité de la thèse soumise au microfilmage. Nous avons tout fait pour assurer une qualité supérieure de reproduction.

S'il manque des pages, veuillez communiquer avec l'université qui a conféré le grade.

La qualité d'impression de certaines pages peut laisser à désirer, surtout si les pages originales ont été dactylographiées à l'aide d'un ruban usé ou si l'université nous a fait parvenir une photocopie de mauvaise qualité.

Les documents qui font déjà l'objet d'un droit d'auteur (articles de revue, examens publiés, etc.) ne sont pas microfilmés.

La reproduction, même partielle, de ce microfilm est soumise à la Loi canadienne sur le droit d'auteur, SRC 1970, c. C-30. Veuillez prendre connaissance des formules d'autorisation qui accompagnent cette thèse.

LA THÈSE A ÉTÉ
MICROFILMÉE TELLE QUE
NOUS L'AVONS REÇUE

NL-339 (r. 82/08)

Canada

63

0-315-15972-3

National Library of Canada | Bibliothèque nationale du Canada

Canadian Theses Division | Division des thèses canadiennes

Ottawa, Canada
K1A 0N4

63881

PERMISSION TO MICROFILM — AUTORISATION DE MICROFILMER

• Please print or type — Écrire en lettres moulées ou dactylographier

Full Name of Author — Nom complet de l'auteur

MICHAEL JEPSON LONDON

Date of Birth — Date de naissance	Country of Birth — Lieu de naissance
JAN. 4 1958	CANADA

Permanent Address — Résidence fixe

NUCLEAR RESEARCH CENTRE
UNIVERSITY OF ALBERTA
EDMONTON ALBERTA T6G 2N5

Title of Thesis — Titre de la thèse

DETERMINING THE NEUTRON-NEUTRON EFFECTIVE RANGE FROM NEUTRON-DEUTERON QUASI-FREE SCATTERING

University — Université

UNIVERSITY OF ALBERTA

Degree for which thesis was presented — Grade pour lequel cette thèse fut présentée

MASTER OF SCIENCE

Year this degree conferred — Année d'obtention de ce grade	Name of Supervisor — Nom du directeur de thèse
1983	JAN M. GREBEN

Permission is hereby granted to the NATIONAL LIBRARY OF CANADA to microfilm this thesis and to lend or sell copies of the film.

The author reserves other publication rights, and neither the thesis nor extensive extracts from it may be printed or otherwise reproduced without the author's written permission.

L'autorisation est, par la présente, accordée à la BIBLIOTHÈQUE NATIONALE DU CANADA de microfilmer cette thèse et de prêter ou de vendre des exemplaires du film.

L'auteur se réserve les autres droits de publication; ni la thèse ni de longs extraits de celle-ci ne doivent être imprimés ou autrement reproduits sans l'autorisation écrite de l'auteur.

Date	Signature
April 25 1983	Michael J London

NL-91 (4/77)

THE UNIVERSITY OF ALBERTA

DETERMINING THE NEUTRON-NEUTRON EFFECTIVE RANGE FROM NEUTRON-DEUTERON QUASI-FREE SCATTERING

by

Michael Jepson London

(C)

A THESIS

SUBMITTED TO THE FACULTY OF GRADUATE STUDIES AND RESEARCH

IN PARTIAL FULFILMENT OF THE REQUIREMENTS FOR THE DEGREE

OF MASTER OF SCIENCE

IN

NUCLEAR PHYSICS

Department of Physics

EDMONTON, ALBERTA

Spring 1983

THE UNIVERSITY OF ALBERTA

RELEASE FORM

NAME OF AUTHOR Michael Jepson London

TITLE OF THESIS DETERMINING THE NEUTRON-NEUTRON EFFECTIVE RANGE FROM NEUTRON-DEUTERON QUASI-FREE SCATTERING

DEGREE FOR WHICH THESIS WAS PRESENTED MASTER OF SCIENCE

YEAR THIS DEGREE GRANTED Spring 1983

Permission is hereby granted to THE UNIVERSITY OF ALBERTA LIBRARY to reproduce single copies of this thesis and to lend or sell such copies for private, scholarly or scientific research purposes only.

The author reserves other publication rights, and neither the thesis nor extensive extracts from it may be printed or otherwise reproduced without the author's written permission.

(SIGNED) Michael J. London

PERMANENT ADDRESS:

NUCLEAR RESEARCH CENTRE
UNIVERSITY OF ALBERTA
EDMONTON T6G 2N5

DATED April 25 1983

THE UNIVERSITY OF ALBERTA

FACULTY OF GRADUATE STUDIES AND RESEARCH

The undersigned certify that they have read, and recommend to the Faculty of Graduate Studies and Research, for acceptance, a thesis entitled DETERMINING THE NEUTRON-NEUTRON EFFECTIVE RANGE FROM NEUTRON-DEUTERON QUASI-FREE SCATTERING submitted by Michael Jepson London in partial fulfilment of the requirements for the degree of MASTER OF SCIENCE.

.....

Supervisor

.....

.....

.....

.....

Date. April 22, 1983

ABSTRACT

An experiment is under way which will attempt to measure the neutron-neutron quasi-free scattering cross section in neutron-deuteron break-up to an accuracy of a few percent. This work is a theoretical study of the reaction as a means of determining the neutron-neutron effective range. Both impulse approximation and three-body models have been used. Some recommendations regarding the experimental geometry are made. The ingredients of a proper theoretical error analysis are identified.

The effective range can be deduced from the experimental cross section with a percentage uncertainty equal to that of the cross section. A further theoretical error of 2% must be included.

ACKNOWLEDGMENTS

The following people were indispensable to me during the completion of this degree:

Tamer Aytimur
Tim Cooper
Pál Doleschall
Jim Easton
Jock Elliot
Jan Greben
Maureen Lavoie
Llanca Letelier
Jim Pasos
John Ritzel
Helmy Sherif
Greta Tratt

Special thanks to Jan Greben for his patience.

Edmonton
April 1983

Mike London

Table of Contents

Chapter — Page

I. INTRODUCTION 1

II. THREE-BODY THEORY 7

a. Notation 7

b. Limitations of Two-Body Theory 10

c. Three-body Equations 13

d. Separable Potential 20

e. Analytic Structure of the Equations 24

f. Methods of Solution 27

III. IMPULSE APPROXIMATION 32

a. Justification 32

b. Model 33

c. Experiment 36

d. Results 38

IV. THREE-BODY CALCULATIONS 52

a. Model 52

b. Results 58

V. CONCLUSIONS 71

a. Theoretical 71

b. Experimental 75

c. Determining effective range 78

BIBLIOGRAPHY 81

APPENDIX A KINEMATICS 87

APPENDIX B DOCODE MANUAL 91

a. General Features 91

b. Outline 92

c. Input 96
d. Sample Run 108
e. Test Run 126
f. Permanent Files 126
g. DOCODE Contents 129
APPENDIX C PARAMETERS OF THE TWO-BODY INTERACTIONS 132

List of Tables

Table		Page
I.1	Survey of measurements of r_{nn}	6
IV.1	Survey of n-D calculations	54
IV.2	Effective range parameters for S-wave potentials	57
IV.3	Number of parameters in the two-body interactions	59
IV.4	Symmetric QFS cross sections	60
IV.5	Near-symmetric QFS cross sections	63
IV.6	Asymmetric QFS cross sections	64
IV.7	Symmetric break-up cross sections	65

List of Figures

Figure		Page
II.1	Simple two-body scattering	11
II.2	Two-body scattering in three body space	12
II.3	Two-body decomposition of three-body scattering	14
II.4	Faddeev decomposition of three-body scattering	17
II.5	Singularities in the kernel of the three-body integral equations	26
II.6	Simple contour of integration	29
II.7	More complicated contour of integration	30
III.1	Schematic of n-D break-up in the impulse approximation	34
III.2	Schematic of experimental setup	37
III.3	Cross section and relative energies vs. ϕ	40
III.4	Proton recoil energy vs. ϕ	41
III.5	Cross section and relative energies vs. outgoing neutron energy	42
III.6	Cross section and relative energies vs. θ	44
III.7	Yamaguchi off-shell n-n function vs. θ	45
III.8	Proton recoil energy vs. θ	46
III.9	Cross section vs. θ and r_{nn}	47
III.10	QFS cross section vs. r_{nn}	49
III.11	Sources of error in r_{nn}	50
IV.1	Symmetric break-up cross section vs. θ	67
IV.2	Sensitivities of the symmetric break-up cross section vs. θ	68
IV.3	Sensitivity of the symmetric break-up cross section to r_{nn} vs. θ	70
V.1	QFS cross section vs. r_{nn}	80

I. INTRODUCTION

The nonexistence of a free neutron target has always made experimental investigation of the pure neutron-neutron (n-n) interaction difficult. Details of the low energy n-n interaction remain much less clear than those of the neutron-proton and proton-proton interactions. Though important in their own right such details could supply notable tests of charge independence and charge symmetry.

One obvious place to attempt to observe the n-n interaction is in the three-nucleon system, either in the bound state (triton) or in neutron-deuteron (n-D) scattering. The difficulty here, as in any interacting many-body system is that the off shell nature of the constituent two-body interactions hampers the observation of on-shell two-body scattering behaviour.

Chew (Ch48,50,52) seems to have been the first to look for two-nucleon information in the three-nucleon system, trying to deduce the free n-n and n-p cross sections from n-D inelastic scattering results using the impulse approximation. Since then this method has been widely used, and with reasonable success, to describe n-D elastic scattering (Ko65 and references therein). Success with n-D and p-D inelastic scattering has been less (references in Du73) especially at low energies. It was not until practical formulations of the three-body problem (Fa60,61,63,65, We63,64, Lo64) and subsequent calculations† that accurate

---

†These had to await a further breakthrough in high-speed computing.

determination of n-n scattering parameters became possible.

n-n final-state interaction (FSI) experiments have been found sensitive to the n-n scattering length (a_{nn}), which has been determined to an accuracy of about 3% (Ku76, Wi79, Ss81). Using phase-equivalent potentials† Haftel (Ha73) and Harper (Hr72) have shown that the triton binding energy (E_t) is sensitive to the off-shell behaviour of nucleon-nucleon (N-N) interactions. The Phillips line (Ph68) demonstrates a direct relationship between E_t and the n-D doublet elastic scattering length. Brayshaw (Br74) has further asserted that there is essentially no off-shell dependence of the three-nucleon system beyond that specified by E_t. This rather strong statement has seen considerable debate (Ha74,75,76, Br75, St76,78).

Quasi-free scattering (QFS), in which one of the target particles remains at rest, is particularly appealing for studying the n-n interaction. Calculations and intuition both suggest that this two-body-like process is almost entirely insensitive to the off shell behaviour of the N-N interactions. Moreover a strong sensitivity of the n-n QFS cross section to the n-n effective range (r_{nn}) has made this a popular place to measure r_{nn}. Determinations of r_{nn} (table I.1) are typically much less accurate than those of a_{nn}, the limiting factors being experimental. For this reason, and because of the generally low sensitivity of n-n QFS to other

---

†potentials that agree on-shell but have different off-shell behaviours

aspects† of the n-n interaction, analysis of theoretical errors has not been extensive. Comparing a measured n-n effective range with the Coulomb-corrected p-p value would provide a simple test of charge symmetry. The corrected n-p (singlet) value provides a similar test of charge independence. Cursory inspection of table I.1, however, reveals that considerable improvement in accuracy is required before any meaningful comparisons can be made.

Experiments other than n-n QFS are in evidence in table I.1 but none appears to offer any advantages in accuracy. The results from FSI measurements are considered unreliable due to an inadequate model and the low sensitivity to r_{nn} in this region (Gu80). Of more interest is the report of von Witsch et al. (Wi80) who claim that the ratio of n-p to n-n QFS cross sections can be measured more accurately and r_{nn} deduced from it with less theoretical uncertainty. While the first claim may be true, their experimental uncertainty of 8% leaves much room for betterment by conventional methods (Ss78). The second claim is discussed in chapter IV.

The latest survey by Šlaus (Ss78,81) points out a systemmatic discrepancy between effective range parameters deduced from n-n QFS and (π^-,γ) experiments (on D). Šlaus et al. (Ss82) propose that a three-nucleon force, implicit in the nature of the strong interaction, is present in the former but not the latter where only two nucleons

---

†in particular higher partial waves, off shell behaviour (St76) and a_{nn}

participate. One might, therefore, regard the difference between r_{nn} measured from two-and three-nucleon experiments as a measure of the presence a three-nucleon force. The dominant component of such a force would be a two-pion exchange term (Mk76). Slobodrian (Sb82) maintains that, short of colliding neutron beams, the only reliable way to study the n-n interaction is via comparison of "mirror processes" in which neutrons and protons are interchanged. He cites Gross et al. (Gr70) who obtained agreement with (π^-,γ) results using ^{3}He(^{3}He,^{4}He)2p and ^{3}H(^{3}H,^{4}He)2n. The comparison method has been criticized (Ss71).

Sauer and Walliser (Sr77) have found that the process of making electromagnetic corrections to p-p data is model dependent. They propose using the assumption of charge symmetry (i.e. equality of n-n and corrected p-p parameters) as a constraint on the off-shell behaviour of the nuclear potential. The correction of n-p data does not appear to suffer from model dependence.

Here at the Nuclear Research Centre an experiment is currently in progress† which will attempt to measure the n-n QFS cross section to within a few percent. This should enable a determination of r_{nn} to a similar (previously unattained) degree of accuracy. To maintain this level of accuracy, a more comprehensive and detailed theoretical understanding of the reaction is required. The purpose of

---

†Details of the experimental setup can be found in section III.C and in Nuclear Research Centre Progress Reports 1979-82.

this work is to provide that understanding. Of course the relationship between r_{nn} and the QFS cross section must be well established. The sensitivity of the outcome to experimental geometry and resolution must be explored. Finally the various theoretical uncertainties that have previously been swamped by experimental error must be either eliminated or quantified. The scale of the investigation is dictated by the anticipated experimental uncertainty.

Such detailed analysis is only possible with the latest three-body computer calculations. We have used a code supplied by Pál Doleschall (Do73) which we believe is the best available for the purpose. The results of its use are presented in chapter IV. Preceeding these (in chapter III) are the results of our own "poor man's" three-body calculations using the impulse approximation. Chapter II is a review of basic three-body theory, intended mainly for perspective.

ref.	reaction	r_{nn}
(Sb70)	comparison on D and ^{3}He-^{3}H	3.1 ±.5[1]
(Ss71)	n-n QFS	2.5[2]
(Ze74)	n-n and n-p FSI	2.13±.4[1]
(Kc75)	n-n and n-p FSI	3.15±.7[1]
(Ad77)	(π^-,γ)	2.9 ±.3
(Bo78)	n-n QFS	2.86[2]
(Su79)	n-n QFS[3]	2.9 ±.4
(Ga80)	(π^-,γ)	2.83±.11
(Gu80)	n-n QFS	2.69±.27
(Wi80)	n-n and n-p QFS n-n QFS	2.65±.18[4] 3.0 ±.2
(Ss81)	n-n QFS (π^-,γ)	2.68±.16[5] 2.83±.16[5]
(No64)	charge independence	2.73±.03[6]
(Hl64)	charge symmetry	2.85[6]
(No71)	charge symmetry	2.79[6]
(Ho75)	meson-exchange	2.76[6]
(La80)	Paris potential	2.88[6]

[1]unreliable, see text
[2]no fitting attempted
[3]not exact QFS, symmetric geometry
[4]may be incorrect, data indicates 2.95±.2 (Do82)
[5]weighted average of experimental results
[6]theoretical prediction

Table I.1 Survey of measurements of r_{nn} from scattering off deuterium.

II. THREE-BODY THEORY

a. Notation

In three-body equations, the interacting particles are labelled 1,2 and 3. Quantities defined on a pairwise basis are labelled by the index of the non-participating particle. Thus V_i indicates the potential between particles j and k (i,j,k cyclic in this discussion).

To simplify later expressions, Lovelace variables (Lo64) are used with all masses set equal to 1. Pairwise relative momentum is denoted by the vector quantity $\bar{p}$;

$$\bar{p}_k=(1/2)(\bar{k}_i-\bar{k}_j) \qquad \text{II.1}$$

where $\bar{k}_i$ is the laboratory momentum of particle i. $\bar{q}_k$ is proportional to the momentum of particle k relative to the (i,j) centre-of-mass:

$$\bar{q}_k=(1/2\sqrt{3})(\bar{k}_i+\bar{k}_j-2\bar{k}_k). \qquad \text{II.2}$$

A free state is labelled by its momenta, and in the three-body case can be expressed in four different but equivalent ways:

$$|q_i\rangle|p_i\rangle(\equiv|q_i p_i\rangle)=|k_1k_2k_3\rangle \qquad \text{II.3}$$

for i=1,2,or3. With Lovelace variables the energy of this

state is simply expressed:

$$E=p_i^2+q_i^2 \qquad \text{II.4}$$

χ_i represents a bound state of (j,k) in two-body space. Accordingly,

$$|I\rangle\equiv|q_i\rangle|\chi_i\rangle \qquad \text{II.5}$$

is the same bound state in three-body space.

The symbol T_i indicates the t-matrix for (j,k) scattering, while the arguments supplied indicate whether it is a matrix element or operator acting in two- or three-body space. In two-body space

$$T_i(p_i,p_i';E)=\langle p_i|T_i(E)|p_i'\rangle \qquad \text{II.6}$$

where E is the two-body energy. In three-body space

$$T_i(p_iq_i,p_i'q_i';E)=\langle q_i|\langle p_i|T_i(E)|p_i'\rangle|q_i'\rangle \qquad \text{II.7}$$

where E is now the total three-body energy. Thus

$$T_i(p_iq_i,p_i'q_i';E)=\langle q_i|T_i(p_i,p_i';E-q_i^2)|q_i'\rangle \qquad \text{II.8}$$
$$=\delta(q_i-q_i')T_i(p_i,p_i';E-q_i^2).$$

Clearly then, the behaviour of $T_i(E)$, in particular the

singularity structure, depends on whether it is used in two- or three-body space. The incorporation of other two-body operators into three-body space follows analogous lines.

The complete potential acting in the three-body system is assumed to be the sum of pairwise potentials

$$V=\Sigma_i V_i \qquad \text{II.9}$$

although there is no reason why the summation could not include a "three-body potential", involving all three particles simultaneously (Fu57, Ph66, chapter I).

In analogy to the two-body case there is a Green† function for the entire process

$$G=(E-H)^{-1} \qquad \text{II.10}$$

defined in terms of the full Hamiltonian

$$H=H_0+V. \qquad \text{II.11}$$

The channel Hamiltonians

$$H_i=H_0+V_i \qquad \text{II.12}$$

and associated Green functions

---

†The terminology of Jackson (Ja75) is adopted here. Read "Green's" if you are stubborn.

$$G_1(E)=(E-H_1)^{-1} \qquad \text{II.13}$$

describe the pairwise interactions. The bound states $|I\rangle$ (equation II.5) are the eigenstates of H_1.

In analogy to the two-body t-matrix, there is assumed to be a t-matrix for 0→0 scattering (0 denoting the state of three free particles):

$$\begin{aligned} T&=V+VGV \\ &=V+VG_0T \end{aligned} \qquad \text{II.14}$$

where G_0 describes the propagation of the 0 state.

b. Limitations of Two-Body Theory

The Lippmann-Schwinger equation, II.14 or

$$\psi=\phi+G_0V\psi \qquad \text{II.15}$$

belongs to the general class of Fredholm equations. Viewed as an operator equation, certain statements about its solution can be made† provided the kernel operator G_0V is compact. In numerical solutions, II.15 is usually converted to a set of matrix equations for which compactness guarantees a finite number of equations. In practical terms, therefore, compactness is elevated to a requirement for solution.

---

†Fredholm theorem. See for example Kreyszig (Kr78).

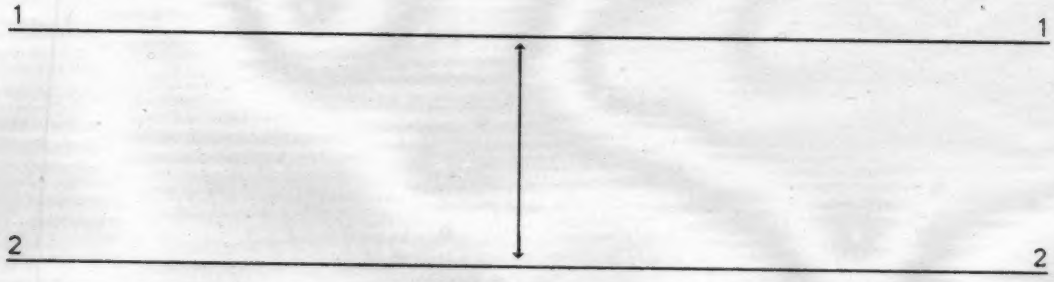

Figure II.1 Two-body scattering in two-body space is a connected process.

In the Hilbert space of quantum mechanics, compactness is roughly equivalent to square integrability (boundedness in the Schmidt norm). More intuitively, the kernel of II.15 is compact for any *connected* process in which no particle or group of particles can be singled out as separate (noninteracting) from the remaining particles.

Simple two-body scattering, depicted in figure II.1, is clearly a connected process, for which equation II.15 is soluble, as long as V satisfies certain basic requirements.† Strictly speaking, the kernel G_0V for most potentials is compact everywhere but at bound state energy poles and on the right-hand energy cut. Nevertheless the problem can be dealt with rigorously by using a few

†See Taylor (Ta72) for example.

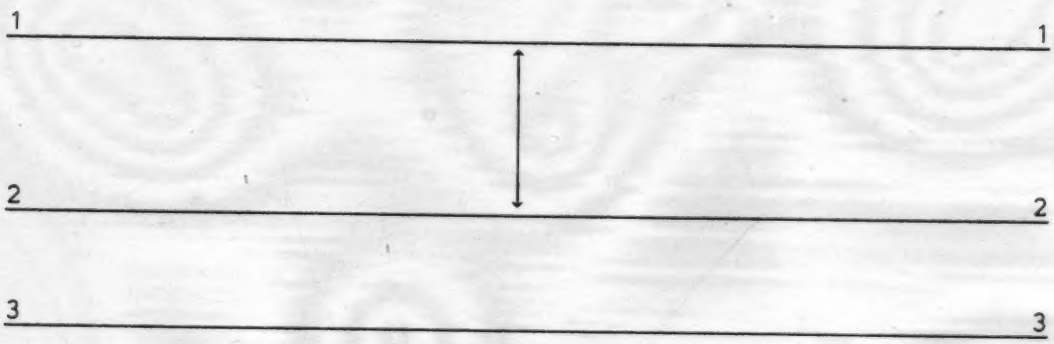

Figure II.2 Two-body scattering in the presence of a spectator particle is a disconnected process in three-body space.

mathematical tricks. These are reviewed by Lovelace (Lo64).

The situation in three-body space is more forbidding. Even the simplest process – two-body scattering in the presence of a spectator particle – is obviously disconnected (figure II.2). Mathematically, writing the two-body Green function in three-body space (following along the lines of equation II.8)

$$\langle p_i q_i | G_0(E) | p_i' q_i' \rangle = \delta(q_i - q_i') \langle p_i | G_0(E - q_i^2) | p_i' \rangle \quad \text{II.16}$$

introduces a δ-function in the third coordinate which leads, upon integration, to a very awkward infinity.

In more general fully-interacting three-body problems the above divergence arises again, and not just as an

isolated factor. Decomposing II.14 using II.9 and iterating,

$$T=\Sigma_i V_i+\Sigma_i V_i G_o T \qquad \text{II.17}$$
$$=\Sigma_i V_i+\Sigma_{i\,j} V_i G_o V_j+\Sigma_{i\,j\,k} V_i G_o V_j G_o V_k+\ldots$$

reveals that there are disconnected terms (for i=j=...) at each order of the expansion (figure II.3). The insolubility of one such problem is discussed in more detail by Afnan and Thomas (Af77). One is forced to conclude that the established mathematical formulation of two-body scattering is unable to describe three-body processes.

c. Three-body Equations

Faddeev (Fa60,61,63,65) approached the mathematical problem of disconnectedness by proposing a different decomposition of the 0→0 t-matrix:

$$T=\Sigma_i T^i \qquad \text{II.18}$$
$$=\Sigma_i [\Sigma_j (\delta_{i\,j} V_i+V_i G V_j)].$$

The T^i are found to satisfy "Faddeev-type" coupled equations:

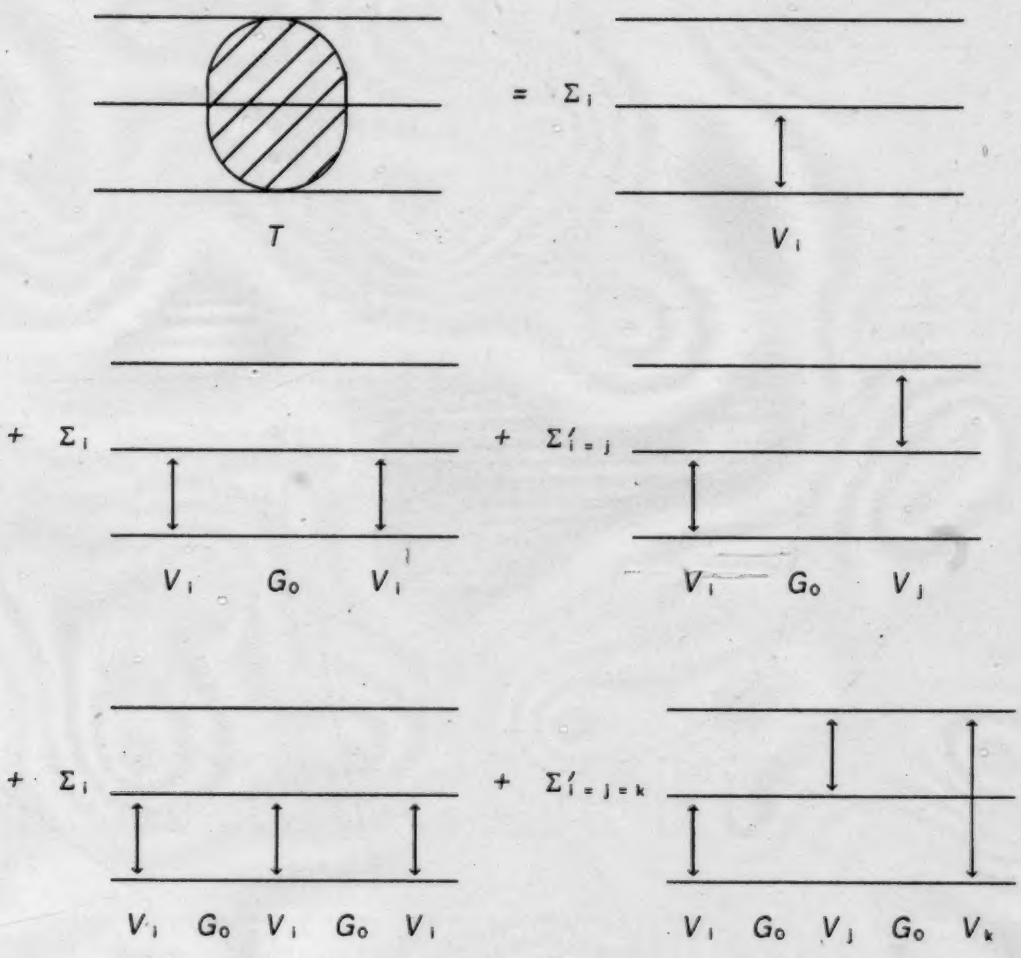

Figure II.3 Expansion of the 0→0 t-matrix in simple two-body interactions leads to an infinite number of disconnected terms. (equation II.17)
$\Sigma'_{i=j=k} \equiv \Sigma_{ijk} - \Sigma_{i=j=k}$

$$T^i = T_i + T_i G_0 (T^j + T^k) \qquad \text{II.19}$$
$$= T_i + T_i G_0 T_j + T_i G_0 T_k$$
$$+ T_i G_0 T_j G_0 T_i + T_i G_0 T_j G_0 T_k$$
$$+ T_i G_0 T_k G_0 T_i + T_i G_0 T_k G_0 T_j$$
$$+ \ldots$$

with connected kernels. Associated with these are Green functions

$$G^i = G_0 V_i G \qquad \text{II.20}$$

which satisfy similar equations:

$$G^i = (G_i - G_0) + G_0 T_i (G^j + G^k). \qquad \text{II.21}$$

II.20 suggests that G^i (or T^i) describes the process in which particles j and k interact last. This process is clearly subdivided by equation II.19 into connected and disconnected parts.† For convenience the completely connected operators

$$Y^i = T^i - T_i \qquad \text{II.22}$$

are then defined, satisfying

II.23

---

†Recall the δ-function of equation II.8 which causes T_i to be singular.

$$Y^i = T_i G_0 \Sigma_{j \neq i} (T_j + Y^j).$$

Intuitively, Faddeev has regrouped the multiple scattering series for the 0→0 interaction such that the infinity of disconnected terms in equation II.17 are all collected into the first term (the two-body t-matricies) of equation II.19 (figure II.4).

For most calculations the T^i are further decomposed:

$$T^i = \Sigma_j M_{ij} \qquad \text{II.24}$$
$$= \Sigma_j (\delta_{ij} V_i - V_i G V_j)$$

or

$$Y^i = \Sigma_j W_{ij} \qquad \text{II.25}$$
$$= \Sigma_j (M_{ij} - \delta_{ij} T_i).$$

From the elements W_{ij} which describe the connected parts of the 0→0 process, can be derived (Fa61,Os71) the amplitudes for the other possible processes, although the connections are not simply made.

To make the derivation of amplitudes for the general I(i,j)J† process more transparent, Lovelace (Lo64) chose to begin rather than end with these amplitudes. Depending on the use of incoming and outgoing scattering wave functions in the derivation, two operators are found:

---

†refer to equation II.5

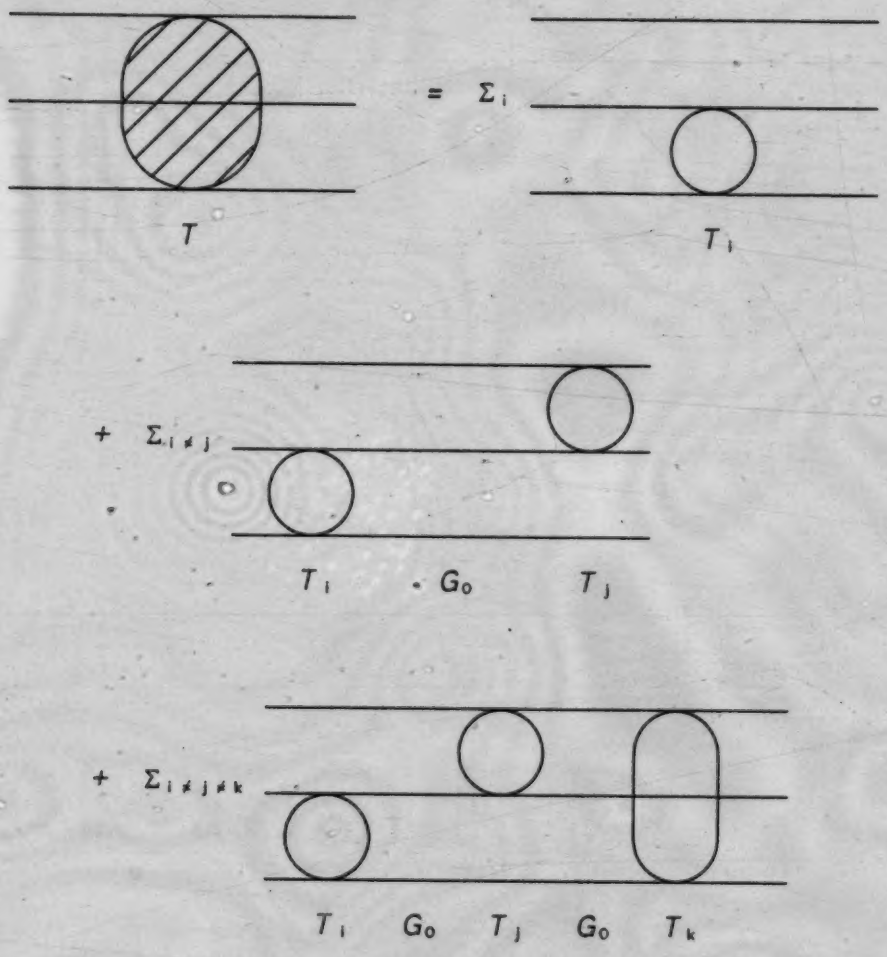

Figure II.4 Faddeev has regrouped the multiple scattering series so that disconnected terms are more easily dealt with. (equation II.19)

$$U_{\uparrow j}=V^{j}+V^{j}GV^{j} \qquad \text{II.26}$$
$$U_{\downarrow j}=V^{j}+V^{j}GV^{j}.$$

Lovelace showed that these satisfy Faddeev-type equations (the "Lovelace equations"):

$$U_{\uparrow j}=V^{j}+\Sigma_{k\neq j}U_{\uparrow k}G_{0}T_{k} \qquad \text{II.27}$$
$$U_{\downarrow j}=V^{j}+\Sigma_{k\neq i}T_{k}G_{0}U_{k\downarrow j}$$

which are compact and soluble but do require both potentials and t-matricies for the two-body interactions. While differing off-shell, both operators yield the same t-matrix for the on-shell process

$$T_{i,j}=\langle I|U_{i\downarrow}^{(-)}|J\rangle \qquad \text{II.28}$$

as required.

The problem of off-shell ambiguity was addressed by Alt, Grassberger and Sandhas (A167) who defined a single type of operator

$$U_{ij}=\bar{\delta}_{ij}G_{j}+U_{\uparrow j} \qquad (\bar{\delta}_{ij}=1-\delta_{ij}) \qquad \text{II.29}$$
$$=\bar{\delta}_{ij}G_{i}+U_{i\downarrow}$$

which also describes the on-shell three-body process. In addition to being more symmetric, these operators satisfy Faddeev-type equations (the "AGS equations") which do not

involve explicit two-body potentials

$$U_{ij}=\bar{\delta}_{ij}G_0+\Sigma_{n\neq j}U_{in}G_0T_n \qquad \text{II.30}$$
$$=\bar{\delta}_{ij}G_0+\Sigma_{n\neq i}T_nG_0U_{nj}.$$

The three-body breakup transition operator can be defined in terms of the bound state transition operators:

$$U_{0j}=G_0^{-1}+\Sigma_{k=1}^{3}T_kG_0U_{kj}. \qquad \text{II.31}$$

Osborn and Kowalski (Os71) have demonstrated the connection between Faddeev and AGS formulations of the problem. The relation

$$W_{ij}=T_iG_0U_{ij}G_0T_j \qquad \text{II.32}$$

identifies W_{ij} as the part of the full 0→0 t-matrix in which particles (j,k) interact first and particles (i,k) interact last. U_{ij} then appears as this part, stripped of its initial and final two-body interactions.

The impulse approximation used in chapter III can be derived as a simplification of the full three-body solution by iterating equation II.31. Choosing particle 1 as a proton, 2 and 3 as neutrons, the transition operator for neutron-induced breakup of the deuteron becomes

$$U_{03}=G_0^{-1}+\Sigma_k T_k G_0 U_{k3} \qquad \text{II.33}$$
$$=G_0^{-1}+(T_1+T_1 G_0 \Sigma_{k\neq 1} T_k G_0 U_{k3})+(T_2+T_2 G_0 \Sigma_{k\neq 2} T_k G_0 U_{k3})$$
$$+T_3 G_0 \Sigma_{k\neq 3} T_k G_0 U_{k3}$$
$$\simeq G_0^{-1}+T_1+T_2.$$

Following equation II.28, the t-matrix for the process is

$$T_{0,3}=\langle 0|U_{03}|3\rangle. \qquad \text{II.34}$$

d. Separable Potential

While three-body equations have been solved for a local potential (Os67,Kl71), the numerical problem is, in general, very difficult.† Even after angular momentum decomposition, which reduces the dimensions from six to two, the remaining integral equations are coupled and infinite in number.

Most calculations, therefore, introduce separable partial wave two-body potentials (the partial wave index is suppressed):

$$V_i(p,p')=\Sigma_{yz} g_{iy}(p)\lambda_{iyz} g_{iz}(p'). \qquad \text{II.35}$$

Although this may seem rather restrictive, it is worth noting that any local potential can be approximated with arbitrary accuracy by a sum of separable terms. In

---

†There are mathematically sound theories (e.g. We64) but for practical calculations simplifying assumptions are required (see Sc74).

particular, the two-term R-type separable potential described in chapter IV has a level of agreement with experimental N-N phase shifts previously available only with non-separable potentials such as the Reid soft-core (Re68).

In the presence of a separable potential, the two-body partial wave t-matrix itself becomes separable:

$$T(p,p',E)=\Sigma_{\gamma z} g_\gamma(p)\tau_{\gamma z}(E)g_z(p'). \qquad \text{II.36}$$

In operator notation,

$$T(E)=|g\rangle\tau(E)\langle g| \qquad \text{II.37}$$

where the conventions of section A still apply, i.e.

$$T_k(E)=\int dq_k{}^3\,|q_k\rangle|g_k\rangle\tau_k(E-q_k{}^2)\langle g_k|\langle q_k| \qquad \text{II.38}$$

in three-body space. To simplify notation, the third variable will be omitted from equations in three-body space on the understanding that a q_i should be present for each subscript i, with three-dimensional integration over repeated subscripts.

In this notation, the "X-amplitude" for rearrangement scattering is defined:

$$X_{ij}=\langle g_i|G_0(E)U_{ij}G_0(E)|g_j\rangle. \qquad \text{II.39}$$

Inserting the separable t-matrix of II.37 into II.30 and taking matrix elements $\langle g_i|G_0(E)\ldots G_0(E)|g_i\rangle$ yields a set of coupled integral equations in one continuous variable for the X_{ij}:

$$X_{ij}(E)=\bar{\delta}_{ij}V_{ij}(E)+\Sigma_{k\neq j}V_{ik}(E)\tau_k(E-q_k^2)X_{kj}(E). \qquad \text{II.40}$$

V_{ij} is an energy-dependent "effective potential":

$$V_{ij}(E)=\langle g_i|G_0(E)|g_j\rangle. \qquad \text{II.41}$$

By taking matrix elements $\langle p_0|\ldots G_0(E)|g_j\rangle$ of equation II.31, analogous equations for the breakup case are obtained

$$X_{0j}=V_{0j}(=O)\dagger+\Sigma_k V_{0k}\tau_k X_{kj} \qquad \text{II.42}$$

where

$$X_{0j}(E)=\langle p_0|U_{0j}(E)G_0(E)|g_j\rangle \qquad \text{II.43}$$

$$V_{0j}(E)=\langle p_0|g_j\rangle. \qquad \text{II.44}$$

After angular momentum decomposition (Do73,A167), equations II.40 become one-dimensional integral equations which can be solved by a variety of methods (some of which are described in section F). The breakup amplitudes X_{0j} can

---

†See equation II.49.

then be calculated from these using II.42.

Although the t-matrix of equations II.36 and II.37 could be expressed in any basis, the ideal (We63,64,Sc74) basis of bound state form factors is used to simplify calculations. In this representation, each form factor for a pairwise interaction can be related on shell to a bound state of the pair:

$$\langle p_i|G_0(E)|g_i\rangle=\langle p_i|x_i\rangle. \qquad \text{II.45}$$

Thus a potential will typically have one form factor for each bound state.

The relation II.45 can be used to attach some physical meaning to the mysterious X-amplitudes. From definition II.39, it is clear that on shell, X_{ij} is the amplitude for scattering from a bound state of (i,k) to a bound state of (j,k):

$$X_{ij}=\langle x_i|U_{ij}|x_j\rangle. \qquad \text{II.46}$$

In other words, looking at equation II.28, $X_{ij}=T_{ij}$ on shell. Similarly, X_{0j} is just the matrix element of U_{0j} between free and bound states:

$$X_{0j}=\langle p_0|U_{0j}|x_j\rangle, \qquad \text{II.47}$$

or $X_{0j}=T_{0j}$ on shell.

Of course, if a particle pair had more than one bound state, X would have to be labelled accordingly. For simplicity and because the deuteron has only one bound state, such labelling has been omitted.

Finally ,II.45 can help to clarify the description of V_{ij} as an "effective potential":

$$V_{ij}=\langle g_i|G_0(E)G_0^{-1}(E)G_0(E)|g_j\rangle \qquad \text{II.48}$$
$$=\langle \chi_i|G_0^{-1}(E)|\chi_j\rangle$$
$$=\langle \chi_i|(E-H_0)|\chi_j\rangle.$$

Similarly,

$$V_{0j}=\langle p_0|g_j\rangle \qquad \text{II.49}$$
$$=\langle p_0|G_0^{-1}(E)G_0(E)|g_j\rangle$$
$$=\langle p_0|(E-H_0)|\chi_j\rangle$$
$$=0 \text{ on the energy shell.}\dagger$$

e. Analytic Structure of the Equations

The first step toward solving integral equations II.40 is a study of the singularity structure of its constituent parts. Because many methods of solution involve analytic extensions of these parts into the complex plane, the following brief account of singularities will not be restricted to the real q axis.

---

†Recall $\langle p_0|(E-H_0)|\chi_j\rangle=\delta(q_0-q_j)\langle p_0|(E-H_0)|\chi_j\rangle$.

In general, the solubility of such an equation depends on the behaviour of the kernel $V\tau$ (as discussed in section B), and of the solution X itself. Of the two contributions to the kernel, that due to the "bare" two-body t-matrix τ is the simplest. In pure two-body scattering, $\tau(E)$ has a simple pole at each energy corresponding to a bound state of the pair. In the three-body case, $\tau(E-q^2)$ will therefore have a pole on the real q axis for each $E-q^2$ corresponding to a bound state energy. For three nucleons this means at most one pole.

Singularities in the "effective potential" V arise from both the three-body propagator G_0 and the form factor $\langle g|p\rangle=g(p)$. For most calculations, Brayshaw (Br68) has argued that the latter source may be ignored. Since the separable potential, defined through the form factors, is only approximate, any reasonable calculation must be relatively insensitive to the exact form of g. If the singularities in g were to play a part, then this requirement would not be met.

When the energy is high enough that the propagation of three free particles can occur, the free Green function exhibits two pairs of branch points of logarithmic singularity with branch cuts between them. Since the positions of these singularities depend on both momentum variables†, while the integration is performed over only one, this particular source presents the greatest barrier to

---

†Recall that $V_{ij}(E)=\langle q_i|V_{ij}(E)|q_j\rangle=V_{ij}(q_i,q_j,E)$.

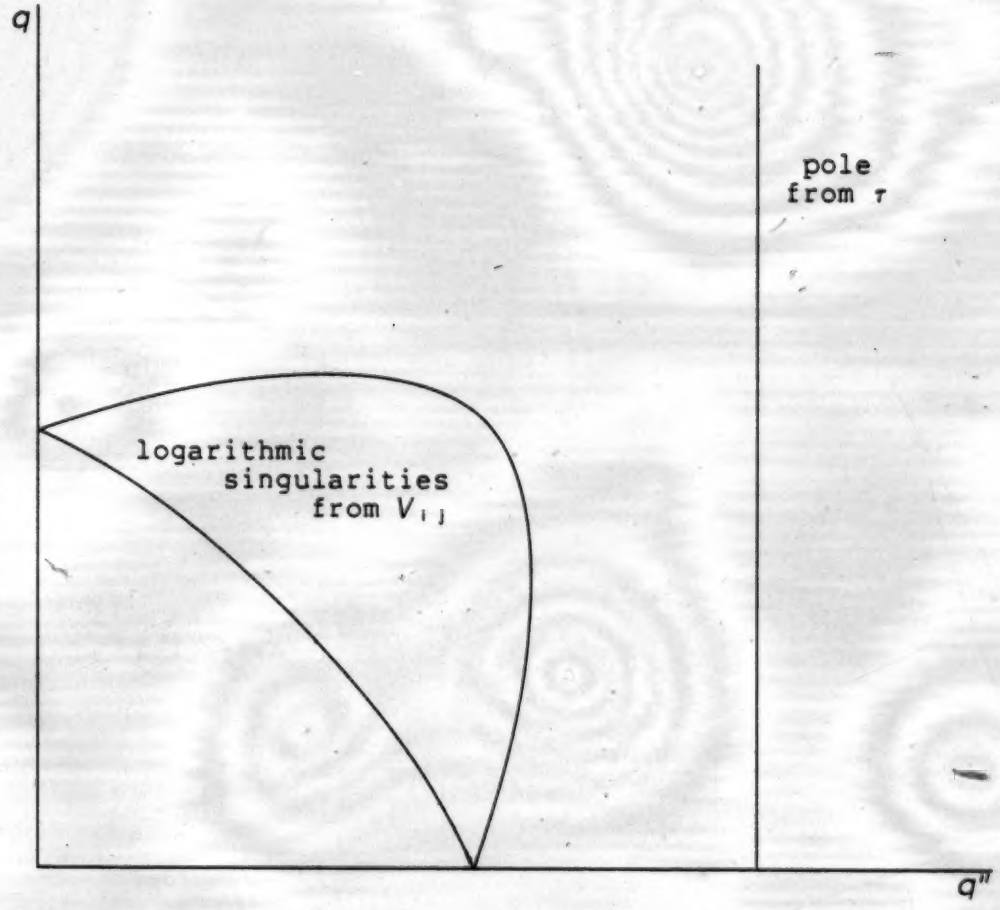

Figure II.5 The integrand of II.49 has singularities in both the variable of integration q'' and the independent variable q.

solution of equations II.40. The locations of all singularities in the kernel (excepting those due to the form factor) are illustrated in figure II.5 as a function of both momentum variables.

Singularities in the amplitudes X_{ij} themselves have been studied in detail by Brayshaw (Br68) who looked at analytic continuations into the complex plane and the ultimate solution of equations like II.40. The complicated structure of these amplitudes is contributed by both the "effective potential" term and the integral term, including those singularities mentioned above which are independent of the variable of integration. In particular, Brayshaw has found the behaviour of the X_{ij} to be compatible with solution by the method of contour deformation.

f. Methods of Solution

Following angular momentum decomposition, equations II.40 reduce to a set of uncoupled, one-dimensional integral equations of the form

$$X(q,q',E)=V(q,q',E) + \int_0^\infty q''^2 dq'' V(q,q'',E)\tau(E-q''^2)X(q'',q',E). \qquad \text{II.50}$$

The challenge of the three-body problem at present, is to solve this type of equation given the singularity structure outlined in the previous section.

The most common approach is to solve II.50 for integration along some contour in the complex q'' plane. Then, from the solution for complex momenta, the physical amplitude, for real momenta, can be calculated. The simplest contour is defined by rotation of the coordinate plane (Ca71), equivalent to integration along the line $q''e^{i\phi}$. This contour clearly avoids the "moving singularities" in the kernel when they take the form indicated in figure II.6. For some values of q', however, the branch cuts assume the more complicated form of figure II.7. In this case, the simple rotation must be supplemented by a detour around the branch point at A and evaluation of the integrand on the second Riemann sheet (where the contour is represented by a broken line). Brayshaw has shown that for small enough ϕ, the method of contour rotation is compatible with the singularities contributed by the X amplitude itself.

A different contour has been used by Ebenhöh (Eb72) who was able to extract the amplitudes for real momenta directly. This avoids the problem of integrating over singularities a second time in computing the amplitudes on the real axis from those in the complex plane.

The presence of "moving singularities" in the kernel of equation II.50 prevents a straightfoward solution using numerical quadrature. While the changing nature of the singularities would require a changing integration mesh, solution of the resulting system of linear equations would demand that the mesh remain constant throughout. Doleschall

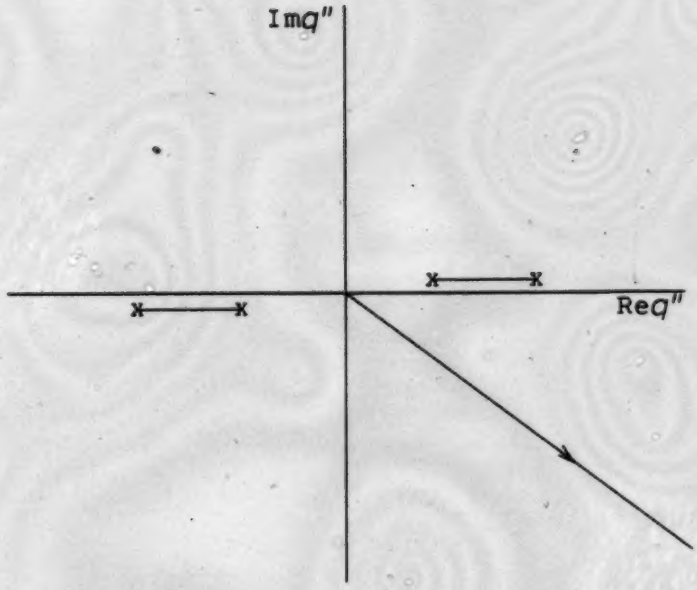

Figure II.6 In their simplest form, the branch cuts in the integrand can be avoided be simple contour rotation.

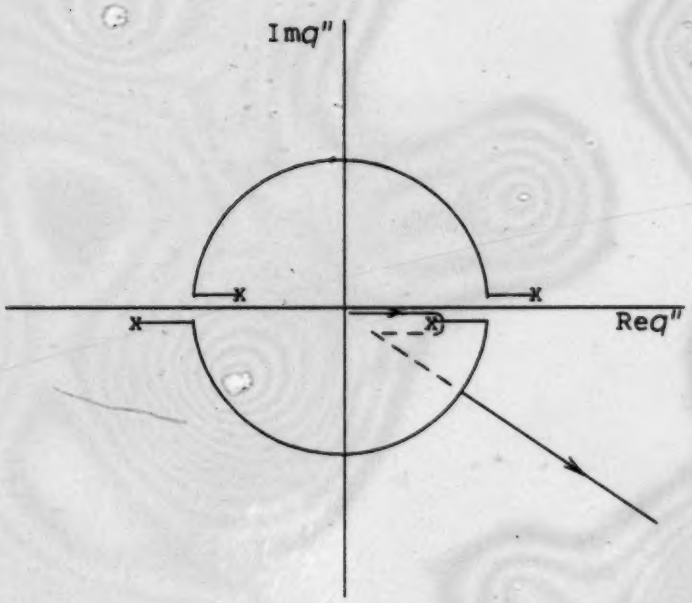

Figure II.7 For some values of q the basic rotated contour must be adjusted to negotiate more complicated branch cuts.

(Do73) (and also Sohre and Ziegelmann (So71)) has developed a modified Gaussian quadrature which gives exact solutions for an $N-1$st degree polynomial using N mesh points. It should be noted on surveying these two popular techniques that analytical integration inevitably requires that the potential have a suitable analytical form with a well behaved extension into the complex plane. Numerical integration, on the other hand, places no such restrictions on form allowing a wider and perhaps more realistic choice of potentials.

A number of calculations have been based on the Fredholm method of iterating equation II.50. A problem arises from the fact that the multiple scattering series so generated does not always converge. Kloet and Tjon (Kl71) enforced convergence by adding a multiplier to the kernel. The transition amplitude, which was derived for a local potential, was then approximated using the Padé method.

By splitting the X-amplitudes into singular and non-singular parts and iterating once, Stuivenberg (St76) effected a solution by analytical integration along the real axis only.

III. IMPULSE APPROXIMATION

a. Justification

Although the impulse approximation was originally used to extract features of the n-n interaction from n-D inelastic scattering (Ch50), its quantitative accuracy has since been surpassed by full-fledged three-body methods. For its simplicity, however, the impulse approximation is still a useful tool of qualitative analysis, especially in the vicinity of quasi-free scattering. We have used it to get a feel for the sensitivities of the D(n,nn)p quasi-free scattering reaction and to guide us in the most efficient use of the lengthy and expensive three-body calculations.

Kinematically, n-n quasi-free scattering can be defined by a three-body final state where the proton has no recoil. Experimentally, this state is evidenced by a peak in the break-up cross section. Except for the effect of the binding energy, then, this is two body n-n scattering with the proton as a spectator and should be well described by the impulse approximation.

As incident energy decreases, the binding energy plays a greater role and the reaction adopts a more three-body character. Under these circumstances, the QFS peak is less pronounced, broadened by the contributions of various multiple scattering terms. The energy of this study, 21.5 MeV (14.3 MeV in the centre-of-mass), is still high enough relative to the deuteron binding energy that the impulse

approximation should give a reasonable account of the kinematics of this reaction and an indication of its suitability for measuring the n-n effective range. Furthermore, the impulse approximation has the added advantage that it includes, implicitly, all relative n-D partial waves in the incident and scattered channels. Stuivenberg (St76) has acknowledged the importance of higher partial waves in this particular reaction.

b. Model

The impulse approximation model for the QFS reaction is illustrated schematically in figure III.1. The kinematics are those of simple n-n elastic scattering modified by the absorption of energy in the breakup of the deuteron (see appendix A).

Yamaguchi S-wave separable potentials (Ya54a)

$$V(k,k')=g(k)\lambda g(k') \qquad \text{III.1}$$

where

$$g(k)=1/(\beta^2+k^2) \qquad \text{III.2}$$

are used for both n-n and n-p interactions. The momentum space proton wave function in the deuteron thus takes the form

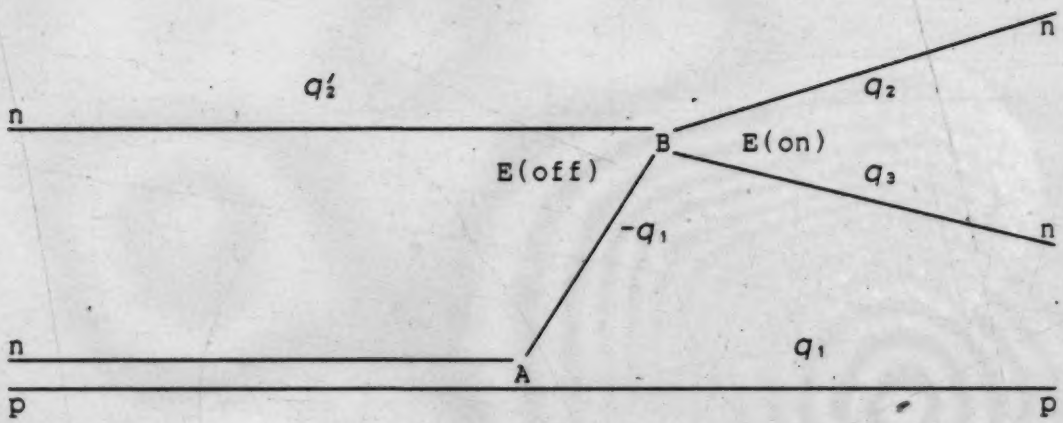

Figure III.1 In the impulse approximation the deuteron wave function (at A) furnishes the momentum distribution for neutrons scattered by the off-shell n-n interaction (at B). The proton acts as a spectator.

$$\psi(p)=N/[(\alpha^2+p^2)(\beta^2+p^2)] \qquad \text{III.3}$$

where N is a normalization constant. It is the peaking of this wave function at zero momentum that is responsible for the peak in the n-D cross section at the QFS geometry.

For the separable potential III.1, the t-matrix for n-n scattering is also separable (see equation II.16)

$$t(k,k';E)=g(k)\tau(E)g(k'). \qquad \text{III.4}$$

For on-shell ($k^2=k'^2=E$) S-wave scattering the effective range expanded t-matrix is used

$$t(k,k;k^2)=(k\cot\delta-ik)^{-1} \qquad \text{III.5}$$
$$=(-1/a+rk^2/2-Pr^3k^4+\ldots-ik)^{-1}$$

where a is the scattering length, r is the effective range and P is the shape parameter. Equations III.4 and III.5 imply that the half-off-shell t-matrix at B in figure III.1 can be approximated by

$$t(k,k';k^2)=[g(k')/g(k)](-1/a+rk^2/2-Pr^3k^4-ik)^{-1}. \qquad \text{III.6}$$

Here the off-shell effect of the potential on the behaviour of the t-matrix can clearly be singled out in the factor $g(k')/g(k)$.

The complete expression for the cross section is

$$\sigma \propto |\psi t|^2 (q_2 q_3 / q_2') \qquad \text{III.7}$$

where the last factor is the kinematic factor in the limit of zero proton recoil (see appendix A). Although approximate, it is considered to be in keeping with the accuracy of the impulse approximation, at least in the vicinity of QFS geometry.

The effective range parameters used in the above interactions are:

n-n	r=2.70fm	n-p	r=2.51fm
(spin singlet)	a=-17.0fm	(spin triplet)	a=-23.7fm
	P=-.017		

c. Experiment

As this study is being conducted in support of an experiment in progress at the Nuclear Research Centre, a few words about the experimental setup are in order. Note that all angles and energies (except relative energies) are described in the laboratory frame of reference.

Incident 21.5±.3 MeV neutrons scatter off a D_2O target into two banks of detectors arranged in four opposing pairs at ±42° to the beam axis with 11° azimuthal spacing between pairs. The detectors have an angular acceptance of 3° in the ϕ direction and 12° in the θ direction. The latter value can be subdivided into two or three equal-sized bins if

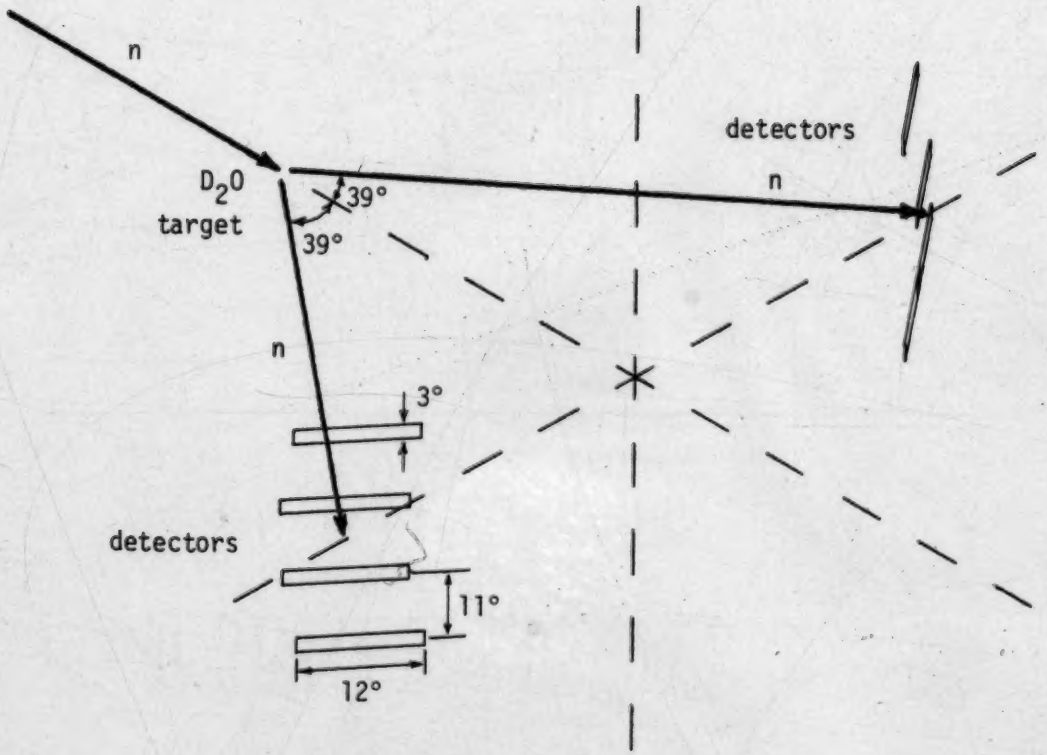

Figure III.2 Schematic diagram of the D(n,nn)p experiment. Detectors are arranged in two banks around a 42° cone. Azimuthal spacing within each bank is 11°.

necessary. The experimental geometry is illustrated schematically in figure III.2.

A n-n QFS reaction is evidenced by coincident neutrons in each detector of a pair. The proton, remaining at rest in exact QFS, cannot be detected. Neutron laboratory energies from 2 to 19 MeV will be measured with a resolution on the order of 1 MeV. Symmetric QFS occurs at a neutron energy of 9.64 MeV. The goal is a measurement of the differential cross section at n-n QFS geometry, to an accuracy better than 5%. A value for r_{nn} can then be deduced by matching the measured cross section to the value predicted by a three-body calculation.

d. Results

For on-shell scattering, equation III.6 reduces to the simple effective range expansion for the t-matrix, since the off-shell function $g(k')/g(k)$ is unity. This t-matrix being defined by measureable† on-shell quantities, should be independent of the off-shell behaviour of the potential.

In the absence of a clear choice for the n-n potential, one should therefore seek out kinematic regions where off-shell effects are minimized, if a reliable estimate of r_{nn} is to be made. Of course the exact QFS geometry is best suited, but the experimental limitations on resolution and acceptable count rate demand an investigation of near-QFS geometries as well.

---

†in theory, at least

From figure III.1, the off-shell function $g(k')/g(k)$ depends on the incoming virtual relative energy $E(off)$ and the real outgoing energy $E(on)$ ($k'^2=E(off)$, $k^2=E(on)$). One could, therefore, regard the difference between $E(on)$ and $E(off)$ as an indication of the model dependence of these calculations. For $E(off)$ closer to $E(on)$, the reaction has more of a two-body character and should yield a more reliable value for r_{nn}. Proton recoil energy, however, is a further test of two-body character and must be monitored as well. It is also a measure of the validity of this approximation.

In the experiment, neutron coincidences are possible in detectors with 169°, 158°, and 147° azimuthal spacing (±3°). As the separation decreases from 180° the calculations become more model dependent, but not greatly so (figure III.3). At 180° the cross section is constant over the azimuthal range of the detectors (3° each). For coincidences in other than opposed detectors, the proton can acquire recoil energies comparable to those of the outgoing neutrons although this problem is alleviated by using energy windows for the neutrons. Figure III.4 shows the magnitude of proton recoil energies encountered, for fixed neutron energies.

In the case of fixed neutron angles and varying energies (figure III.5), model dependence increases away from the QFS value of 9.64*MeV* while the constant on-shell energy implies that the cross section will only be sensitive to the magnitude of the on-shell amplitude but not to its

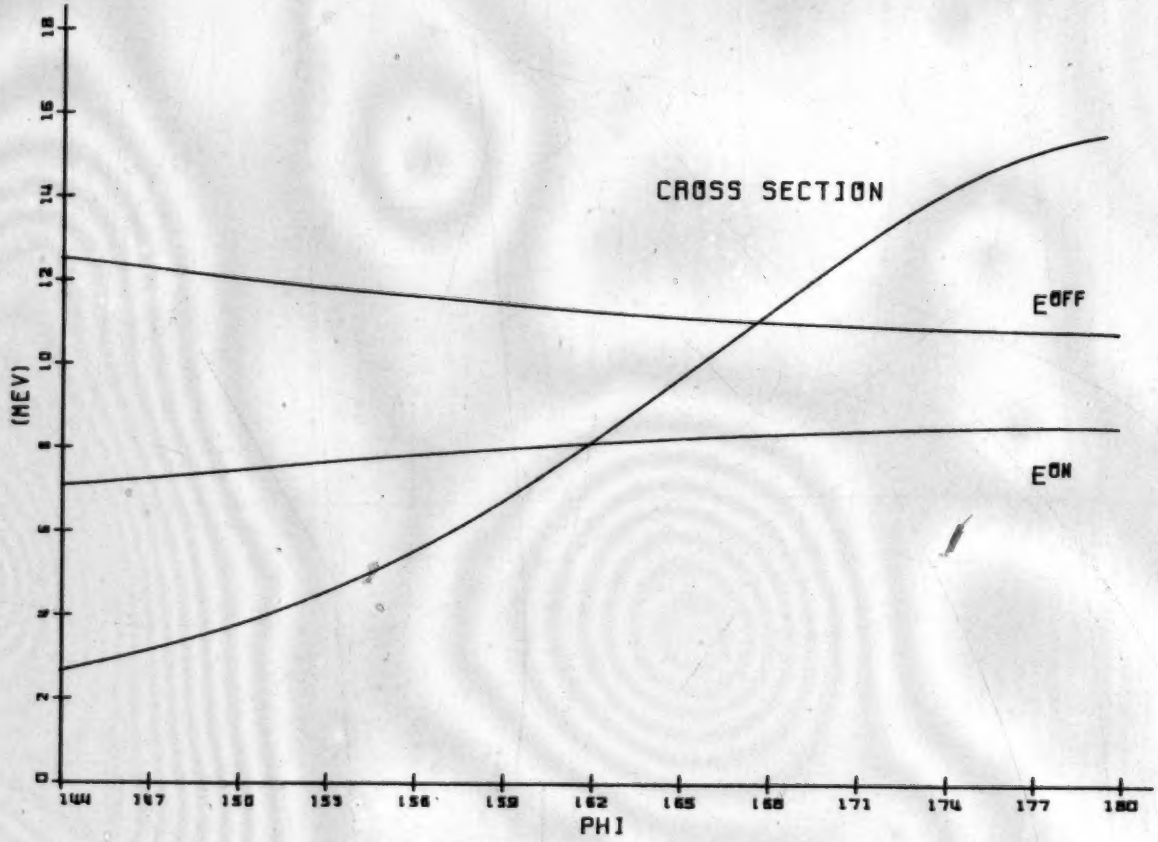

Figure III.3 Break-up cross section and relative neutron energies vs. azimuthal separation of outgoing neutrons (ϕ_2-ϕ_3). $\theta_2=\theta_3=41.7°$, $E_2=E_3$. Cross section from the impulse approximation (not normalized).

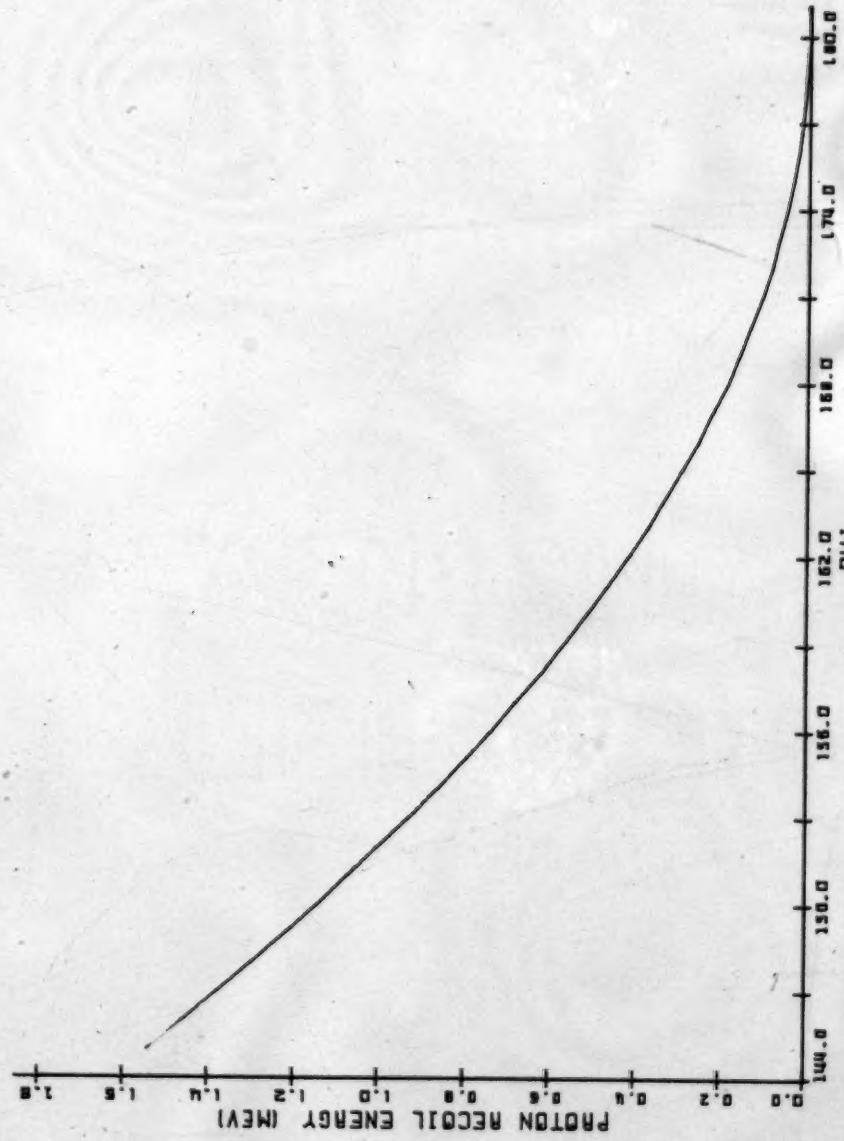

Figure III.4 Proton recoil energy vs. azimuthal separation of outgoing neutrons ($\phi_2-\phi_3$). $\theta_2=\theta_3=41.7°$, $E_2=E_3$.

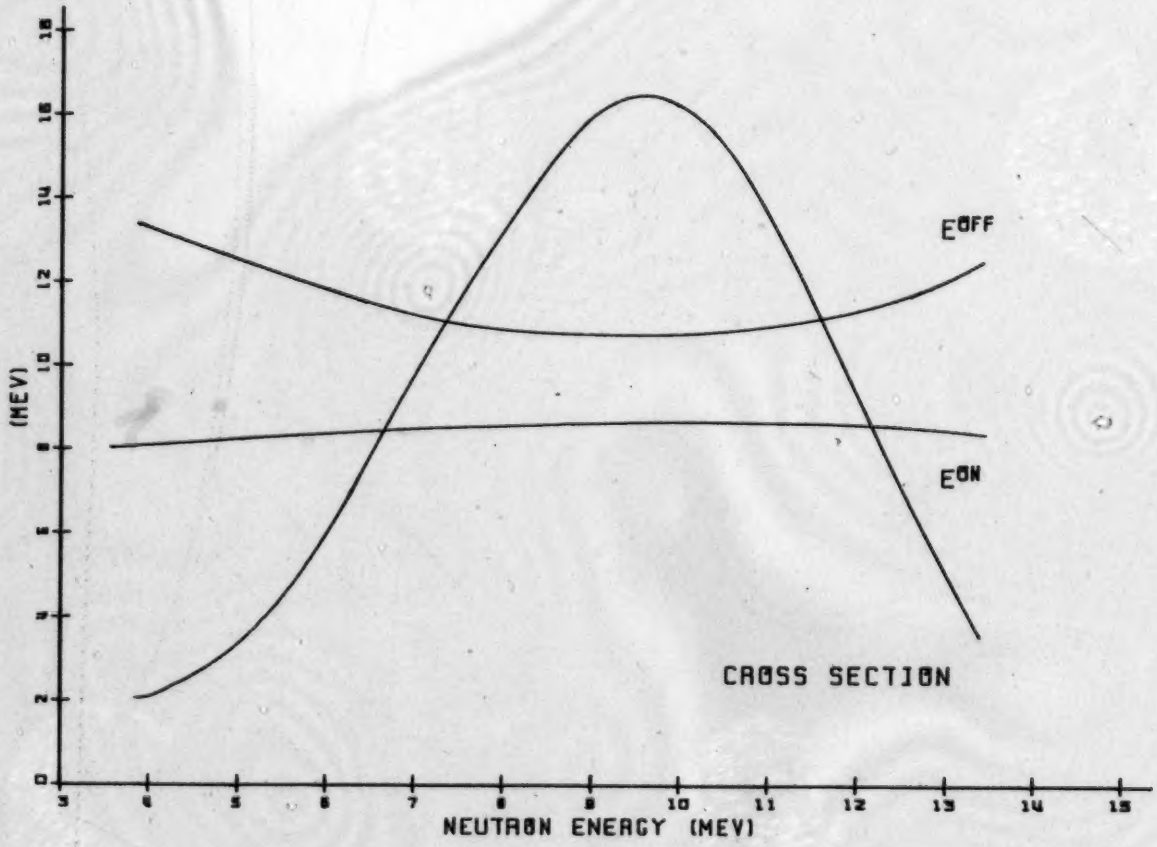

Figure III.5 Break-up cross section and relative neutron energies vs. energy of outgoing neutron (E_2). $\phi_2-\phi_3=180°$, $\theta_2=\theta_3=41.7°$. Cross section from the impulse approximation (not normalized).

k-dependence. Over the range of energy resolution (1*MeV*) model dependence is constant but the peaking in cross section is still discernable.

In contrast to the above results. the two-body nature of the reaction seems to persist through variations in the detector elevation angle θ relative to the beam axis. For symmetric opposed neutron flight paths both on- and off-shell energies increase with angle (figure III.6), the net effect being that the influence of off-shell potential behaviour is constant (figure III.7). This, and the generally small proton energies encountered (figure III.8), indicate that the 12° angular acceptance of the detectors should not pose a serious problem.

The cross section, however, is quite sensitive to θ and peaks at an angle of 39°, somewhat smaller than the 41.7° at which the kinematically defined QFS occurs. This is clearly because of the on-shell t-matrix which increases as θ (and hence $E(on)$) decreases, displacing the peak from that due to the deuteron wave function alone. The fact that the cross section changes by a factor of two over the angular range of the detector will have to be accounted for either through an averageing process or, perhaps better, through the binning mentioned in the previous section.

The suppression of off-shell effects over a range of symmetric, non-QFS angles, coupled with an almost linear relationship between $E(on)$ and θ, suggests a variation in the σ vs. θ relationship via the effective range term in the

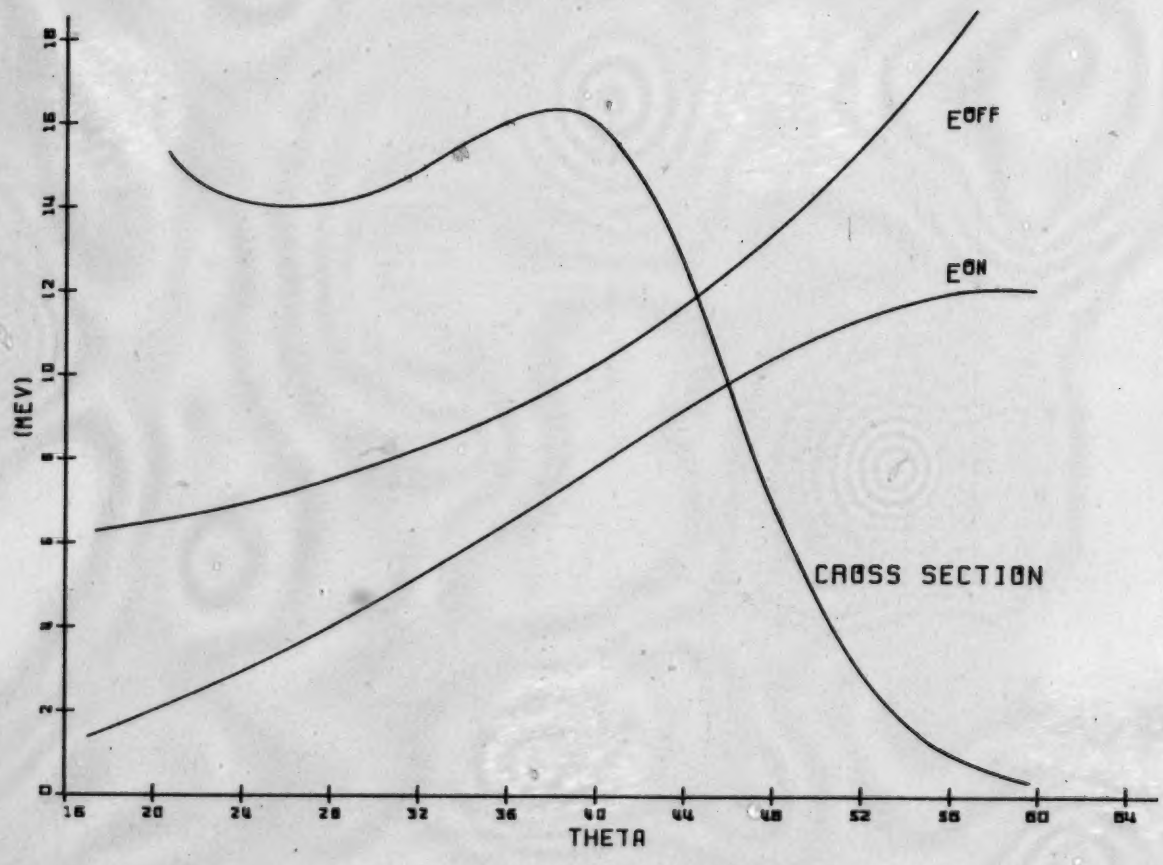

Figure III.6 Break-up cross section and relative neutron energies vs. polar angle (θ) of outgoing neutrons for symmetric geometry. $\theta_2=\theta_3$, $\phi_2-\phi_3=180°$, $E_2=E_3$. Cross section from the impulse approximation (not normalized).

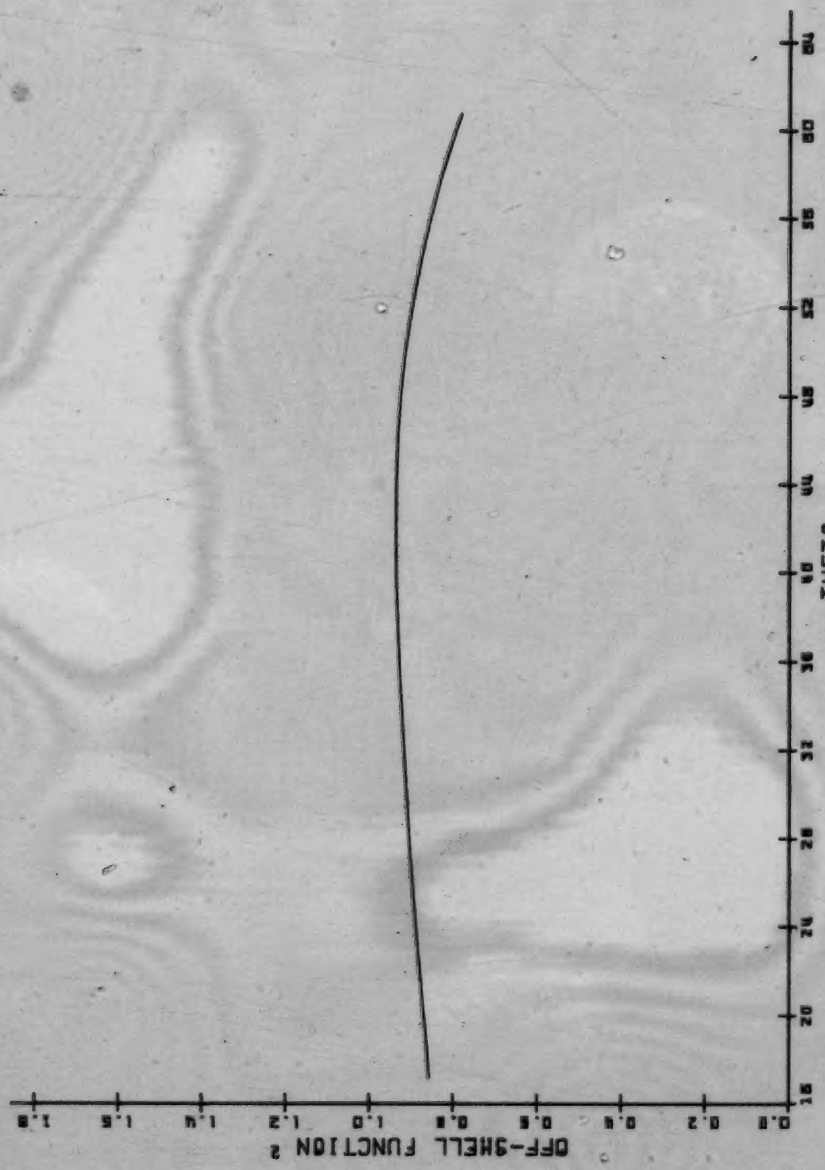

Figure III.7 Yamaguchi off-shell function $[g(k')/g(k)]^2$ vs. polar angle (θ) of outgoing neutrons for symmetric geometry. $\theta_2=\theta_3$, $\phi_2-\phi_3=180°$, $E_2=E_3$.

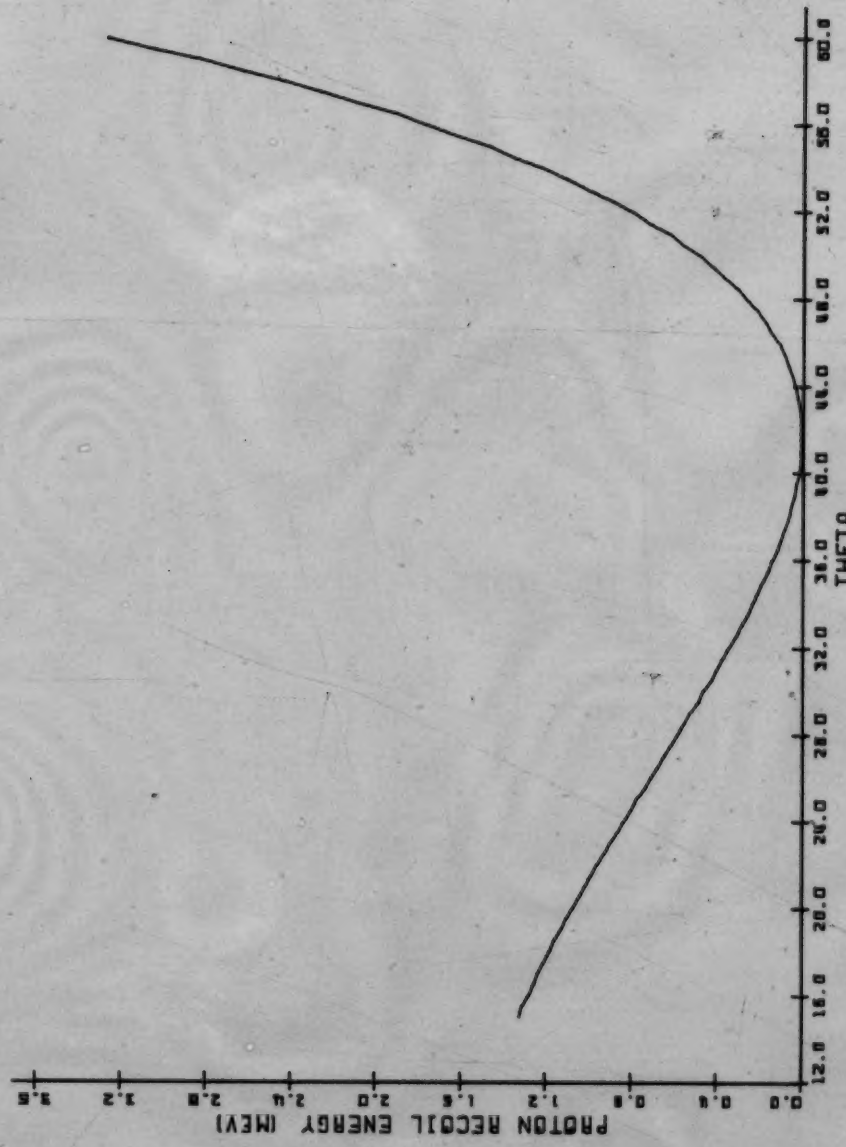

Figure III.8 Proton recoil energy vs. polar angle (θ) of outgoing neutrons for symmetric geometry. $\theta_2=\theta_3$, $\phi_2-\phi_3=180°$, $E_2=E_3$.

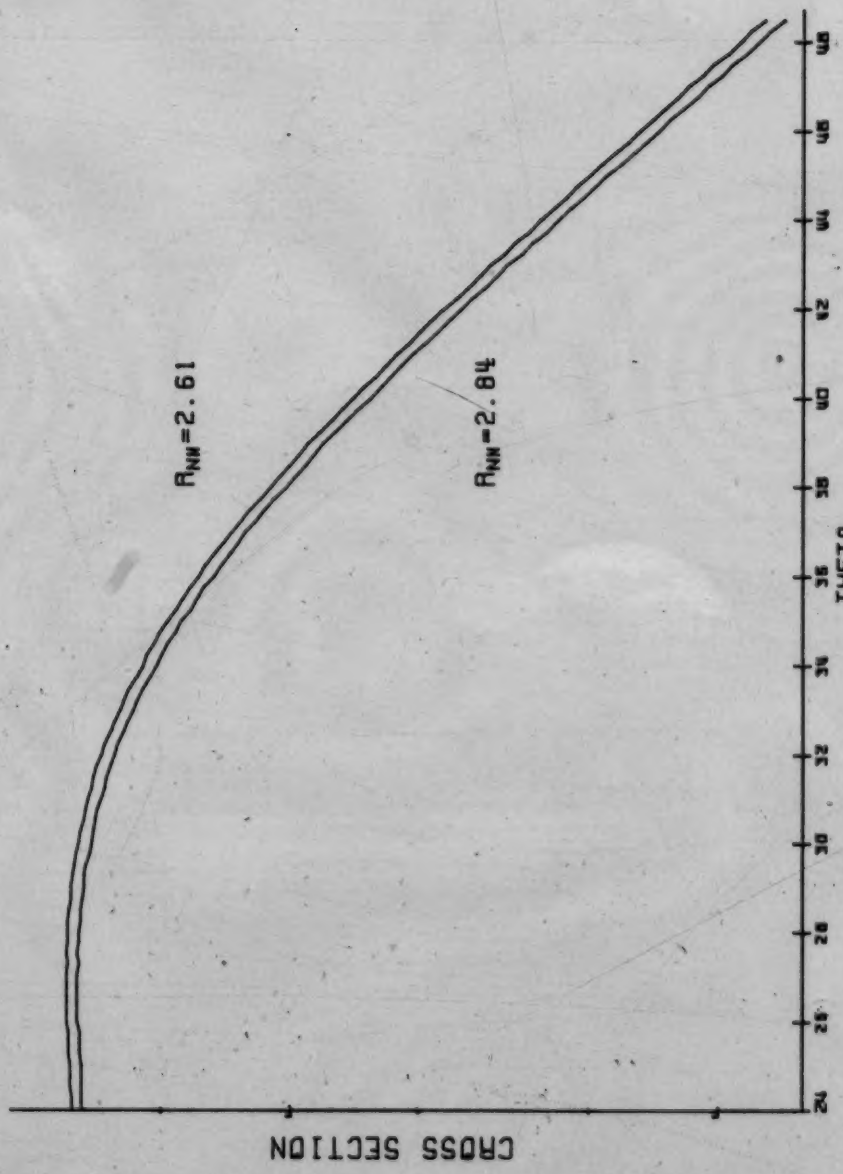

Figure III.9 Break-up cross section for two values of R_{NN} vs. polar angle (θ) of outgoing neutrons for symmetric geometry. $\theta_2=\theta_3$, $\phi_2-\phi_3=180°$, $E_2=E_3$. Cross section from the impulse approximation (not normalized). Logarithmic scale.

expanded on-shell t-matrix (equation III.5). Figure III.9 demonstrates that this shape dependence is too small to be of any use.

The relationship between σ and r_{nn} is roughly linear with a slope of -1 over the conceivable range of r_{nn} (figure III.10). From this, a determination of r_{nn} to within a few percent seems at least feasible.

As a guide to identifying possible sources of error in the experiment, equation III.7 can be inverted to yield r as a function of σ, a, and P, whence

$$(\Delta r)^2=[(\partial r/\partial\sigma)\Delta\sigma]^2+[(\partial r/\partial a)\Delta a]^2+[(\partial r/\partial Q)\Delta Q]^2 \qquad \text{III.8}$$

In the last term, the shape parameter P has been incorporated into $Q=Pr^3$. Comparison of common potentials, both theoretical and empirical, suggests that there is some correlation between P and r which would permit treating Q as an independent parameter.

For reasonable choices of the above uncertainties, the normalization of the cross section arises as the largest source of error for all possible relative outgoing neutron energies (see figure III.11). Even at the reasonable level of 5% overall uncertainty, the cross section still contributes an error in r that is as large as some recently reported values (table I.2). One must therefore hope either for a significant improvement in the measurement of detector efficiency or for a noticeable sensitivity of the shape of

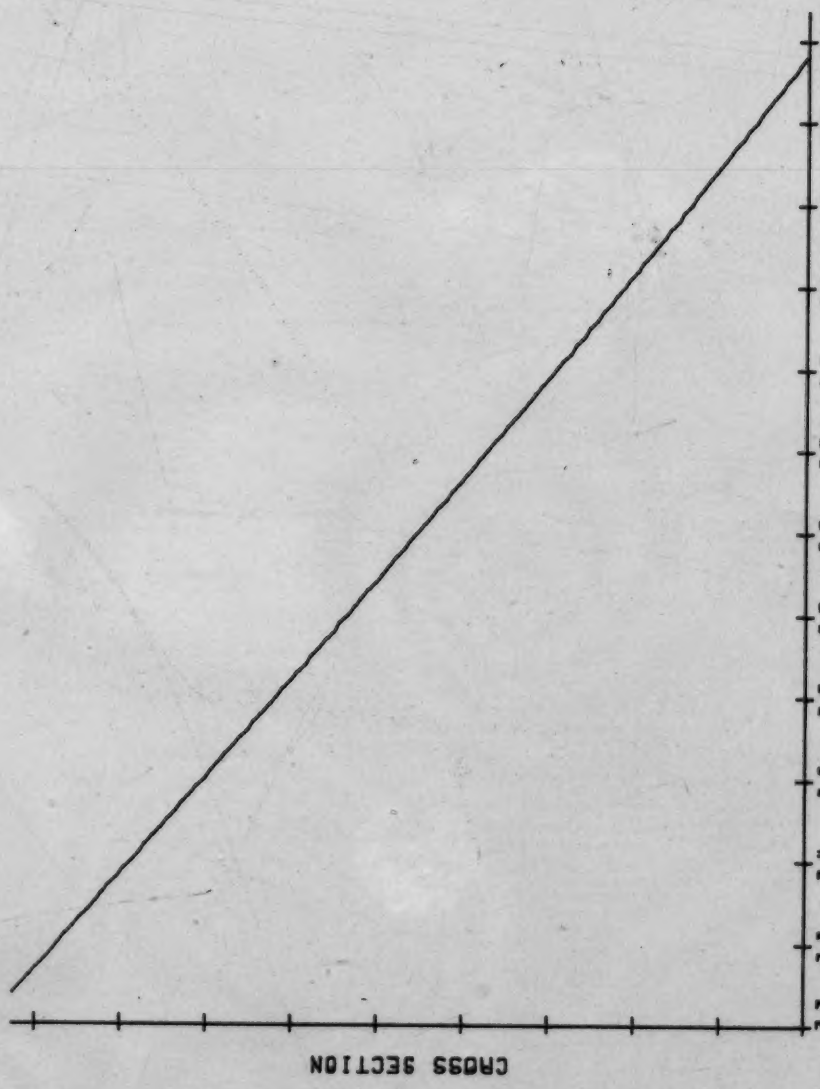

Figure III.10 QFS cross section vs. n-n effective range for symmetric geometry. $\theta_2=\theta_3=41.7°$, $\phi_2-\phi_3=180°$, $E_2=E_3$. Cross section from the impulse approximation (not normalized).

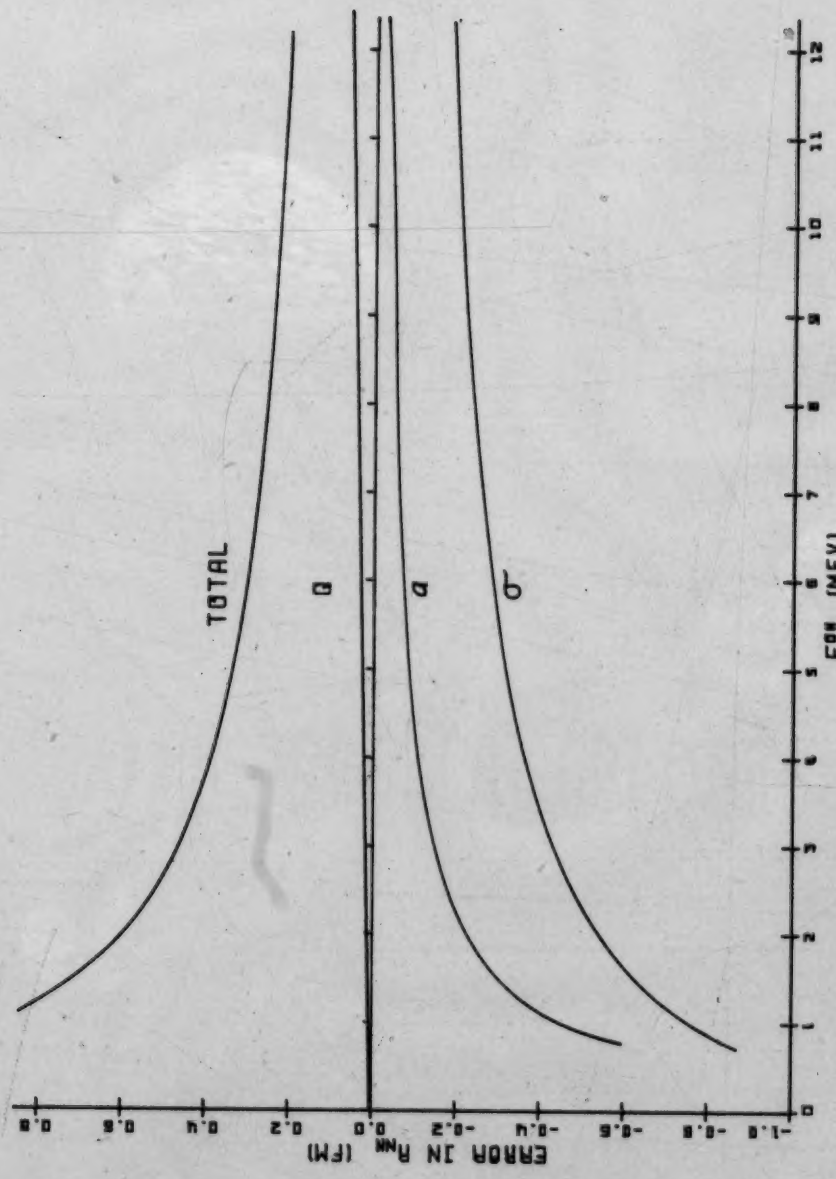

Figure III.11 Absolute uncertainty in r_{nn} due to uncertainties in cross section and parameters of the effective range expansion vs. relative outgoing neutron energy ($E(on)$). $a_{nn}=-19\pm2$fm, $r_{nn}=2.7$fm, $Q=.5\pm.1$, $\Delta\sigma=5\%$. $\theta_2=\theta_3=41.7°$, $\phi_2-\phi_3=180°$, $E_2=E_3$.

the cross section to r.

By way of comment on the liberal use of the effective range expanded t-matrix in this part, it is instructive to consider the expansion in terms of the dimensionless parameter rk:

$$k\cot\delta=(1/r)(-r/a+(rk)^2/2-P(rk)^4+\ldots). \qquad \text{III.9}$$

For reasonably behaved coefficients, $rk<1$ should guarantee convergence of this series, whereas the reaction at hand yields $rk\approx1.2$. While this does not preclude convergence, it is true that the third term contributes as much as 7% in this particular case.

IV. THREE-BODY CALCULATIONS

a. Model

Three-body calculations were carried out with the computer code of P. Doleschall (Do73). Our version of the the program package (which we call DOCODE) is written in IBM-compatible FORTRAN and runs on the University of Alberta's AMDAHL 470/V6 computer.

The program solves the AGS equations (II.30) for separable N-N interactions (II.35). The reduced integral equations (II.50) are integrated numerically by Gaussian quadrature. Those parts of the kernel which contain only simple poles (from τ) are dealt with in a straightforward principal value integral. For the remaining more singular parts (containing logarithmic singularities and cuts) a special quadrature is constructed based on the mesh used for the simpler quadrature. The method relies on some smoothness in τ. Splitting of the kernel into "singular" and "regular" parts is done in such a way that the special quadrature is independent of energy and two-body interactions.

Integration yields a system of linear algebraic equations which are solved by the Padé approximant method (Ba71) using MacDonald's ϵ algorithm (Md64). The total interaction is constructed as a sum of partial wave three-body t-matrices up to $19/2^+$ total angular momentum and parity. To speed up calculations, orbital angular momentum which would normally include states up to $\ell=11$ is truncated

at ℓ=8 with no effect on results reported in the original calculations (Do73). Our calculations show a 2% difference between n-n quasi-free scattering cross sections with truncation at ℓ=7 and ℓ=8. For partial waves beyond $7/2^+$, quadrature is replaced by Sloan's unitary first-order approximation (Sl69). This is a type of first-order approximation to the multiple scattering series with unitarity built in. Our calculations in the quasi-free scattering region indicate an effect of .2% in the combined $9/2^+$ and $11/2^+$ partial waves and .04% in the combined $11/2^-$ and $13/2^-$ partial waves, due to this substitution.

Except for the numerical treatment, the distinguishing feature of any three-body calculation is the type of two-body interactions employed (see table IV.1). For most practical purposes, the mathematical complexity of the problem demands the use of separable potentials. Limits on sheer computing power place further restrictions on the rank of potentials, precluding for example an accurate series approximation to a proven local potential, or even the inclusion of an OPEP tail.

Initial calculations with DOCODE reported by Doleschall used rank one Yamaguchi (separable) potentials in S-, P- and D-wave interactions. Later the program was modified to accept generalized Yamaguchi potentials which were designed to improve the description of the mixed-state deuteron and to fit the experimental phase shifts in all partial waves. In particular, the polynomial form of the numerator enables

reference	reaction	potentials	rank	partial waves
(Aa65,66)	break-up, elastic	Yamaguchi	1	S
(Ph66)	break-up, elastic bound state	Yamaguchi[1]	1	S,P,D
(Ml69)	bound state	Yukawa[2]	2	S
(Sl69)	elastic	Yamaguchi		
(Ca71)	break-up (FSI)	Yamaguchi Tabakin	1	S
(Kl71)	break-up	Yukawa[2]	2	S
(Eb72)	break-up	Yamaguchi	1	S
(Hr72)	bound state	Reid soft-core[2,3]	2	S,T
(Pi72)	elastic	Yamaguchi	1	S
(Do73,74,82)	break-up	gen. Yamaguchi R-type	2	S,T,P,D
(Du73)	break-up (QFS)	Yamaguchi Tabakin	1	S,P,D
(Ha73)	bound state	Yukawa[2,3]	2	S
(Sk75)	elastic	Reid soft-core[3]		S,T,P,D
(Be76)	elastic	de Tourreil[3] and Sprung		S,T,P
(St76,78)	break-up	gen. Yamaguchi[3,4]	2	S
(Bn77)	break-up	Yamaguchi	1	S,T,P

[1]including three-body force
[2]local potential
[3]including phase-equivalent transformations
[4]from G. Koopmans, internal report, Vrije Universiteit

Table IV.1 Survey of three-nucleon calculations. n-D system with separable potentials unless otherwise noted. T indicates tensor force ($^3S_1$-$^3D_1$).

reproduction of nodes in the $^1S_0$†, $^3S_1$ and $^3P_0$ phase shifts. Currently the program accepts both generalized Yamaguchi and R-type (recently developed by Doleschall) potentials of any rank in any partial wave. Coupling between partial waves, as in the $^3S_1$-$^3D_1$ tensor interaction, is also available.

The generalized Yamaguchi potential, in the k-th partial wave, has the form factor

$$g^k(p)=[p^k\Sigma_{i=0}^{m}\gamma_i p^{2i}]/[\Pi_{i=0}^{k}(1+\beta_i p^2)] \qquad \text{IV.1}$$

with m no larger than 2 for the potentials presently in use. This form will hereafter be designated as Y-type, as a reminder that it is more general than the traditional Yamaguchi potential (Ya54a,b) which inspired it. Of course in the case of rank one S-wave form factors this distinction is pure formality. The R-type form factor, for which there is no published description, is very similar:

$$g^k(p)=[p^k/(1+\beta p^2)^k]\Sigma_{i=1}^{m}[\gamma_i/(1+\beta p^2)^i] \qquad \text{IV.2}$$

With some rearrangement, it can be seen that the R form factor is really a reduced form of the Y, with $\beta_0=0$ and $\beta_i=\beta$. The smaller number of parameters in this form factor (through its restricted form) allows its practical use for larger values of m (up to 5 in our calculations).

---

†Standard spectroscopic notation ($^{2s+1}\ell_j$) is used.

Note the distinction between the number of *terms* in a form factor (m) and the *rank* of the potential (number of *channels* or, in most cases, form factors, indexed by y and z in equation II.35). This terminology will be used throughout. Furthermore, to streamline notation, the rank of an S-wave potential may be indicated by a prefix on the type designation, as in 1Y, 2R, etc.

Both types of potentials are used in rank one and two singlet S-wave forms, this being the most important partial wave. Triplet S-wave potentials (n-p only) are rank one except for a rank four tensor interaction (abbreviated 4T) used with the 2R singlet interaction. P-wave interactions are exclusively Y-type and include the $^1P_1$, $^3P_1$, $^3P_2$ and $^3P_0$ partial waves, the latter represented by a rank two potential. D-wave interactions are rank one R-type and include the $^1D_2$ and $^3D_2$ partial waves. The $^3D_1$ interaction is only present when tensor forces, which are R-type, are included. All interactions allowed by the generalized Pauli exclusion principle (ℓ+s+t odd) have been used. Traditional Yamaguchi and Y-type tensor interactions have been used by Doleschall (Do74) but have proven unable to fit even the two-body experimental data.

Parameters for all interactions were obtained from a weighted χ^2 fit to accepted low energy nucleon-nucleon data (Mg69) including singlet and triplet S-wave scattering length and effective range, P_d, Q_d A_d/A_s and p-p phase shifts up to 460*MeV*. The latter were used to construct both

n-p and n-n interactions by increasing the assigned experimental uncertainties below 10*MeV*, thereby diminishing the weights of the lower energy phase shifts. In this respect the calculations are charge independent. In fact, wherever both n-n and n-p interactions are present in the higher partial waves, they are identical. But since the more important S-wave effective range parameters were allowed to differ between n-n and n-p interactions the calculations may be regarded as charge dependent.

Interactions obtained from the same two-body input data are nominally considered on-shell equivalent although there may be on-shell differences due to differences in overall form. Effective range parameters used for S-wave potentials are summarized in table IV.2. Table IV.3 contains a list of

interaction	a	r
^1S_o nn	-17.0	2.84
^1S_o np	-23.7	2.51
$^1\tilde{S}_o$ nn	-17.0	2.61
$^1\tilde{S}_o$ np	-23.7	2.69
$^3S_1$	5.4	1.77
1T4RA	5.4	1.74
4T4RA3	5.4	1.76

Table IV.2 Effective range parameters for the S wave two-body interactions. (units of *fm*)

all partial wave potentials with the number of parameters available for fitting in each form factor. The actual values of parameters can be found in appendix C.

b. Results

The calculated n-n QFS cross sections for the various two-body potentials are shown in table IV.4-6. In the abbreviated notation for the potentials the first term is a n-n interaction, the second is n-p. n-p cross sections are included to explore the results of von Witsch et al. (Wi80). In addition to the overall differences in form between Y and R potentials we had available to us the choice of rank (of singlet S-wave potential), form of triplet interaction, presence of P and D-waves and value of the n-n effective range. Except for the last quantity, the effects of these are treated as independent.

The complete† 2R interaction is the most sophisticated we have used both in terms of complexity and fit to the experimental two-body data. For this reason it is considered to be the most reliable. Assuming this, the most striking feature of table IV.4 is the failure of the 1R interaction to produce the correct magnitude of cross section. This is believed to be due not to some peculiarity in the 1R interaction but rather to the more general fact that symmetric QFS is indeed off-shell independent, but only if rank two (or higher) interactions are used. By the same

---

†including higher partial waves

interaction	m	number of parameters β	γ
^1S_0Y	0	1	1
^3S_1Y	0	1	1
2^1S_0Y	0	1	1
	1	2	2
2^3P_0Y	2	4	3
	1	3	2
^3P_1Y	2	4	3
^3P_2Y	1	3	2
^1P_1Y	2	4	3
^1S_0R	5	1	5
2^1S_0R	5	1	5
	5	1	5
^1D_2R	4	1	4
^3D_2R	4	1	4
^3D_3R	4	1	4
1T4RA3	5	2	10
4T4RA3	5	2	10
	5	2	10
	5	2	10
	5	2	10

Table IV.3 Number of terms and individual parameters available for fitting. Refer to equations IV.1 and IV.2. The construction of tensor interactions is shown in appendix C.

interaction	n-n	n-p	n-p/n-n
^1S_0Y ^1S_0Y ^3S_1Y	.2447	.7924	3.238
$^1\tilde{S}_0Y$ ^1S_0Y ^3S_1Y	.2661	.7892	2.966
2^1S_0Y 2^1S_0Y ^3S_1Y	.2428	.7931	3.266
$2^1\tilde{S}_0Y$ ^1S_0Y ^3S_1Y	.2629	.7901	3.005
^1S_0R ^1S_0R ^3S_1R	.2255	.7847	3.480
^1S_0R $^1\tilde{S}_0R$ ^3S_1R	.2268	.7805	3.441
$^1\tilde{S}_0R$ ^1S_0R ^3S_1R	.2468	.7808	3.164
^1S_0R ^1S_0R 1T4RA	.2288	.7698	3.365
2^1S_0R 2^1S_0R ^3S_1R	.2443	.7828	3.204
2^1S_0R 2^1S_0R 4T4RA3	.2425	.7763	3.201
2^1S_0R 2^1S_0R 4T4RA3 P	.2440	.7738	3.171
2^1S_0R 2^1S_0R 4T4RA3 P D	.2403	.7783	3.239

Table IV.4 Centre-of-mass cross sections for n-n and n-p QFS at neutron polar angles of 41.7°, 41.7°. (units of mb/sr^2MeV) $\phi_2-\phi_3=180°$. Phase space factor not included.

token, the remarkable accuracy of the 1Y potential is regarded as accidental although not entirely unexpected, given its unusually good agreement (for a potential with only two free parameters) with higher energy phase shifts (St76). Ignoring the 1R calculations, variations in the cross section predicted by pure S-wave calculations are less than 1%.

A somewhat stronger result is the lack of any appreciable sensitivity to the presence of a tensor force, exhibited by both 1R and 2R calculations. The fact that a rank one tensor force was used in the former case while a rank four tensor force was used in the latter case reinforces the generality of this result.

The effect of adding D-wave terms is roughly double that of P-wave terms but opposite in direction. This kind of interference between odd and even partial waves has been observed in other kinematic regions of the three-nucleon system (Ku81, Ke78). The combined effect of adding P- and D-wave interactions is on the order of 1% (decrease in cross section).

The one feature to which all calculations were sensitive, and with considerable consistency, was the value of r_{nn}. For a decrease of 8.1% in r_{nn}, symmetric QFS cross sections increased by 8.3-9.4%. In determining a value for r_{nn} from a measured cross section, therefore, percentage errors in the cross section can be equated directly to those in r_{nn}.

A slight inconsistency will be noted in the use of a 1Y n-p potential in the nominally 2Y calculation with r_{nn}=2.61*fm*. This was done to simplify (i.e. cheapen) calculations, assuming that this potential plays little part in n-n QFS. Our results show that its effect even on n-p QFS is minimal. Given this, and the agreement between 1Y and 2Y calculations anyway, the substitution should not prejudice results.

The cross section for symmetric n-p QFS is, in fact, insensitive to everything except the triplet interaction which all but uniquely determines the magnitude. Consequently the ratio of n-p to n-n QFS cross sections, used by von Witsch et al., behaves very much like the n-n QFS cross section alone. For the 8.1% change in r_{nn} this ratio fell by 8.0-9.1%. It is therefore no more sensitive to the value of r_{nn} than is the n-n QFS cross section, nor is its sensitivity any more consistent from one calculation to the next.

The geometry of the von Witsch experiment was actually slightly asymmetric, close to that of table IV.5. All of the remarks concerning symmetric QFS, however, can be applied to this case as well. This includes the *theoretical* result that the ratio of n-p to n-n QFS cross sections is no more reliable an indicator of r_{nn} than the n-n QFS cross section itself.

For radical departures from symmetry, as in table IV.6, differences due to two-body input are much clearer. The

interaction	n-n	n-p	n-p/n-n
^1S_oY ^1S_oY ^3S_1Y	.2291	.8056	3.552
$^1S\tilde{o}Y$ ^1S_oY ^3S_1Y	.2490	.8012	3.218
2^1S_oY 2^1S_oY ^3S_1Y	.2271	.8067	3.552
$2^1S\tilde{o}Y$ ^1S_oY ^3S_1Y	.2457	.8026	3.267
^1S_oR ^1S_oR ^3S_1R	.2115	.8011	3.788
^1S_oR $^1S\tilde{o}R$ ^3S_1R	.2127	.7964	3.744
$^1S\tilde{o}R$ ^1S_oR ^3S_1R	.2313	.7961	3.442
^1S_oR ^1S_oR 1T4RA	.2143	.7947	3.708
2^1S_oR 2^1S_oR ^3S_1R	.2296	.7985	3.478
2^1S_oR 2^1S_oR 4T4RA3	.2280	.7947	4.486
2^1S_oR 2^1S_oR 4T4RA3 P	.2332	.8057	3.455
2^1S_oR 2^1S_oR 4T4RA3 P D	.2313	.8100	3.502

Table IV.5 Centre-of-mass cross sections for n-n and n-p QFS at neutron polar angles of 33.5°, 49.5°. (units of *mb/sr²MeV*) $\phi_2-\phi_3=180°$. Phase space factor not included.

interaction	n-n	n-p	n-p/n-n
^1S_0Y $^1\tilde{S}_0Y$ ^3S_1Y	.1734	.7518	4.336
$^1\tilde{S}_0Y$ ^1S_0Y ^3S_1Y	.1872	.7418	3.963
2^1S_0Y 2^1S_0Y ^3S_1Y	.1721	.7571	4.339
$2^1\tilde{S}_0Y$ ^1S_0Y ^3S_1Y	.1850	.7490	4.049
^1S_0R ^1S_0R ^3S_1R	.1685	.7741	4.594
^1S_0R $^1\tilde{S}_0R$ ^3S_1R	.1705	.7631	4.476
$^1\tilde{S}_0R$ ^1S_0R ^3S_1R	.1825	.7648	4.191
^1S_0R ^1S_0R 1T4RA	.1763	.8365	4.745
2^1S_0R 2^1S_0R ^3S_1R	.1831	.7646	4.176
2^1S_0R 2^1S_0R 4T4RA3	.1799	.7675	4.266
2^1S_0R 2^1S_0R 4T4RA3 P	.2177	.7955	3.654
2^1S_0R 2^1S_0R 4T4RA3 P D	.2273	.8263	3.635

Table IV.6 Centre-of-mass cross sections for n-n and n-p QFS at neutron polar angles of 18.2°, 61.3°. (units of mb/sr^2MeV) $\phi_2-\phi_3=180°$. Phase space factor not included.

effect of the tensor force is slightly enhanced but negligible compared to the increase in cross section produced by the addition of P- and D-waves. These now appear indispensible to the calculation, especially since in this kinematic region their effects do not cancel. Sensitivity to r_{nn} at these angles is slightly reduced but no more off-shell dependent.

The properties of the break-up reaction at symmetric non-QFS neutron angles, as predicted by the impulse approximation, seemed interesting enough to warrant further study with the full three-body calculations. Furthermore with the large angular acceptance of the detectors in the present experiment, an accurate prediction of the cross section throughout this region might be useful. This point

	angle					
interaction	**32.7**	**35.7**	**38.7**	**41.7**	**44.7**	**47.7**
$^1S_0Y\ ^1S_0Y\ ^3S_1Y$	3.502	3.830	4.099	4.045	2.784	1.167
$^1\tilde{S}_0Y\ ^1S_0Y\ ^3S_1Y$	3.721	4.096	4.416	4.398	3.069	1.319
$2^1S_0Y\ 2^1S_0Y\ ^3S_1Y$	3.476	3.801	4.067	4.017	2.755	1.145
$2^1S_0R\ 2^1S_0R$ 4T4RA3 P	3.347	3.708	4.031	4.036	2.803	1.189
$2^1S_0R\ 2^1S_0R$ 4T4RA3 P D	3.367	3.709	4.001	3.976	2.745	1.158

Table IV.7 Laboratory break-up cross sections for symmetric geometries. (units of mb/sr^2MeV) $\theta_2=\theta_3$, $\phi_2-\phi_3=180°$, $E_2=E_3$.

is discussed further in chapter V.

Table IV.7 lists the predictions of the various models for the break-up cross section with equal outgoing neutron angles. The most prominent feature of the results when viewed graphically (figure IV.1) is that the cross section peaks around 40.5° (corresponding to a proton recoil energy of 7keV). This is not as low as the impulse approximation predicts but still significantly lower than the QFS angle of 41.7°. This is important in view of the steep drop in cross section above 42°, much steeper than that predicted by the impulse approximation.

The sensitivity to various aspects of the two-body input is best illustrated by ratios of cross sections (figure IV.2). Sensitivity to the rank of potential, represented by the ratio of 1Y to 2Y cross sections, is fairly constant throughout the angular range of interest. The effect of D-wave interactions, measured by the ratio of complete 2R calculations with and without D-wave components, increases monotonically with angle. From the results at 41.7° it can be assumed that the effect of P-wave interactions also increases with angle although smaller and opposite in sign to the D. Discrepancy between the predictions of the 2Y and complete 2R calculations, interpreted as the effect of the form (or off-shell content) of two-body potential used, decreases monotonically with angle. Overall, there seems to be no "preferred" angle at which undesireable sensitivity to two-body input is

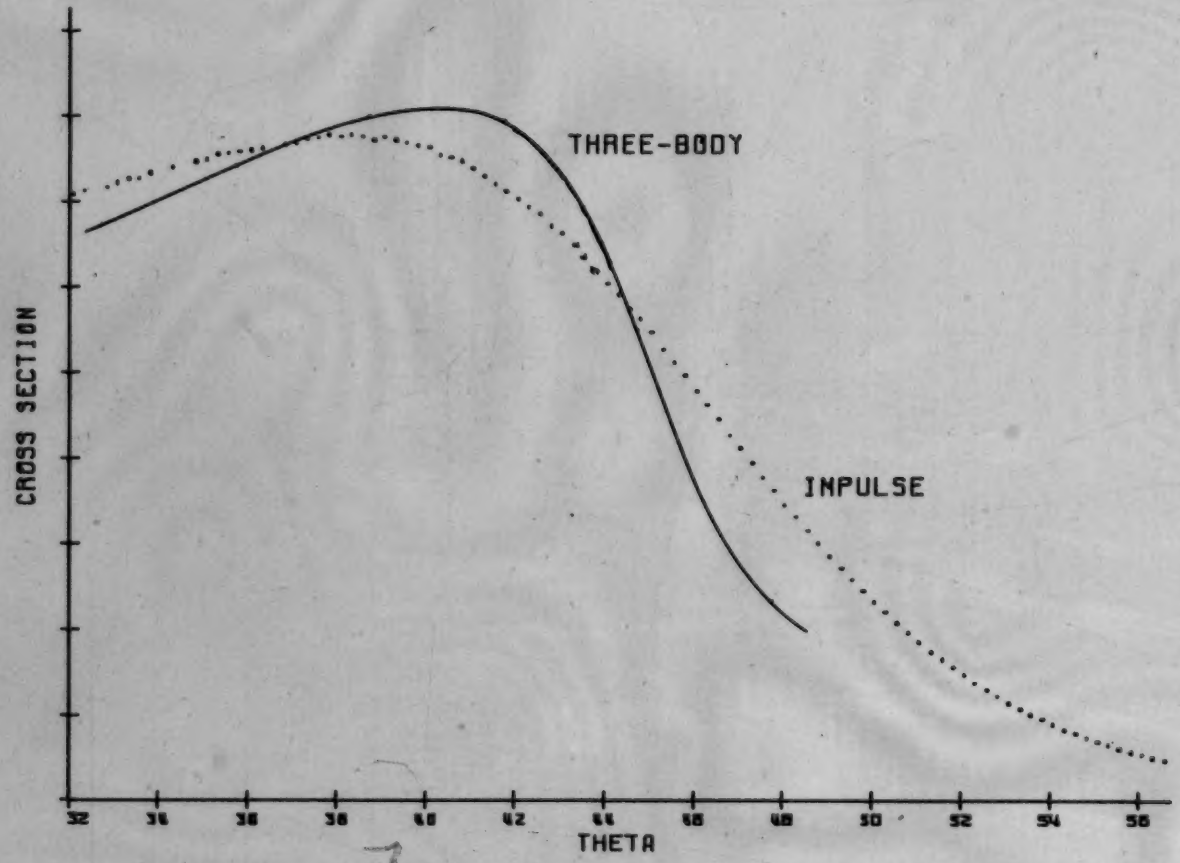

Figure IV.1 Break-up cross section vs. polar angle (θ) of outgoing neutrons for symmetric geometry. $\theta_2=\theta_3$, $\phi_2-\phi_3=180°$, $E_2=E_3$. Complete 2R three-body calculation. Prediction of impulse approximation is overlaid for comparison (not normalized).

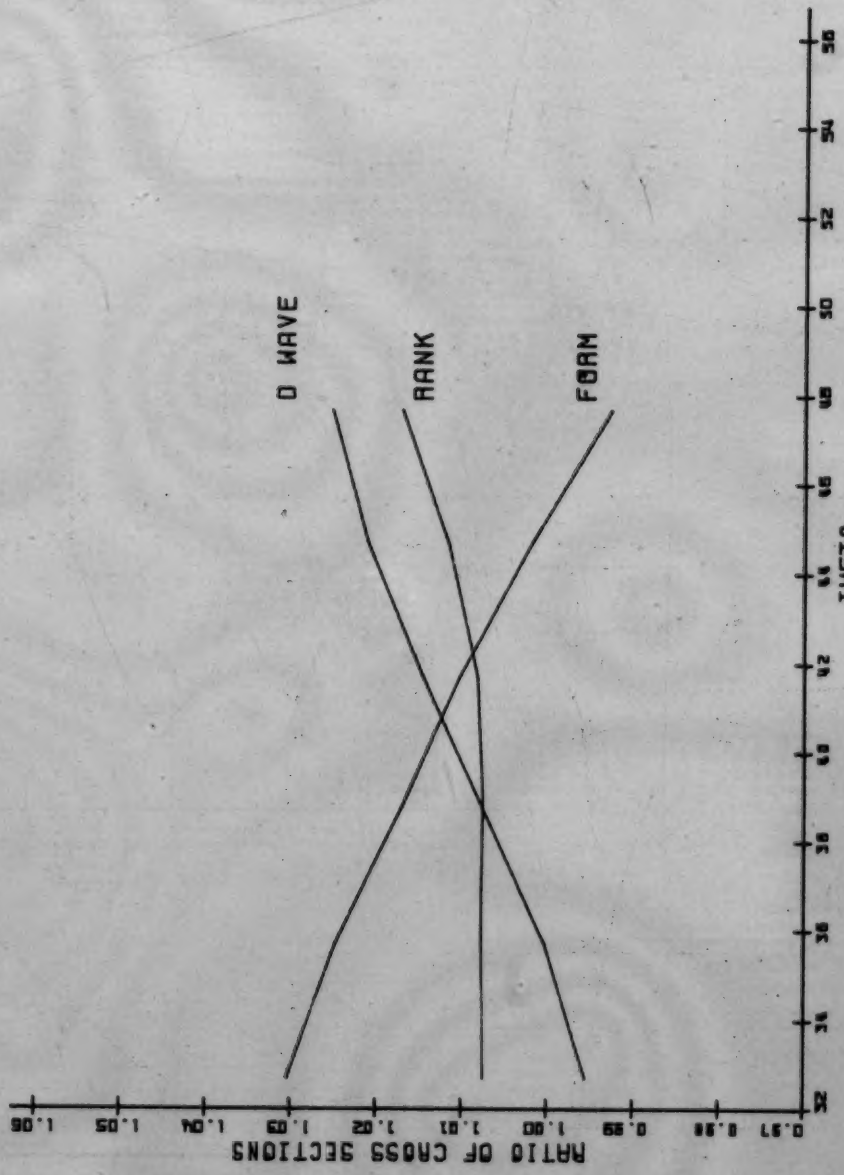

Figure IV.2 Ratios of break-up cross sections vs. polar angle (θ) of outgoing neutrons for symmetric geometry. $\theta_2=\theta_3$, $\phi_2-\phi_3=180^\circ$, $E_2=E_3$. Three-body calculations. See text for details.

minimized.

Sensitivity to r_{nn}, calculated with the 1Y potential, is significantly greater than the above sensitivities and rises steadily with angle (figure IV.3). For the 8.1% change in r_{nn} the change in cross section varies between 6% and 12% over the range of one detector.

Finally, predictions of FSI calculations with the 2R interactions, detailed in our published results (Do82), illuminate the different character of this region and its unsuitability for a measurement of r_{nn}. Both n-n and n-p FSI cross sections show significant sensitivities† to the presence of P and D-wave interactions but not to the tensor force.

---

†up to 30% compared with 1.5% for symmetric QFS

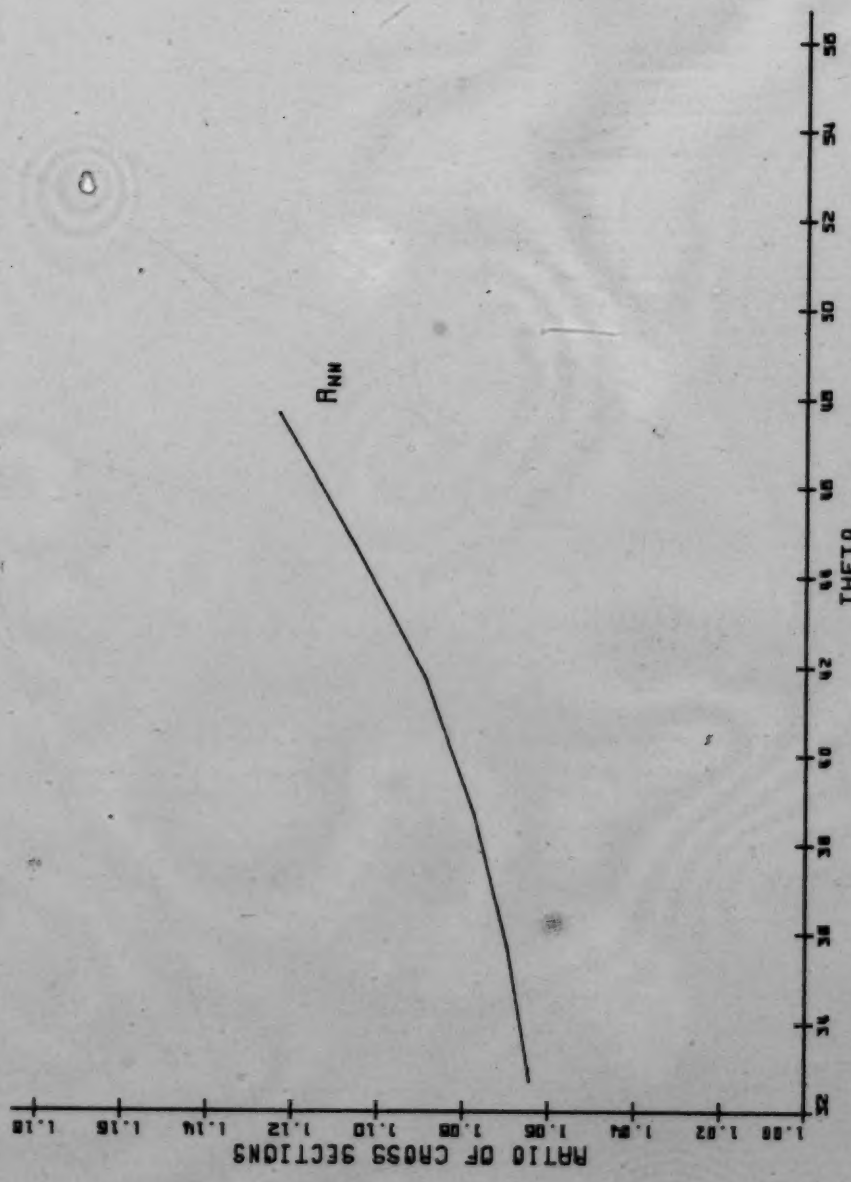

Figure IV.3 Ratio of break-up cross sections for r_{nn}=2.61,2.84*fm* vs. polar angle (θ) of outgoing neutrons for symmetric geometry. $\theta_2=\theta_3$, $\phi_2-\phi_3=180°$, $E_2=E_3$. Three-body calculations. See text for details.

V. CONCLUSIONS

Ideally the presence of experimental and theoretical errors in the determination of some quantity should be reflected in a final numerical uncertainty in that quantity and the experiment should be carried out in such a way as to minimize this uncertainty. While this should be a guiding precept in the present experiment, we see in trying to extract this two-body parameter from its cloak of three-body interactions that the situation is not so clear cut. The experiment, from design through to analysis, must be designed not only around known theory but around sources of theoretical uncertainty as well.

a. Theoretical

Except for a few instances where quantitative evidence was available (see section IV.A), we have assumed there to be no errors in the numerical methods, approximations or other aspects of the actual three-body calculations. While this may not be true, and discrepancies between supposedly similar calculations are routinely reported in the literature, its assessment is certainly beyond the scope of this work. Likewise, (although this point is seldom disputed, Sb82) the entire formulation of three-body interactions is assumed to be correct (i.e. capable in principle of reproducing the experimental data). Consequently the greatest identifyable source of theoretical uncertainty rests with the choice of two-body input to the

problem.

Sensitivity of the break-up cross section to higher (P and D) partial waves in the two-body interaction is smallest at symmetric QFS but still significant at the level of accuracy required in the present case. Their inclusion, therefore, must be viewed as essential, although no error due to their form, etc. is considered.

The effect of the tensor force is similarly small but noticeable. Its inclusion, however, introduces a source of uncertainty due not just to its off-shell behaviour but to a certain ignorance of its correct on-shell behaviour. In the impulse approximation, the break-up cross section is directly proportional to the square of the S-wave component of the deuteron wave function. This quantity in turn depends on (though not necessarily in proportion to) the overall normalization of that component of the wave function. Comparison of the pure S-wave triplet potentials (P_d=0) used in the three-body calculations with the Reid soft-core potential (P_d=6.5%) shows a difference of 1.8% in peak values of the square of the wave function. Aside from the obvious difference between tensor and pure S-wave interactions, the actual amount of D-state attributable to the deuteron wave function is still an open question. It is currently placed at between 4% and 7%, from which we could place an upper limit of 1% on the error from this source.†

---

†The obvious test of this is to perform two calculations differing only in their values of the D-state probability. As this quantity is input directly to the fitting routine, the job would not be difficult (only expensive).

In chapter IV it was stated that symmetric QFS is insensitive to the form of the two-body potential used as long as rank two or higher potentials are used. The first observation regarding this statement is that a survey of two rather similar potentials could hardly be called statistically significant. Nevertheless we have some faith in the complete 2R interaction partly because the 4T (R-type) tensor force succeeds where others have failed (Do74) in reproducing the two-body data. Furthermore it seems natural to use the 2R potential with this tensor force in order that all even partial waves have the same form.

The second observation is that symmetric QFS is probably unconditionally off-shell independent but that reasonable separation of on- and off-shell behaviour can only be achieved with rank two or higher potentials. Evidence for this is seen in appendix C where parameters in the first form factor of rank two S-wave potentials are very close to those of the rank one potentials of the same type, whereas parameters in the second form factor are vastly different. In effect the on- and off-shell properties are concentrated in the first and second form factors respectively. Likewise the tensor potential is constructed, according to the prescription of Ghirardi and Rimini (Gh64), by embodying the deuteron properties in the first pair (S- and D-wave) of form factors.

This places the assertion of von Witsch et al. (Wi80) - that differences among potential forms can lead to

differences of up to 10% in predicted cross sections – in a new context. The calculations cited are based on rank one potentials for which the idea of phase equivalence has limited meaning. Four of the six potentials of Bruinsma et al. (Bn74, Kü75), for instance, were fitted only to the scattering length and effective range. Furthermore the greatest disagreement with the Yamaguchi potential was observed with the "linear" and "quadratic" form factors, rather arbitrary functions which would provide no guarantee of reasonable on-shell behaviour.

The question of rank, or more generally total number of parameters available for fitting, is particularly important in the present case where it is wished to vary r_{nn} without violating unitarity or known on-shell behaviour. The 1Y potential with only two free parameters is capable of reproducing only the scattering length and effective range exactly. If one is changed while the other is held constant the remaining two-body behaviour varies without constraint. If more parameters were present to "take up the slack", r_{nn} could be changed without such undesireable consequences. And if the off-shell behaviour is isolated in a separate form factor it too can remain unaffected by changes in r_{nn}.

One source of error not considered that is well within our grasp stems from the use of p-p phase shifts to generate n-n and n-p interactions. It is worth considering because the very phase shifts that are of interest, those at low energy, are the ones most affected by the Coulomb repulsion.

We do not assign an error to this source but note that the p-p phase shifts could be corrected by established methods (Di81). Assuming the weaker hypothesis of charge symmetry this would produce better n-n interactions at least. The a priori equation of n-n and n-p phase shifts should not prejudice the ultimate test of charge independence available from the experimental value of r_{nn}.

The above constitutes a prescription for accurate three-body calculations along with a feel for the limits of that accuracy. There is no such discussion relevant to the impulse approximation as this method is inherently inexact and has been used for qualitative analysis only.

b. Experimental

The optimum placement of detectors for a determination of r_{nn} from the QFS cross section is guided by a number of experimental and theoretical factors. Assuming fixed azimuthal spacing, proton recoil energy is minimized by centreing detectors at θ=41.7°. Moving outward from this angle increases theoretical sensitivity to r_{nn} and decreases uncertainty due to the form of two-body interaction used. Cross section, however, drops off rather quickly beyond 42° yielding a reduced count rate and less certainty about the theoretical shape of the curve. Detectors with ±6° angular acceptance would incorporate a large chunk of this region if centred at 41.7°.

Aside from considerations of count rate, large changes in cross section as a function of geometry are important in terms of proper normalization of data. To compare experimental points, measured with finite resolutions, to a theoretical differential cross section curve, the latter must be integrated over the appropriate regions of phase space. This demands an accurate knowledge of the theoretical cross section as a function of several parameters. When the cross section is changing rapidly, as with variations in θ, the reliability of such integrals suffers. For this reason, notwithstanding other theoretical arguments to the contrary, it may be better to centre the detectors at some angle less (by a few degrees) than 41.7°. This was done in a recent experiment (Gu80) although no explanation was given.

Experimentally the "differental" cross section can be obtained by dividing the total cross section for a small region of phase space by the volume of that region, effectively identifying the average cross section over the region with the differental cross section at the centroid. For a cross section linear in all variables this procedure introduces no error. In the vicinity of a maximum, however, or any region in which the cross section is concave downwards, such substitution will result in systematic underestimation of the differential cross section. Using the smallest possible region of phase space ($\Delta E_2 = 1 MeV$, $\Delta\phi_2 = \Delta\phi_3 = 3^\circ$, $\Delta\theta_2 = \Delta\theta_3 = 4^\circ$), this effect is estimated at up to 2% in the present experiment. As this has been shown to

translate directly into a comparable error on r_{nn}, we see the importance of comparing apples with apples.

In practice it may only be necessary to integrate over the range of symmetric (equal θ) geometries. The curve can be obtained from a fit to the results of three-body calculations. From figures III.3 and III.5 it appears that changes in the cross section in other directions are less but a firm statement about this must await further three-body calculations.

If the detectors are subdivided three ways in the θ direction, the possibility arises of observing different points on the kinematic locus of QFS. For the correct choices of energy bins, the two most asymmetric angle combinations will be roughly centred on a point along this locus. The remaining symmetric and slightly asymmetric combinations are definitely off this locus but may nonetheless be compared to the appropriate three-body calculations. The large angle symmetric combination will be the least useful due to the aforementioned steep drop in cross section.

Events that are symmetric in ϕ may similarly be used although their enhanced three-body character may cause greater uncertainty due to dependence on off-shell properties of the two-body interaction. The larger number of permutations available in the next-to-symmetric combination (169°) means that count rates at this geometry should be comparable to those at symmetric geometry.

c. Determining effective range

r_{nn} will ultimately be determined using the relationship between r_{nn} and cross section predicted by three-body calculations. Figure V.1 shows four points on this curve, calculated with the 1Y and 2Y potentials.† Fitted to these, by a multiplicative constant only, is the curve predicted by the impulse approximation. As this neglects rescattering effects, it is expected to yield a slightly greater sensitivity of σ to r_{nn}. As can be seen the opposite is found, indicating that the experimental cross section is an even better measure of r_{nn} than simple theory suggests.

In the most exhaustive theoretical treatment allowed by this study, there remain two sources of uncertainty. Discrepancies among cross sections predicted by calculations with differing forms of two-body input are less than 1%. Since only two forms were considered we increase this error estimate to 1.5%. Guided by the impulse approximation, uncertainty due to the disputed deuteron D-state probability is placed at 1%. Assuming these add in quadrature, a "theoretical error" of less than 2% can be claimed.

If a further "experimental error" of 2% is present, we conclude that r_{nn} can be determined from a one point measurement of cross section (at symmetric QFS) with an uncertainty of about 3%. By fitting points from several

---

†For purposes of discussion the differential cross section is used. As discussed above, for actual comparisons this must be integrated over certain directions in phase space.

near-QFS geometries this figure may be reduced even further. If on the other hand experimental error is placed at the otherwise reasonable level of 5%, theoretical error analysis is pointless.

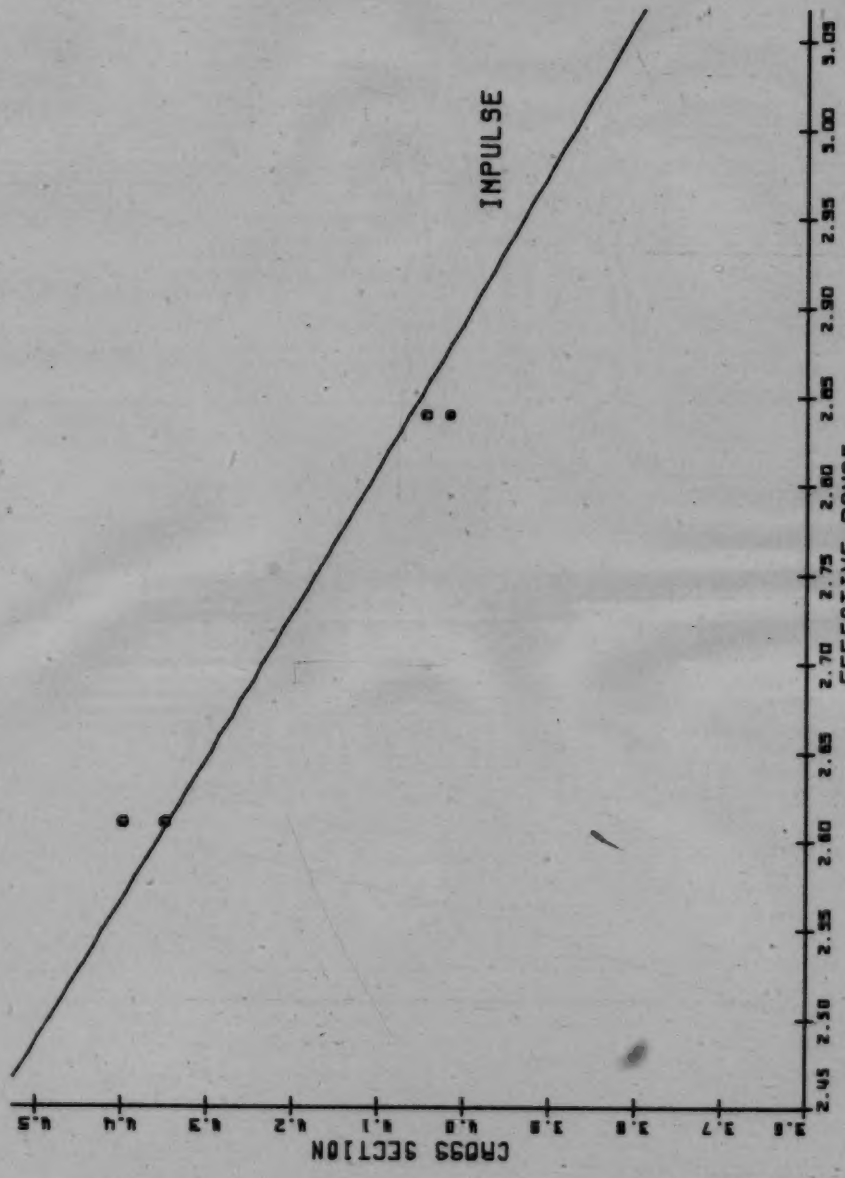

Figure V.1 Theoretical points (from three-body calculations) on the σ vs. r_{nn} curve. Line is predicted by impulse approximation (normalized to the points).

BIBLIOGRAPHY

(Aa65) Aaron, R., R. D. Amado and Y. Y. Yam. Phys. Rev. 140(1965)B1291

(Aa66) Aaron, R. and R. D. Amado. Phys. Rev. 150(1966)857

(Af77) Afnan, I. R. and A. W. Thomas. in *Modern Three-Hadron Physics*. A. W. Thomas ed. Springer-Verlag (1977)

(Ad77) Alder, J. C., W. Dahme, B. Gabioud, W. Hening, C. Joseph, J. G. Loude, N. Morel, H. Panke, A. Perrenoud, J.-P. Perrenoud, D. Reuker, G. Strassner, J. T. Tran, P. Troül, E. Winkelmann and C. Zupančič. Proc. 7th Int. Conf. on high energy physics and nuclear structure, Zurich, 1977. Birkhäuser Verlag (1977)

(Al67) Alt, E. O., P. Grassberger and W. Sandhas. Nucl. Phys. B2(1967)167

(Am69) Amado, R. D. Annual Review of Nuclear Science 19(1969)61

(Ba71) Baker, George A., Jr. and John L. Gammel ed. *The Padé Approximant in Theoretical Physics*. Academic Press (1971)

(Be76) Benayoun, J. J., J. Chauvin, C. Gignoux and A. Laverne. Phys. Rev. Lett. 36(1976)1438

(Bo78) Bovet, E., F. Foroughi and J. Rossel. Nucl. Phys. A304(1978)29

(Br68) Brayshaw, D. D. Phys. Rev. 176(1968)1855

(Br74) Brayshaw, D. D. Phys. Rev. Lett. 32(1974)382

(Br75) Brayshaw, D. D. Phys. Rev. Lett. 34(1975)1478

(Br76) Brayshaw, D. D. Phys. Rev. C13(1976)1024

(Bn74) Bruinsma, J., W. Ebenhöh, J. H. Stuivenberg and R. van Wageningen. Nucl. Phys. A228(1974)52

(Bn77) Bruinsma, J. and R. van Wageningen, Nucl. Phys. A282(1977)1

(Ca71) Cahill, R. T. and I. H. Sloan. Nucl. Phys. A165(1971)161

(Ch48) Chew, Geoffrey F. Phys. Rev. 74(1948)809

(Ch50) Chew, Geoffrey F. Phys. Rev. 80(1950)196

(Ch52) Chew, Geoffrey F. and Gian Carlo Wick. Phys. Rev. 85(1952)636

(Di81) van Dijk, W. University of Alberta (1981) also Y. Nogami and W. van Dijk. McMaster University

(Dd77) Dodd, L. R. in *Modern Three-Hadron Physics*. A. W. Thomas ed. Springer-Verlag (1977)

(Do72) Doleschall, P. Phys. Lett. 40B(1972)443

(Do73) Doleschall, P. Nucl. Phys. A201(1973)264

(Do74) Doleschall, P. Nucl. Phys. A220(1974)491

(Do82) Doleschall, P., J. M. Greben and M. London. Phys. Lett. 112B(1982)303

(Du73) Durand, M. Nucl. Phys. A201(1973)313

(Eb72) Ebenhöh, Wolfgang. Nucl. Phys. A191(1972)97

(Fa60) Faddeev, L. D. JETP 39(1960)1459

(Fa61) Faddeev, L. D. Doklady 6(1961)384

(Fa63) Faddeev, L. D. Doklady 7(1963)600

(Fa65) Faddeev, L. D. *Mathematical Aspects of the Three-Body Problem*. Daniel Davey and Co. (1965)

(Fu57) Fujita, J. and H. Miyazawa. Prog. Theor. Phys. 17(1957)360

(Ga80) Gabioud, B., J.-C. Alder, C. Joseph, J.-F. Loude, N. Morel, A. Perrenoud, J. P. Perrenoud, M. T. Tran, E. Winkelmann, W. Dahme, H. Panke, D. Renker, Č. Zupančič, G. Strassner and P. Truöl. Ninth International Conference on the Few Body Problem, Eugene (1980)

(Gh64) Ghirardi, G. C. and A. Rimini. J. Math. Phys. 5(1964)722

(Gr70) Gross, E. E., E. V. Hungerford, J. J. Malanify and R. W. Woods Phys. Rev. C1(1970)1365

(Gu80) Guratzsch, H., B. Kühn, H. Kumpf, J. Mösner, W. Neubert, W. Pilz, G. Schmidt and S. Tesch. Nucl. Phys. A342(1980)239

(Ha71) Haftel, Michael I. and Frank Tabakin. Phys. Rev. C3(1971)921

(Ha73) Haftel, Michael I. Phys. Rev. C7(1973)80

(Ha74) Haftel, Michael I. Phys. Rev. Lett. 33(1974)1229

(Ha75) Haftel, Michael I. Phys. Rev. Lett. 34(1975)1480

(Ha76) Haftel, Michael I., E. L. Petersen and J. M. Wallace. Phys. Rev. C14(1976)419

(Hr72) Harper, E. P., Y. E. Kim and A. Tubis. Phys. Rev. C6(1972)1601

(Hl64) Heller, L., P. Signell and N. R. Yoder. Phys. Rev. Lett. 13(1964)557

(He65) Hetherington, J. H. and L. H. Schick. Phys. Rev. 137B(1965)935

(Ho75) Holinde, K. and R. Machleidt. Nucl. Phys. A256(1975)479

(Ja75) Jackson, J. D. *Classical Electrodynamics*. Wiley (1975)

(Kc75) Kecskemeti, T. Czibok and B. Zeitnitz. Nucl. Phys. A254(1975)110

(Ki74) Kim, Y. E. and A. Tubis. Annual Review of Nuclear Science 24(1974)69

(Kl71) Kloet, W. M. and J. A. Tjon. Phys. Lett. 37B(1971)460

(Ke78) Koersner, I., L. Glantz, A. Johansson, B. Sundqvist and P. Doleschall. Uppsala Tandem Accelerator Lab Report TLU 61/78(1978)

(Ko65) Kottler, H. and K. L. Kowalski. Phys. Rev. 138(1965)B619

(Kr78) Kreyszig, Erwin. *Introductory Functional Analysis with Applications*. Wiley (1978)

(Kü75) Kühn, B., H. Kumpf, J. Mösner, W. Neubert and G. Schmidt. Nucl. Phys. A247(1975)21

(Ku81) Kulkarni, J., J. Rapaport, R. W. Findlay, G. Randers-Pehrson and R. D. Koshel. Nucl. Phys. A367(1981)157

(La80) Lacombe, M., B. Loiseau, J. M. Richard, R. Vinh Mau,

J. Côté, P. Pirès and R. de Tourreil. Phys. Rev. C21(1980)861

(Lo64) Lovelace, C. Phys. Rev. B135(1964)1225

(Md64) MacDonald, J. R. J. Appl. Phys. 35(1964)3034

(Mg69) MacGregor, Malcolm H., Richard A. Arndt and Robert M. Wright. Phys. Rev. 182(1969)1714

(Ml69a)Malfliet, R. A. and J. A. Tjon. Nucl. Phys. A127(1969)161

(Ml69b)Malfliet, R. A. and J. A. Tjon. Phys. Lett. 29B(1969)391

(Ml70) Malfliet, R. A. Ph.D. thesis. University of Utrecht (1970)

(Ml71) Malfliet, R. A. and J. A. Tjon. Ann. of Phys. 61(1971)425

(Ma64) Mathews, Jon and R. L. Walker. *Mathematical Methods of Physics*. Benjamin (1964)

(Mk76) McKellar, B. H. J. in *Few-Body Dynamics* A. N. Mitra, I. Šlaus, V. S. Bhasin and V. K. Gupta ed. North-Holland (1976)

(No64) Noyes, H. P. Stanford University report SLAC-PUB-59 (1964)

(No71) Noyes, H. P. and H. M. Lipinski. Phys. Rev. C4(1971)995

(Os67) Osborn, T. A. SLAC Report 79(1967)

(Os71) Osborn, T. A. and K. L. Kowalski. Ann. of Phys. 68(1971)361

(Pi72) Pieper, S. C. Nucl. Phys. A193(1972)529

(Ph66a)Phillips, A. C. Phys. Lett. 20(1966)50

(Ph66b)Phillips, A. C. Phys. Rev. 142(1966)984

(Ph66c)Phillips, A. C. Phys. Rev. 145(1966)733

(Ph68) Phillips, A. C. Nucl. Phys. A107(1968)209

(Re68) Reid, Roderick V., Jr. Ann. of Phys. 50(1968)411

(Ro67) Rodberg, Leonard S. and Roy M. Thaler. *The Quantum Theory of Scattering*. Academic Press (1967)

(Sa67) Sandhas, W. Nucl. Phys. B2(1967)167

(Sa72) Sandhas, W. Acta Phys. Aus. supp.IX(1972)57

(Sa74) Sandhas, W. Acta Phys. Aus. supp.XIII(1974)679

(Sr77) Sauer, P. U. and H. Walliser. J. Phys. G3(1977)1513

(Sh73) Schaposnik, F. A. and H. J. de Vega. Nuovo Cimento 13A(1973)923

(Sc74) Schmid, Erich W. and Horst Ziegelmann. *The Quantum Mechanical Three-Body Problem.* Vieweg (1974)

(Ss71) Šlaus, I., J. W. Sunier, G. Thompson, J. C. Young, J. W. Verba, D. J. Margaziotis, P. Doherty and R. T. Cahill. Phys. Rev. Lett. 26(1971)789

(Ss78) Šlaus, I. in Proc. Int. Conf. on nuclear structure, J. Phys. Soc. Japan 44(1978)supp. p. 57

(Ss82) Šlaus, I., Y. Akaishi and H. Tanaka. Phys. Rev. Lett. 48(1982)993

(Sl69) Sloan, Ian H. Phys. Rev. 185(1969)1361

(Sb70) Slobodrian, R. J., H. Meiner, J. Ernst, J. S. C. McKee, H. E. Conzett, A. D. Bacher and F. G. Resmini. in *The Three-Body Problem in Nuclear and Particle Physics.* J. S. C. McKee and P. M. Rolph ed. North-Holland (1970)

(Sb81) Slobodrian, R. J. and P. Doleschall. Phys. Lett. 101B(1981)1

(Sb82) Slobodrian, R. J. Phys. Rev. Lett. 49(1982)300

(So71) Sohre, F. and H. Ziegelmann. Phys. Lett. 34B(1971)579

(Su77) Soukup, J. Ph.D. Thesis. University of Alberta

(Su79) Soukup, J., J. M. Cameron, H. W. Fielding, A. H. Hussein, S. T. Lam and G. C Neilson. Nucl. Phys. A322(1979)109

(Sp81) Sperisen, F., W. Grüebler, V. König, P. A. Schmelzbach, B. Jenny, K. Elsener, C. Schweizer, J. Ulbricht, and P. Doleschall. Phys. Lett. 102B(1981)9

(Sk75) Stolk, C. and J. A. Tjon. Phys. Rev. Lett. 35(1975)9859

(St76) Stuivenberg, J. H. Ph.D. Thesis. Vrije Universiteit

(1976)

(St78) Stuivenberg, J. H. and R. van Wageningen. Nucl. Phys. A304(1978)141

(Tb64) Tabakin, F. Ann. of Phys. 30(1964)51

(Ta72) Taylor, John R. *Scattering Theory*. Wiley (1972)

(Th81) Thomas, A. W. seminar notes. University of Alberta (1981)

(To73) de Tourreil, R. and D. W. L. Sprung. Nucl. Phys. A201(1973)193

(Vi67) Villars, F. *Collision Theory*. in *Fundamentals in Nuclear Theory*. International Atomic Energy Agency (1967)

(Wa67) Watson, K. M. and J. Nuttall. *Topics in Several Particle Dynamics*. Holden-Day (1967)

(We63) Weinberg, Steven. Phys. Rev. 131(1963)440

(We64) Weinberg, Steven. Phys. Rev. B133(1964)232

(Wi79) von Witsch, W., B. Gomez Moreno, W. Rosenstock, K. Ettling and J. Bruinsma. Nucl. Phys. A329(1979)141

(Wi80) von Witsch, W., B. Gomez Moreno, W. Rosenstock, R. Franke and B. Steinheuer. Nucl. Phys. A346(1980)117

(Ya54a) Yamaguchi, Yoshio. Phys. Rev. 95(1954)1628

(Ya54b) Yamaguchi, Yoshio and Yoriko Yamaguchi. Phys. Rev. 95(1954)1635

(Ze74) Zeitnitz, B. R. Maschuw, P. Suhr, W. Ebenhöh, J. Bruinsma and J. H. Stuivenberg. Nucl. Phys. A321(1974)13

(Zi69) Ziman, J. M. *Elements of Advanced Quantum Theory*. Cambridge University Press (1969)

APPENDIX A KINEMATICS

The n-D break-up reaction, whether described by the impulse approximation or three-body methods, is governed by overall conservation of momentum and energy. Referring to figure III.1, for a neutron incident along the z axis momentum conservation yields three equations

$$q_1' = q_1\cos\theta_1 + q_2\cos\theta_2 + q_3\cos\theta_3 \qquad \text{A.1}$$
$$0 = q_1\sin\theta_1\cos\phi_1 + q_2\sin\theta_2\cos\phi_2 + q_3\sin\theta_3\cos\phi_3$$
$$0 = q_1\sin\theta_1\sin\phi_1 + q_2\sin\theta_2\sin\phi_2 + q_3\sin\theta_3\sin\phi_3 .$$

Energy conservation must include the binding energy of the deuteron ($E_d = 2.225 MeV$) which is absorbed in the break-up:

$$q_1'^2 - E_d = q_1^2 + q_2^2 + q_3^2 . \qquad \text{A.2}$$

The factor $\hbar^2/(2m)$, which relates the energy of a free particle to its wave vector (or momentum expressed in fm) has been omitted. For purposes of these calculations, where the free momentum of a particle is seldom needed, the q's are most conveniently expressed in units of $Mev^{1/2}$ thereby avoiding this factor.

To use the effective range expanded t-matrix (in the impulse approximation), one must compute relative neutron energies. The usual definitions of relative momentum κ and reduced mass μ

$$\bar{\kappa}=(\bar{k}_1-\bar{k}_2)/2 \qquad \mu=m_1m_2/(m_1+m_2)=m/2\dagger \qquad \text{A.3}$$

yield a relative energy

$$E=\hbar^2\kappa^2/2\mu=(\hbar^2/2m)|\bar{k}_1-\bar{k}_2|^2/2 \qquad \text{A.4}$$

In our chosen units, therefore, we have for the relative outgoing neutron energy (in *MeV*)

$$E(on)=|\bar{q}_2-\bar{q}_3|^2/2 \qquad \text{A.5}$$

and similarly

$$E(off)=|\bar{q}_2'+\bar{q}_1|^2/2. \qquad \text{A.6}$$

To express these in fm^{-2} for use with the conventional effective range expansion we need the factor $\hbar^2/m$ $=41.47 MeV fm^2$.

For a fixed incident neutron energy, equations A.1 and A.2 constitute a system of four equations in nine unknowns; hence the expression of the differential cross section as a function of five variables, usually the two outgoing neutron solid angles and one neutron energy. Choosing, as is done in the experiment, the outgoing neutron angles leaves but one free variable which is often chosen to be the arc length along the curve of possible neutron energy pairs (the

---

†We assume a uniform nucleon mass of 939*MeV*.

kinematic curve or *locus*). Differential cross section is frequently described in terms of this energy variable (*arc length projection*). Selecting a point on the kinematic curve, by measuring neutron energies, leaves no free variables and hence a results in a *kinematically complete* experiment. Choosing, instead, the conditions of QFS yields a different locus which defines pairs of outgoing neutron polar angles and energies. As to the azimuthal angles, the requirement of zero proton recoil fixes their difference at 180° (coplanar geometry) and the azimuthal symmetry of the problem makes their sum irrelevant.

The kinematic factor used in the impulse approximation (equation III.7) comes from an integration over the final state (outgoing) phase space. Following Taylor (Ta72 p.348) and recalling that in our units free momentum is expressed as $\sqrt{2m}q$, we begin with the general result (in the laboratory frame)

$$\sigma(\bar{q}_2,\bar{q}_3,p \leftarrow \bar{q}_1',D)= \qquad \text{A.7}$$
$$(2\pi)^4(\sqrt{2m})^7/2q_1' \int d\Omega_2 q_2^2 dq_2 d\Omega_3 q_3^2 dq_3 \delta(E_1'-E_d-E_2-E_3)|t|^2$$

where D indicates the deuteron target, p indicates the proton at rest in the final state (under the assumption of zero proton recoil), E' and E are the initial and final state energies:

$$E'=E_2'-E_d \qquad E=E_1+E_2+E_3. \qquad \text{A.8}$$

For purposes of the integration the t-matrix is assumed constant. Using $E=q^2$, $dE=2qdq$ and dividing by the appropriate differential phase space volume

$$d\sigma/d\Omega_2 d\Omega_3 dE_2= \qquad \text{A.9}$$
$$(2\pi)^4(\sqrt{2m})^7/2q_2' \ (q_2/2)\int(q_3/2)dE_3\delta(E_2'-E_d-E_2-E_3)|t|^2.$$

The remaining integral serves only to determine the second outgoing neutron energy q_2, which is uniquely defined by the chosen conditions. Consequently,

$$d\sigma/d\Omega_2 d\Omega_3 dE_2=(2\pi)^4\sqrt{2}(\sqrt{m})^7(q_2q_3/q_2')|t|^2. \qquad \text{A.10}$$

APPENDIX B DOCODE MANUAL

a. General Features

The program analyzes a given three-body reaction using the AGS form of the Faddeev equations. The two-body partial wave potentials must be separable

$$V(p,p')=\Sigma_{\gamma,z} g_\gamma(p)\lambda_{\gamma,z} g_z(p') \qquad \text{B.1}$$

where summation is up to the rank of the potential. The form factor, g, has either the generalized Yamaguchi (or Y-type) form

$$g^k(p)=[p^k\Sigma_{i=0}^{m}\gamma_i p^{2i}]/[\Pi_{i=0}^{k}(1+\beta_i p^2)] \qquad \text{B.2}$$

or the so-called R-type form

$$g^k(p)=[p^k/(1+\beta p^2)^k]\Sigma_{i=1}^{m}[\gamma_i/(1+\beta p^2)^i] \qquad \text{B.3}$$

where k is the angular momentum. The latter type has been recently suggested by Doleschall as it provides a good fit to experimental data including nodes in the $^1S_0$, $^3S_1$ and $^3P_0$ phase shifts. For this form, Doleschall finds m=5 to be adequate in the three-nucleon calculation. Given the quantum numbers of the interacting particles and the geometry of the reaction, the program can produce cross sections and polarizations for elastic scattering and three particle

breakup. The program can also be used just to generate kinematics. Results are available in both the laboratory and c.m. frames.

A complete source listing is contained in the file DOCODE. An index to the programs and subprograms in this listing is provided at the end of this manual. Main program names carry the prefix PR.

b. Outline

The calculation is distributed among various main programs which are run in the sequence indicated in figure B.1. Global communications is carried out via sequential files assigned to I/O data sets 1 and 2. These are referred to as files 1 and 2. In addition, certain other files, described below, must be preserved between steps of the calculation.

The GAUS program reads Gaussian mesh points from data set 2 (data file GAQUAD, included in the program package) and prepares file 1 for use by the Gaussian quadrature routine. Since this task is independent of the specific problem being programmed, it need be run only once for the implementation of this calculation on a particular computer. GAUS must be compiled under *FORTX.

The normal starting point of the calculation is QUAD. It separates the kernels into singular and non-singular parts and performs a special Gaussian quadrature for the singular part. Mesh points for this quadrature are created

here and written into file 1.

KERE deals with two-body interactions. Using the parameters of the two-body form factors it calculates two-body propagators and t-matrices. These are placed in file 2 for future use.

The pair of programs, FAMA and PADE, must be run once for each combination of total three-body angular momentum and parity. FAMA calculates the kernel of the (reduced) integral equation using the special quadrature performed by QUAD and the mesh points for the regular quadrature, also supplied by QUAD. PADE solves the resulting set of algebraic equations using the Padé approximant technique. The three-body T-matrices thus obtained are placed in file 2 for unlimited use by the following two programs. PADD is a double precision version of PADE.

ELAS computes elastic scattering cross sections and polarizations with or without the inclusion of Rutherford scattering. BRUP computes breakup cross sections and polarizations for a given geometry. QFS and FSI geometries can be specifically selected.

Finally, there is an auxilliary program, FITI, which takes experimental two-body data and produces, by a simple search technique, the parameters of the two-body interactions in the form required by KERE. As this program does not communicate directly with KERE via the global files 1 and 2, the results of a FITI run must be transferred manually to KERE. FITI does, however, retain results on data

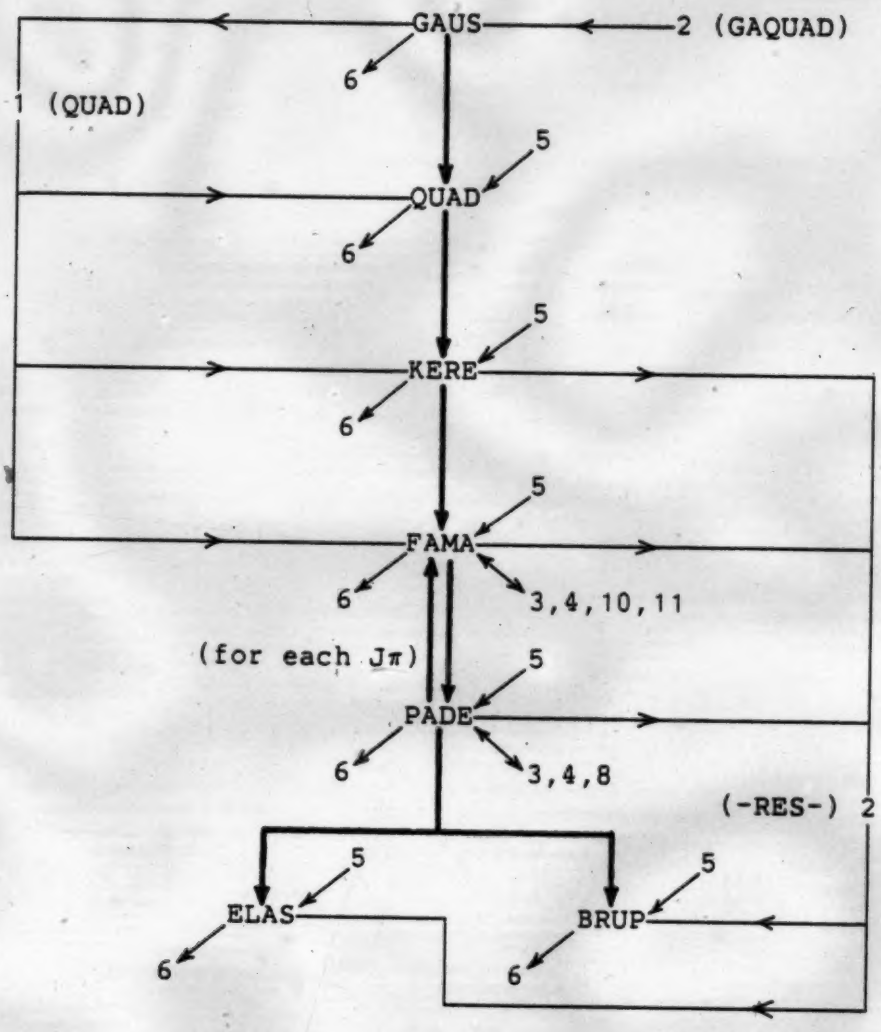

Figure B.1 DOCODE consists of several main programs which are run in the sequence indicated by the heavy lines. Programs communicate with each other via data sets 1 and 2. Other data sets are used for program control (5), diagnostics/results (6) and storing intermediate results.

set 2 for its own use and can be run repeatedly until the desired covergence in the search routine is achieved.

The bulk of the execution of each main program is carried out in a subroutine which has the name of the main program prefixed by DO (e.g. DOGAUS, DOQUAD, etc.) The main programs are used to read the TEST array and to initialize various parameters. Since some of these will change according to the problem being considered or (in the case of FAMA and PADE) the particular step in the calculation, editing and recompilation of main programs will frequently be necessary. This is the reason for divorcing the main body of the calculation from the main programs.

Many of the variables assigned in the main programs are checked, during the calculation, for consistency among themselves and with the input data. These variables are listed here along with the explanation of the input. If an error is found the program signals (via the output file), providing the required value of the variable, and stops. Thus, when in doubt, a quick run of the program is sufficient to establish the value of any such parameter.

Subroutine HIBA is the universal error flagging routine. It prints an error code number on the output file and stops the calculation. The error code for an incorrect parameter as above is zero.

The complete program package contains a number of main programs and subroutines which are not needed for our purposes. Questions about these and about the package in

general should be directed to its author:

Dr. P. Doleschall
Central Research Institute for Physics
H-1525 Budapest
Box 49
Hungary

J. Svenne at the University of Manitoba also has a good understanding of the program, although his version is not as recent as the one described here.

c. Input

Input data are listed here for each program, with brief explanations following. Each line of the form

VARIABLE LIST (FORMAT)

represents one line or card of input. The format is given in FORTRAN. Repeated lines are indented, with the incremented index variable given in FORTRAN DO-loop style.

The TEST array is used to choose various program options. Each element must be given the value 0 or 1.

The FORTRAN data set reference number for input is 5. Output is produced on data set 6.

Main Program PRGAUS

The only input to PRGUAS is fixed and contained in file GAQUAD, which must be assigned to data set 2.

Main Program PRQUAD

```
TEST                                                    (3(I1,2X))
(MASS(I),I=1,3)                                       (6(1PE11.4,2X))
(SPIN(I),I=1,3)                                        (17(I2,2X),I2)
(CHARGE(I),I=1,3)                                      (17(I2,2X),I2)
repeat for J=1,NTC
   (TWQ(I,J),I=1,DTWQ)                                 (17(I2,2X),I2)
(if TEST1=0) SYM,LLMAX,N1,M2,NG1,NG2,NG3,K,L,TLMM,TC1,TC2
                    (4(I2,2X),3(I3,2X),3(I2,2X),2(F6.4,2X))
(if TEST1=1) LLMAX,N1,M2,NG1,NG2,NG3      (3(I2,2X),3(I3,2X))
```

TEST(1)=1 ONLY LLMAX,N1,N1,NQ,NS MUST BE READ.
TEST(2)=1 THE WEIGHTS OF SPECIAL QUADRATURES ARE WRITTEN ON THE LINEPRINTER.
TEST(3)=1 THE INTEGRALS ARE WRITTEN OUT.

NTC total number of two-body channels, taking into account the ranks of the separable potentials (number of TWQ cards or lines)

TWQ two-body quantum numbers
- TWQ(1,J) specifies interacting pair
- TWQ(2,J) number of form factor in the separable expansion (0 for a rank one interaction, 1,...,N for a rank N interaction)
- TWQ(3,J) angular momentum of pair (X2)
- TWQ(4,J) parity of pair wavefunction
- TWQ(5,J) number of L,S pairs
- TWQ(6,J),TWQ(7,J)=L,S (X2)
- TWQ(8,J),TWQ(9,J) second L,S pair (-1 if none)

If there are identical particles, identical interactions need not be duplicated in TWQ; the program will generate these.

SYM=-1 for identical fermions
1 for identical bosons
0 for distinct particles

LLMAX=max[L of pair]+[l of pair relative to third particle]

N1 number of Gaussian mesh points for P,D waves (6 for three nucleons)

M2 number of Gaussian mesh points for S waves (9 for three nucleons)

$N1 \leq M2$

If numbers are chosen which produce disallowed mesh points DSQ is printed and the program stops.

NG1-3,K,L number of mesh points

TLMM average of two largest L's

TC1,TC2 specify a transformation on the mesh points to smooth out branch points in the T matrix

$$y=\left(1-\left(\frac{1-x}{2}\right)^{1+TC1}\right)^{\frac{1}{1+TC2}}$$

```
Internally checked variables
WSD1
WSD2
N2
NTC    number of two-body channels (rows in TWQ)
DTWQ   number of columns in TWQ (=9)
TLMM   average of two largest L's


Main Program PRKERE

TEST                                                    (3(I1,2X))
(if TEST1=0) NFE1,NFE2                                  (2(I2,2X))
(if TEST1=1 or TEST2=1) TC3,TC4,M                    (2(F3.1,2X),I2)
                        (EBO(I),I=1,NTC)             (6(1PE11.4,2X))
repeat for I=1,NTC
   (CIPA(J,I),J=1,2)                                    (2(I3,2X))
   repeat for J=1,TWQ(5,I)
      (BETA(K,J,I),K=1,L)                            (5(E13.6,2X))
      (GAMMA(K,J,I),K=1,N2)                          (5(E13.6,2X))
   (LAMBDA(J,I),J=1,N1)                              (5(E13.6,2X))
(EINF(I),I=1,7)          (F4.1,2X,E13.6,2X,4(F4.1,2X),F5.1)
(LIM(3,I),I=1,NTC)                                   (6(E11.4,2X))
(NF(I),I=1,NTC)                                     (17(I2,2X),I2)


TEST(1)=1   THE FILE CH2 IS EMPTY AND THE TWO-BODY AND
            ENERGY DEPENDENT PARAMETERS MUST BE READ,
            OTHERWISE THE  NFE1,NFE2 PARAMETERS MUST BE
            READ AND THE NEW INFORMATION IS WRITTEN
            AFTER THE NFE1,NFE2 POSITION.
TEST(2)=1   NEW TWO-BODY AND ENERGY DEPENDENT PARAMETERS,
            OTHERWISE ONLY THE ENERGY DEPENDENT PARAMETERS
            MUST BE READ
TEST(3)=1   THE FORM FACTORS AND THE CFF COEFFICIENT WILL
            BE WRITTEN ON THE LINEPRINTER.

NFE1,NFE2 not generally used, see TEST(1)
TC3,TC4 are like TC1,TC2
M
EBO(J) bound state energy corresponding to interaction J
       (line J of TWQ))
     <0 if unbound
The target must be bound: EBO(EINF(1))>0
CIPA coulomb interaction parameters
   CIPA(1,I)=0 (coulomb option does not work)
   CIPA(2,I)=m where m>0 specifies a generalized Yamaguchi
             form factor
```

$$g^k(p)=[p^k\Sigma_{i=0}^{m}\gamma_i p^{2i}]/[\Pi_{i=0}^{k}(1+\beta_i p^2)]$$

and m<0 specifies an R-type form factor

$$g^k(p)=[p^k/(1+\beta p^2)^k]\Sigma^{-m}_{i=1}[\gamma_i/(1+\beta p^2)^i]$$

BETA,GAMMA parameters of the form factors, in the same order as TWQ
ℓ=TWQ(4+2J,I)
L=$\ell/2$+m+1 if m≥0
L=1 if m<0
N2=m+1 if m≥0
=-m if m<0
LAMBDA strength of the potential
N1=DIM(I)
EINF energy information
EINF(1) line in TWQ of incident channel
EINF(2) three-body c.m. energy
=[m(target)/m(total)]E(lab)-E(binding)
EINF(3)=N1 maximum number of special mesh points (from QUAD)
EINF(4)=N2 even number (The principal value integral requires an even number of points around the singularity)
EINF(5)=N3
EINF(6)=N4
EINF(7)=NFP
LIM(3,I)=0 if third momentum interval extends to infinity
NF(I)=6 or 9
number of special mesh points in first interval for each two-body channel
The NF(I) can not all be the same unless QUAD uses identical quantities (program bug).

Internally checked variables
NTC number of two-body channels (rows in TWQ)
DTWQ number of columns in TWQ (=9)
NLS number of L-S pairs
CCN number of coupled channels
NG
BD1 maximum number of β's in any interaction
GD1 maximum number of γ's in any interaction
NFP size of breakup propagator matrix

Main Program PRFAMA

```
TEST                                                    (7(I1,2X))
NG,JT,PAR                                               (3(I2,2X))
(if TEST3=1) (FFIND(I),I=1,NTC)                        (17(I2,2X),I2)
```

TEST(1)=1 THE SUBMATRICES AND THE INHOMOGENEOUS TERM IS PRINTED.

TEST(2)=1 THE COULOMB DISTORTED SUBMATRICES ARE NOT MULTIPLIED BY THE CHANNEL COULOMB PENETRATION FACTOR, OTHERWISE THEY ARE MULTIPLIED FROM LEFT.

TEST(3)=1 THE INTEGER ARRAY FFIND(NTC) MUST BE READ. THE FFIND(I)=-2 ROWS AND COLUMNS AND THE FFIND(I)=-1 ROWS ARE NOT CALCULATED. FROM FFIND(J)=-1 COLUMNS ONLY THE ON-SHELL ELEMENTS OF THE FFIND(I)=2 ROWS ARE CALCULATED. THE I,J SUBMATRICES WITH FFIND(I).GE.1 AND FFIND(J).GE.1 OR WITH FFIND(I)=2 AND FFIND(J)=0 OR WITH THE REVERSE ARE CALCULATED.

TEST(4)=1 ONLY THE ONE-STEP ITERATION IS CALCULATED.

TEST(5)=1 TWO PARALLEL CALCULATIONS ARE PERFORMED THE FIRST WITH THE COULOMB DISTORTION, THE SECOND WITHOUT THE COULOMB DISTORTION.

TEST(6)=1 THE TABULATED FORM FACTORS ARE USED.

TEST(7)=1 THE EARLIER INTERRUPTED CALCULATION WILL BE CONTINUED (IN THIS CASE THE DATA SETS 3 AND 8 MUST BE CATALOGED).

NG number of Gaussian mesh points
JT total three-body angular momentum (X2)
PAR total three-body parity
FFIND(I) weighting of interaction I

Internally checked variables

NTC number of two-body channels (rows in TWQ)
DTWQ number of columns in TWQ (=9)
NLS number of L,S pairs
CCN number of coupled channels
BD1 maximum number of β's in any interaction
GD1 maximum number of γ's in any interaction
NA1
N1 =EINF(3)
N2 =EINF(4)
N3 =EINF(5)
N4 =EINF(6)
NT =N1+N2+N3+N4+1
NFP size of break-up propagator matrix
put=1 if no break-up calculations are to be made
WSD1
WSD2
NCH number of three-body channels (rows in THQ)
FCD2
DM dimension of kernel
EQN number of three-body channels compatible with incident channel
NA number of open outgoing channels
ROD1
ROD2

If necessary, make a short run to establish NCH,
a second run to establish DM, EQN and NA.

Main Programs PRPADE, PRPADD

```
TEST                                                    (7(I1,2X))
I,TOL                                                  (I3,2X,E7.1)
(if TEST2=1) FIDI                                          (I2)
repeat for J=1,FIDI
   (TOFI(I,J),I=1,NTC)                                (17(I2,2X),I2)
```

```
TEST(1)=1   THE RESULTS ARE PUNCHED.
TEST(2)=1   THE INTEGER FIDI AND THE INTEGER ARRAY
            TOFI(NTC,FIDI) MUST BE READ AND FIDI NUMBER OF
            CALCULATIONS WILL BE PERFORMED WITH
            (AFFIN(I)=TOFI(I,J),I=1,NTC),J=1,FIDI.
TEST(3)=1   THE FULL SOLUTION WILL BE CALCULATED.
TEST(4)=1   THE OFF-SHELL T-MATRIX ELEMENTS
            FOR THE BREAK-UP ARE CALCULATED.
TEST(5)=1   TWO PARALLEL CALCULATIONS WILL BE PERFORMED
            THE FIRST WITH THE COULOMB DISTORTION,
            THE SECOND WITHOUT THE COULOMB DISTORTION.
TEST(6)=1   THE CONVERGENCE WILL BE CHECKED ONLY ONCE.
TEST(7)=1   THE BREAK-UP TMATRICES ARE NOT PRINTED.

I maximum number of iterations of Padé approximation
 =odd number
TOL tolerance of approximation
    condition is 2[P(n,n)-P(n+1,n+1)]<TOL[P(n,n)+P(n+1,n+1)]
For three nucleons the approximation should converge in 24
iterations.
FIDI number of different calculations to be performed (with
     different potential weightings)
TOFI(I,J)=FFIND(I) for the Jth calculation

Internally checked variables
ITM  =I
NTC   number of two-body channels (rows in TWQ)
FIDI  see above
NT
BP2
DI1
N1
EQN   number of three-body channels compatible with incident
      channel
NCH   number of three-body channels (rows in THQ)
NA    number of open outgoing channels
DM    dimension of kernel
BR2
BR3
CDM
```

```
CEQN
SDM
SEQN
BP3
```

Main Program PRELAS

```
TEST                                                    (6(I1,2X))
NFE1,NFE2                                               (2(I2,2X))
LINM,LFIM,NRM                                           (3(I2,2X))
(if TEST3=1) I                                             (I3)
             (TIND(I),I=1,TDIM)                    (17(I2,2X),I2)
(CHARGE(I),I=1,3)                                  (17(I2,2X),I2)
```

```
TEST(1)=1   THE DIFFERENTIAL CROSS SECTIONS AND THE
            POLARIZATIONS ARE CALCULATED.
TEST(2)=1   THE NFE1,NFE2 SET IS CALCULATED, OTHERWISE
            THE LAST SET.
TEST(3)=1   ONLY A CERTAIN SET OF T-MATRICES IS INCLUDED
            (TDIM AND TIND(TDIM) MUST BE GIVEN), OTHERWISE
            ALL DIFFERENT T-MATRICES ARE INCLUDED (THE FIRST
            OF THE T-MATRICES WITH IDENTICAL QUANTUM
            NUMBERS).
TEST(4)=1   THE T-MATRICES ARE NOT PRINTED.
TEST(5)=1   NEW CHARGES MUST BE READ AND THE RUTHERFORD
            IS ADDED ACCORDING TO THE NEW CHARGES.
TEST(6)=1   THE ELASTIC OFF-DIAGONAL T-MATRICES ARE
            SYMMETRIZED.

NFE1,NFE2=1 usually, see TEST(2)
LINM≥maximum value of initial orbital angular momentum
      of projectile with respect to target
LFIM≥maximum value of final orbital angular momentum
      of projectile with respect to target
LRM number of points from zero  at which the Rutherford
    cross section is to be excluded
I=TDIM number of matrices used
TIND(I) indicies of matrices used (matrices are indexed
        in the order that they are calculated by PADE)
CHARGE(I)

Internally checked variables
NTM
TDIM  number of matrices used
NTC   number of two-body channels (rows in TWQ).
DTWQ  number of columns in TWQ (=9)
NLS   number of L,S pairs
CCN   number of coupled channels
BD1   maximum number of β's in any interaction
GD1   maximum number of γ's in any interaction
EQNM
```

NCHM
NAM

Main Program PRBRUP

```
TEST                                                    (10(I1,2X))
CSPR,POPR                                                (2(I2,2X))
NFE1,NFE2                                                (2(I2,2X))
LINM,LFIM,SIG                                            (3(I2,2X))
MA,NX,MJP,MLP,MPA                                        (5(I2,2X))
(if TEST3=1) TDIM                                              (I3)
             (TIND(I),I=1,TDIM)                    (17(I2,2X),I2)
(if TEST8=1) repeat for J=1,MA
                (SFKV(I,J),I=1,4)                  (6(1PE11.4,2X))
(if TEST6=0) repeat for J=1,MA
                (ANGLES(I,J),I=1,4)                (6(1PE11.4,2X))
(if TEST6=1 and TEST8=0) (PAA(I),I=1,NX)           (6(1PE11.4,2X))
                         repeat for J=1,MA
                          (ANGLES(I,J),I=1,4)(6(1PE11.4,2X))
```

TEST(1)=1 THE POLARIZATIONS ARE CALCULATED
TEST(2)=1 THE NFE1,NFE2 SET IS CALCULATED, OTHERWISE THE LAST SET.
TEST(3)=1 ONLY A CERTAIN SET OF T-MATRICES IS INCLUDED (TDIM AND TIND(TDIM) MUST BE GIVEN), OTHERWISE ALL DIFFERENT T-MATRICES ARE INCLUDED (THE FIRST OF THE T-MATRICES WITH IDENTICAL QUANTUM NUMBERS).
TEST(4)=1 THE T-MATRICES ARE NOT PRINTED.
TEST(5)=1 THE COULOMB EFFECTS ARE NOT INCLUDED.
TEST(6)=1 THE INPUT AND THE RESULTS ARE GIVEN IN THE C.M. SYSTEM, OTHERWISE IN THE LABORATORY SYSTEM.
TEST(7)=1 THE TABULATED FORM FACTORS ARE USED.
TEST(8)=1 IN CASE OF TEST(6)=1 THE QUASI-FREE SCATTERING OF THE PARTICLE MPA IS CALCULATED, OTHERWISE THE LABORATORY CROSS SECTIONS. THE ARRAY SFKV(4,MA) MUST BE GIVEN AND THE KINEMATICS IS TAKEN BETWEEN THESE LIMITS.
TEST(9)=1 ONLY THE KINEMATICS IS CALCULATED.
TEST(10)=1 THE ARCLENGTH PROJECTION, OTHERWISE THE EQUIDISTANCE STEP IS USED.

CSPR number of cross section printouts required
POPR number of polarization printouts required
NFE1,NFE2=1 usually, see TEST(2)
LINM≥maximum value of initial orbital angular momentum of projectile with respect to target
LFIM≥maximum value of final orbital angular momentum of projectile with respect to target
SIG=-1 no Coulomb distortion factors
MA number of angle pairs

NX number of points on the kinematic curve
=odd number to put quasifree geometry at centre of range
$2 \leq NX \leq 80$
MJP,MLP indicies of detected particles
MPA index of spectator particle
TDIM number of matrices used
TIND(I) indicies of matrices used (matricies are indexed in the order that they are calculated by PADE)
SFKV kinematic limits
There are three possible kinematic loci (figure B.2). SFKV specifies two energy windows in terms of arc length along the kinematic curve (MeV). The second window can be ignored by choosing an interval of $(10^{-30}, 10^{30})$ in cases A and B or an interval of $(a, a+\epsilon)$ in case C. If in doubt, a preliminary run with a large window can help to establish the type of curve and the required intervals.

Internally checked variables
NTM
MA number of angle pairs
NX number of points on the kinematic curve, see above
TDIM number of matrices used
NTC number of two-body channels (rows in TWQ)
DTWQ number of columns in TWQ (=9)
NLS number of L,S pairs
CCN number of coupled channels
BD1 maximum number of β's in any interaction
GD1 maximum number of γ's in any interaction
N1
NFP size of break-up propagator matrix
NT
TMF

Main Programs PRFITI, PRFITE

```
TEST                                              (3(I1,2X))
MASS                                            (3(F4.1,2X))
CHARGE                                            (3(I2,2X))
I,J,K,L,ICH,TOL                                (5(I2,2X),E8.1)
repeat for J=1,NTC
   (TWQ(I,J),I=1,DTWQ)                          (17(I2,2X),I2)
(EBO(I),I=1,NTC)                               (6(1PE11.4,2X))
(NOO(I),I=1,NTC)                               (17(I2,2X),I2)
(ENERGY(I),I=1,NT)                             (6(1PE11.4,2X))
(NOO(I),I=1,NTC)                                 (16(I3,2X))
I                                                        (I3)
(FOFA(1,J),J=1,NFF)                             (10(F6.1,2X))
repeat for NV=1,NTC
   INP,ITM,NST,J,ICH                               (5(I2,2X))
   SEPQ(1),SEPQ(2)                               (2(E10.3,2X))
   SEPQ(3),SEPQ(4),SEPQ(5)                       (3(E10.3,2X))
   repeat for J=1,2
```

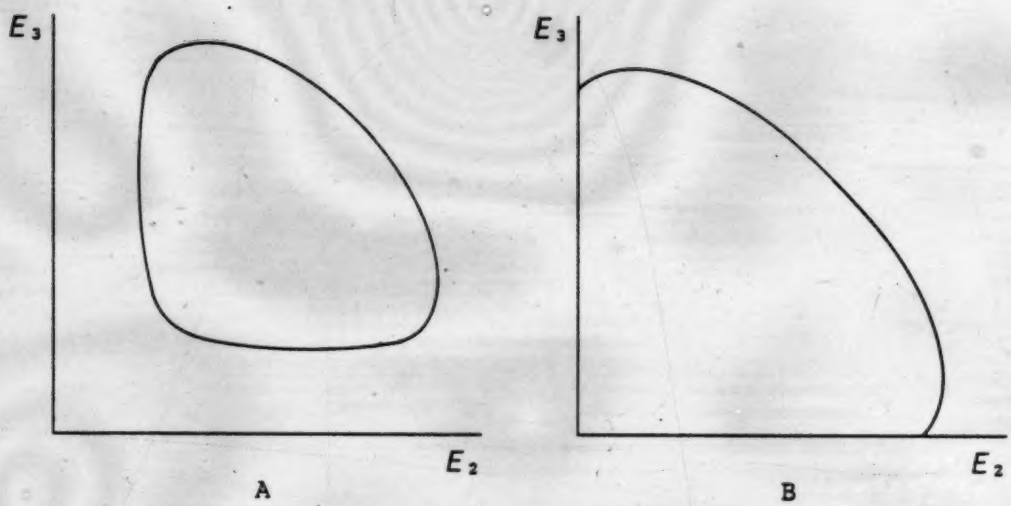

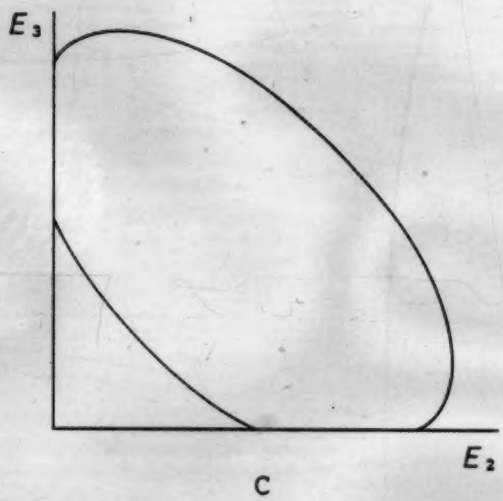

Figure B.2 The energy locus has three possible forms.

```
   (PHAS(I,J),I=1,NT)                                    (6(1PE11.4,2X))
(if TEST3=0 and M=2) (SDM(I),I=1,NT)                     (6(1PE11.4,2X))
(if TEST3=1 and M=1) (PHERR(I,J),I=1,NT)                 (6(1PE11.4,2X))
(if TEST3=1 and M=2) repeat for J=1,2
                       (PHERR(I,J),I=1,NT)               (6(1PE11.4,2X))
                     (SDM(I),I=1,NT)                     (6(1PE11.4,2X))
                     (MERR(I),I=1,NT)                    (6(1PE11.4,2X))
(EVA(I),I=1,NT)                                           (17(I2,2X),I2)
(PTVA(I),I=1,3)                                          (6(1PE11.4,2X))
(WF(I),I=1,8)                                            (6(1PE11.4,2X))
(VOP(I),I=1,NFP)                                          (17(I2,2X),I2)
(STP(I),I=1,NFP)                                         (6(1PE11.4,2X))
(LIM(I),I=1,2*NFP)                                       (6(1PE11.4,2X))
(FMFP(K,J,NV),K=1,NPP)                                    (6(E11.4,2X))
(FMF(K,J,NV),K=1,NPP)                                     (6(E11.4,2X))
(FMFE(K,J,NV),K=1,NPP)                                    (6(E11.4,2X))
(BETA(K,J,NV),K=1,L)                                      (5(E13.6,2X))
(GAMMA(K,J,NV),K=1,NPM1)                                  (5(E13.6,2X))
(LAMBDA(J,NV),J=1,NL),(KAPPA(J,NV),J=1,M)                 (5(E13.6,2X))
```

```
TEST(1)=1   THE FINAL PARAMETERS WILL BE PUNCHED.
TEST(2)=1   THE BETA(0, , )=....=BETA(L, , ).
TEST(3)=1   THE ERRORS MUST BE READ AND THE USUAL CHI2 IS
            CALCULATED.

MASS in nucleon masses
CHARGE
I=NTC number of two-body channels (rows in TWQ)
J=DTWQ number of columns in TWQ (=9)
K=NT number of experimental energies
L=NG
ICH=1 if input (starting values) is from data set 2
    (from a previous FITI run)
TOL fitting tolerance (never used)
TWQ two-body quantum numbers, see PRQUAD
EBO(J) bound state energy corresponding to interaction J
       (line J of TWQ)
      <0 if unbound
NOO orthogonality indicies
ENERGY experimental energies
NOO(I)=CIPA(2,I)=m for interaction I (row I of TWQ)
I=NFF number of points (energies) for fitting
FOFA energies
INP index of incoming particle
ITM maximum total number of steps in fit
NST maximum number of steps for any one parameter
J overrides TEST2
ICH as above
SEPQ(1) scattering length
SEPQ(2) effective range
SEPQ(3) D-state probability
SEPQ(4) quadrupole moment
SEPQ(5) asymptotic D/S
```

PHAS experimental phase shifts
PHERR errors in experimental phase shifts
The error is used to determine the weight of each phase shift in fitting to the experimental data. In order to fit nn and np interactions with pp data, the low energy phase shifts are given artificially large errors.
SDM mixing parameters
MERR errors in mixing parameters
EVA(I)=1 if the data for ENERGY(I) is to be included in the chi-squared
=0 otherwise
PTVA(I)=0 phase shift turning values (not used)
WF weight factors for fitting
WF(1) phase shifts
WF(2) mixing parameters
WF(3) D wave
WF(4) scattering length
WF(5) effective range
WF(6) D-state probability
WF(7) quadrupole moment
WF(8) asymptotic D/S
VOP order of parameter variation
The indexing of parameters, using the notation $\beta_{\ell}^{(\gamma)}$, $\lambda_{\gamma z}$ (see equations B.1-3), is as follows:

1	2	3	4	5	6	7	8	9	10	11
$\beta_0^{(1)}$	$\beta_1^{(1)}$	$\gamma_0^{(1)}$	$\gamma_1^{(1)}$	λ_{11}	λ_{12}	$\beta_0^{(2)}$	$\beta_1^{(2)}$	$\gamma_0^{(2)}$	$\gamma_1^{(2)}$	λ_{22}

If a number outside the possible range is encountered, fitting returns to the first parameter. If a zero is encountered the remaining parameters are ignored.
STP step size for parameter variation
LIM limits of parameter variation, in pairs (upper lower)
zero indicates no limit
FMFP arguments of the form factor
FMF values of the form factor
FMFE errors in the form factors
BETA, GAMMA, LAMBDA starting values of the potential parameters
KAPPA multiplies the form factor
=1 normally

Internally checked variables
NTC number of two-body channels (rows in TWQ)
DTWQ number of columns in TWQ (=9)
NT
NG
NLS number of L,S pairs
CCN number of coupled channels
BD1 maximum number of β's in any interaction
GD1 maximum number of γ's in any interaction
NFF

d. Sample Run

The following control files demonstrate the n-D QFS calculation denoted by $2'S_0R,2'S_0R,4T4RA3,P,D$. This calculation, the most sophisticated we have presently available, uses rank two R-type singlet S-wave potentials with a rank four tensor force and higher partial waves (P,D) added. The complete interaction, in the order specified in the TWQ matrix, could be described by:

nn: $2'S_0R,2^3P_0Y,^3P_1Y,^3P_2Y,'D_2R$

np: $2'S_0R,'P_1Y,2^3P_0Y,^3P_1Y,^3P_2Y,'D_2R,^3D_2R,^3D_3R,4T4RA3$

The complete control files are reproduced both to illustrate one convenient method for editing and running the main programs and to provide the necessary values of internal program variables and array dimensions.

The procedure followed is to copy each main program from the master source file of main programs, DOMAST, make the necessary changes via the system editor (still in batch mode), and compile into a temporary object deck. In this way the master file is never actually tampered with. Note that the batch output echoes the original file, not the edited version. The subroutines, which never change, reside in the (non-library) file DOLIBR, in object form.

The three-body T-matrices are calculated up to $19/2^+$ three-body angular momentum and parity. For this, the usual partial wave limit for three nucleons, several hours of time

on the AMDAHL are required. Higher states must be added in pairs; ($19/2^-$,$21/2^-$), ($21/2^+$,$23/2^+$), etc. Similarly, if desired, the cutoff must be reduced by pairs.

Up to $9/2^+$, certain parameters are constantly changing and JOBFAPA is used to run individual iterations of FAMA-PADE. Beyond this limit Sloan's approximation is used and internal variables remain constant, allowing the remaining iterations to be performed by JOBFAIT.

The use of GAUS is not shown. As is usually the case the preexistence of file QUAD is assumed.

Control file JOBQUAD

```
$SIGNON CSID PROUTE=PHYS T=5M PRIO=N
PASSWORD
$COPY DOMAST(44,94) TO -PRQUAD
$EDIT -PRQUAD
SET VERIFY=OFF
R 23 28
      COMMON /DINAR/SUMR(585),SUMI(585),WSQ(585),TWQ(189)
      NTC=21
      DTWQ=9
      WSD1=13
      WSD2=5
      N2=9
STOP
$RUN *FORTG SCARDS=-PRQUAD SPRINT=*DUMMY* O=-OBJECT
$RUN -OBJECT+DOLIBR 1=QUAD 6=QUADOUT 19=-DEB
0  0  0
 1.0000E+00    1.0000E+00    1.0000E+00
 1    1    1
 0    1    1
-1   24    6    9   40   64   40  21   9   4  1.0000  0.0000
 1    1    0    1    1    0    0   -1   -1
 1    2    0    1    1    0    0   -1   -1
 1    1    0   -1    1    2    2   -1   -1
 1    2    0   -1    1    2    2   -1   -1
 1    0    2   -1    1    2    2   -1   -1
 1    0    4   -1    1    2    2   -1   -1
 1    0    4    1    1    4    0   -1   -1
 2    1    0    1    1    0    0   -1   -1
 2    2    0    1    1    0    0   -1   -1
 2    0    2   -1    1    2    0   -1   -1
 2    1    0   -1    1    2    2   -1   -1
 2    2    0   -1    1    2    2   -1   -1
 2    0    2   -1    1    2    2   -1   -1
 2    0    4   -1    1    2    2   -1   -1
 2    0    4    1    1    4    0   -1   -1
 2    0    4    1    1    4    2   -1   -1
 2    0    6    1    1    4    2   -1   -1
 2    1    2    1    2    0    2    4    2
 2    2    2    1    2    0    2    4    2
 2    3    2    1    2    0    2    4    2
 2    4    2    1    2    0    2    4    2
$COPY QUADOUT TO *PRINT*
$SIGNOFF
```

Control file JOBKERE

```
$SIGNON CSID PROUTE=PHYS T=10M PRIO=N
PASSWORD
$COPY DOMAST(95,201) TO -PRKERE
$EDIT -PRKERE
SET VERIFY=OFF
R 33 51
      COMMON /DINAR/TWQ(189),DIM(21),ATQ(84),CIPA(42),
     1               IDIN(42),TNM(63),NF(21),EBO(21),Q(21),
     2               LIM(63),HSNO(21),HSNOC(21),PV(420),
     3               BETA(168),GAMMA(210),LAMBDA(84),
     4               GPT(64),GWT(64)
      COMMON /CDINA/EIVA(420),EIVAC(420),TAU(420),TAUC(420),
     1               CFH(84),CFHC(84),CFF(1680),CFFC(1680),
     2               TAHE(2100),TAHEC(2100),
     3               CFHE(8400),CFHEC(8400)
      COMMON TWQH(189),PH(420),TPFF(202)
      NTC=21
      DTWQ=9
      NLS=2
      CCN=4
      BD1=4
      GD1=5
      NT=20
      NG=64
      NFP=100
STOP
$RUN *FORTG SCARDS=-PRKERE SPRINT=*DUMMY* O=-OBJECT
$EMPTY KEREOUT
$EMPTY NDRES
$RUN -OBJECT+DOLIBR 1=QUAD 2=NDRES 6=KEREOUT 19=-DEB
1  0  0
1.0  0.0  64
-1.0000E+00  -1.0000E+00  -1.0000E+00  -1.0000E+00  -1.0000E+00  -1.0000E+00
-1.0000E+00  -1.0000E+00  -1.0000E+00  -1.0000E+00  -1.0000E+00  -1.0000E+00
-1.0000E+00  -1.0000E+00  -1.0000E+00  -1.0000E+00  -1.0000E+00   2.2250E+00
-1.0000E+00  -1.0000E+00  -1.0000E+00
  0   -5
 4.605000E-03
 1.550000E-01  -6.500000E+00   1.913000E+01  -1.797000E+01   6.185000E+00
-2.788200E-01   0.000000E+00
```

```
 0    -5
 1.409000E-02
-3.749000E+00    1.015000E+01   -3.189000E+00   -4.846000E+00    2.634000E+00
 0.000000E+00    1.275000E-01
 0     2
 1.069000E-02    1.069000E-02    1.069000E-02    1.069000E-02
 1.000000E+00    4.072000E-03    1.226000E-04
-4.054000E-03    0.000000E+00
 0     1
 5.315000E-03    5.315000E-03    5.315000E-03
 1.000000E+00   -1.752000E-02
 0.000000E+00    2.519000E-03
 0     2
 1.560000E-02    1.423000E-02    6.113000E-03    6.113000E-03
 1.000000E+00    5.406000E-03    2.605000E-04
 5.763000E-03
 0     1
 1.186000E-02    1.191000E-03    1.191000E-03
 1.000000E+00    2.919000E-03
-6.409000E-04
 0    -4
 6.775000E-03
 3.198000E+00   -6.900000E+00    4.116000E+00    5.860000E-01
-3.232000E-05
 0    -5
 4.922000E-03
 2.140000E-01   -8.801000E+00    2.650000E+01   -2.467000E+01    7.757000E+00
-3.206300E-01    0.000000E+00
 0    -5
 9.814000E-03
-3.970000E+00    1.077000E+01   -3.305000E+00   -5.375000E+00    2.880000E+00
 0.000000E+00    1.828000E-01
 0     2
 5.000000E-02    2.445000E-02    5.201000E-03    5.201000E-03
 1.000000E+00   -6.557000E-03    9.907000E-04
 1.152000E-02
 0     2
 1.069000E-02    1.069000E-02    1.069000E-02    1.069000E-02
 1.000000E+00    4.072000E-03    1.226000E-04
-4.054000E-03    0.000000E+00
 0     1
 5.315000E-03    5.315000E-03    5.315000E-03
```

```
 1.000000E+00  -1.752000E-02
 0.000000E+00   2.519000E-03
  0     2
 1.560000E-02   1.423000E-02   6.113000E-03   6.113000E-03
 1.000000E+00   5.406000E-03   2.605000E-04
 5.763000E-03
  0     1
 1.186000E-02   1.191000E-03   1.191000E-03
 1.000000E+00   2.919000E-03
-6.409000E-04
  0    -4
 6.775000E-03
 3.198000E+00  -6.900000E+00   4.116000E+00   5.860000E-01
-3.232000E-05
  0    -4
 8.625000E-03
 2.562000E+00  -5.036000E+00   2.889000E+00   5.850000E-01
-1.427000E-04
  0    -4
 9.988000E-03
 1.542000E+01  -2.833000E+01   1.374000E+01   1.700000E-01
-1.053000E-06
  0    -5
 4.860000E-03
 4.710000E-01  -8.185000E+00   2.146000E+01  -1.747000E+01   4.724000E+00
 4.988000E-03
 7.633818E-03  -4.591094E-02   2.661634E-02   0.000000E+00   0.000000E+00
-2.034986E-01   0.000000E+00   0.000000E+00   0.000000E+00
  0    -5
 5.868000E-03
 2.979000E+00  -4.688000E+00  -1.396000E+00   4.293000E+00  -1.880000E-01
 8.062000E-03
 5.947873E-02  -3.544604E-02  -5.049303E-02  -2.136605E-03   0.000000E+00
 0.000000E+00   2.982000E-01   4.834000E-02  -1.952000E-02
  0    -5
 1.483000E-02
 8.472000E-01  -2.396000E+00   2.928000E-01   2.307000E+00  -5.100000E-02
 9.960000E-03
-1.088496E-03   5.548746E-02  -1.101823E-05  -4.560621E-04   0.000000E+00
 0.000000E+00   4.834000E-02   6.277000E-02   6.498000E-03
  0    -5
 8.243000E-03
```

```
 2.388000E+00  -1.295000E+00  -3.045000E-01  -1.798000E-01   0.000000E+00
 9.430000E-03
 6.263965E-02   3.418646E-02  -2.175946E-02   4.105694E-04   0.000000E+00
 0.000000E+00  -1.952000E-02   6.498000E-03  -3.532000E-02
18.0   1.210833E+01   9.0   4.0   6.0   0.0  100.0
 0.0000E+00   0.0000E+00   0.0000E+00   0.0000E+00   0.0000E+00   0.0000E+00
 0.0000E+00   0.0000E+00   0.0000E+00   0.0000E+00   0.0000E+00   0.0000E+00
 0.0000E+00   0.0000E+00   0.0000E+00   0.0000E+00   0.0000E+00   0.0000E+00
 0.0000E+00   0.0000E+00   0.0000E+00
 9   9   6   6   6   6   6   9   9   6   6   6   6   6   6   6   6   9
 9   9   9
$COPY KEREOUT TO *PRINT*
$SIGNOFF
  0   -5
 3.281000E-03
 5.968000E+00  -2.057000E+01   2.858000E+01  -1.463000E+01  -3.480000E-01
 1.223000E-02
-1.864143E-01   3.170841E-01  -2.974037E-01   0.000000E+00   0.000000E+00
 0.000000E+00   4.221000E-02  -1.812000E-02   3.203000E-03
  0   -5
 7.566000E-03
 5.585000E+00  -9.092044E+00  -1.090000E+00   1.443000E+00   4.154000E+00
 1.716000E-02
 2.415000E-01  -7.391055E-01   4.206000E-01  -7.593000E-02   1.436000E-01
 0.000000E+00  -1.812000E-02   1.368000E-01  -1.911000E-02
  0   -5
 1.462000E-02
 3.672000E+00  -3.866260E+00  -6.024000E-01  -4.273000E-02  -1.616000E-01
 1.063000E-02
-4.837000E-02   5.679124E-02   3.403000E-02   5.567000E-03   4.044000E-02
 0.000000E+00   3.203000E-03  -1.911000E-02  -2.666000E-02
-1.0000E+00  -1.0000E+00   2.2250E+00
  0    0
 1.890000E-02
 1.000000E+00
-1.585000E-01
  0    0
 1.542000E-02
 1.000000E+00
-1.481000E-01
  0    0
 1.398000E-02
```

```
 1.000000E+00
 1.032000E-02    1.032000E-02    0.000000E+00
-1.288000E-02
-1.594000E-01
 3.0    1.290833E+01    9.0    4.0    6.0    0.0   100.0
 0.0000E+00    0.0000E+00    0.0000E+00
 9    9    9
```

Control file JOBFAPA

```
$SIGNON CSID PROUTE=PHYS T=60M PRIO=D
PASSWORD
$COPY DOMAST(202,414) TO -PRFAMA
$EDIT -PRFAMA
SET VERIFY=OFF
R 35 46
      COMMON /DINAR/TWQ(189),DIM(21),ATQ(84),CIPA(42),
     1              IDIN(42),TNM(63),FFIND(21),BOO(21),
     2              EBO(21),Q(21),LIM(63),
     3              BETA(168),GAMMA(210),
     4              BVN(405),PV(420),
     5              THQ(183),SMD(61),FCO(400),
     6              TPFF(2),TPF(2)
      COMMON /CDINA/ROWS(1),ROWSC(1),CFFC(1),
     1              CFF(1680),WSQ(585)
      COMMON /LDINA/KERN(400),KERNH(400),TAU(420),IHT(3081),
     1              KERNC(1),KERNHC(1),TAUC(1),IHTC(1),
     2              TWQH(189),ZK(3721),ZKC(1)
R 93 94
      DEFINE FILE 3(2500,805,U,IP3)
      NSM=2500
R 99 100
      DEFINE FILE 10(100,1200,U,IP10)
      NWM=100
R 102 116
      NTC=21
      DTWQ=9
      NLS=2
      CCN=4
```

```
      BD1=4
      GD1=5
      N1=9
      NT=20
      NCH=61
      DM=1027
      EQN=3
      NA=3
      FCD2=20
      WSD1=13
      WSD2=5
STOP
$RUN *FORTG SCARDS=-PRFAMA SPRINT=*DUMMY* O=-OBJ1
$CREATE -DIAC TYPE=SEQ SIZE=2500P MAXSIZE=3000P
$CREATE -MATR TYPE=SEQ SIZE=2000P MAXSIZE=2500P
$CREATE -QUAD TYPE=SEQ SIZE=140P MAXSIZE=150P
$CREATE -FAMA TYPE=SEQ SIZE=50P
$EMPTY FAMAOUT
$RUN -OBJ1+DOLIBR 1=QUAD 2=NDRES 3=-DIAC 4=-MATR 6=FAMAOUT 10=-QUAD 11=-FAMA 19=-DEB
0  1  1  0  0  0  0
16   9  -1
 2   2   1   1   1   1   0   2   2   1   1   1   1   1   0   0  -2   2
 2   2   2
$COPY FAMAOUT TO *PRINT*
$DESTROY -PRFAMA
$DESTROY -DIAC
$DESTROY -QUAD
$DESTROY -FAMA
$COPY DOMAST(598,787) TO -PRPADE
$EDIT -PRPADE
SET VERIFY=OFF
R 47 56
      COMMON /DINAR/AFFIN(21),FFIND(21),BOO(21),O(21),THF(21),
     1              TNM(63),TOFI(84),ITF(3),BOL(3),DIV(3),
     2              THQ(183),SMO(61),ZK(3721),
     3              BOPA(1830),DIPA(1830)
      COMMON /CDINA/XRI(9),PCH(9),BRUP(1647),
     1              KERN(400),IHT(3081),IHTC(1),
     2              SOL(1),ROWS(1),ROWSC(1)
      COMMON /DINDP/PRI(81),ITRR(6162),ITRI(6162),
     1              PCOR(729),PCOI(729),
     2              PCOTR(2187),PCOTI(2187)
```

```
R 72 80
      NTC=21
      N1=9
      NT=20
      NCH=61
      DM=1027
      EQN=3
      NA=3
      TOD2=4
      ITM=81
STOP
$RUN *FORTG SCARDS=-PRPADE SPRINT=*DUMMY* O=-OBJ2
$CREATE -TEM1 TYPE=SEQ SIZE=700P MAXSIZE=1000P
$CREATE -TEM2 TYPE=SEQ SIZE=700P MAXSIZE=1000P
$EMPTY PADEOUT
$RUN -OBJ2+DOLIBR 2=NDRES 3=-TEM1 4=-MATR 6=PADEOUT 8=-TEM2 19=-DEB
0  1  0  1  0  0  1
 81  3.0E-03
 3
 2   2   1   1   1   1   0   2   2   1   1   1   1   1   0   0  -2   2
 2   2   2
 2   2   1   1   1   1  -2   2   2   1   1   1   1   1  -2  -2  -2   2
 2   2   2
 2   2  -2  -2  -2  -2  -2   2   2  -2  -2  -2  -2  -2  -2  -2  -2   2
 2   2   2
$COPY PADEOUT TO *PRINT*
$SIGNOFF
J=1
      NCH=34
      DM=582
      EQN=2
      NA=2
J=3
      NCH=53
      DM=899
      EQN=3
      NA=3
J=5
      NCH=60
      DM=1011
      EQN=3
      NA=3
```

```
J=7,9,...
      NCH=61
      DM=1027
      EQN=3
      NA=3
```

Control file JOBFAIT

```
$SIGNON CSID PROUTE=PHYS T=20M PRIO=D P=400
PASSWORD
$COPY DOMAST(202,414) TO -PRFAMA
$EDIT -PRFAMA
SET VERIFY=OFF
R 35 46
      COMMON /DINAR/TWQ(189),DIM(21),ATQ(84),CIPA(42),
     1               IDIN(42),TNM(63),FFIND(21),BOO(21),
     2               EBO(21),Q(21),LIM(63),
     3               BETA(168),GAMMA(210),
     4               BVN(405),PV(420),
     5               THQ(183),SMD(61),FCO(400),
     6               TPFF(2),TPF(2)
      COMMON /CDINA/ROWS(3081),ROWSC(1),CFFC(1),
     1               CFF(1680),WSQ(45)
      COMMON /LDINA/KERN(1),KERNH(1),TAU(420),IHT(3081),
     1               KERNC(1),KERNHC(1),TAUC(1),IHTC(1),
     2               TWQH(189),ZK(1),ZKC(1)
R 93 94
      NSM=0
      CONTINUE
R 102 116
      NTC=21
      DTWQ=9
      NLS=2
      CCN=4
      BD1=4
      GD1=5
      N1=9
      NT=20
      NCH=61
```

```
      DM=1027
      EQN=3
      NA=3
      FCD2=20
      WSD1=1
      WSD2=5
STOP
$RUN *FORTG SCARDS=-PRFAMA SPRINT=*DUMMY* O=-OBJ1
$CREATE -MATR TYPE=SEQ SIZE=100P
$CREATE -FAMA TYPE=SEQ SIZE=50P
$EMPTY FAMAOUT
$RUN -OBJ1+DOLIBR 1=QUAD 2=NDRES 4=-MATR 6=FAMAOUT 11=-FAMA 19=-DEB
0  1  0  1  0  0  0
16   9   1
$IF RC >> 0 $SIGNOFF
$COPY DOMAST(598,787) TO -PRPADE
$EDIT -PRPADE
SET VERIFY=OFF
R 47 56
      COMMON /DINAR/AFFIN(21),FFIND(21),BOO(21),Q(21),THF(21),
     1              TNM(63),TOFI(84),ITF(3),BOL(3),DIV(3),
     2              THQ(183),SMD(61),ZK(1),
     3              BOPA(1),DIPA(1)
      COMMON /CDINA/XRI(9),PCH(9),BRUP(1647),
     1              KERN(1),IHT(3081),IHTC(1),
     2              SOL(1),ROWS(3081),ROWSC(3081)
      COMMON /DINDP/PRI(1),ITRR(2),ITRI(2),
     1              PCOR(9),PCOI(9),
     2              PCOTR(1),PCOTI(1)
R 72 80
      NTC=21
      N1=9
      NT=20
      NCH=61
      DM=1027
      EQN=3
      NA=3
      TOD2=4
      ITM=1
STOP
$RUN *FORTG SCARDS=-PRPADE SPRINT=*DUMMY* O=-OBJ2
$EMPTY PADEOUT
```

```
$RUN -OBJ2+DOLIBR 2=NDRES 4=-MATR 6=PADEOUT 19=-DEB
0  1  0  1  0  0  1
  1  3.0E-03
 3
-1  -1  -1  -1  -1  -1  -1  -1  -1  -1  -1  -1  -1  -1  -1  -1  -2  -1
-1  -1  -1
-1  -1  -1  -1  -1  -1  -2  -1  -1  -1  -1  -1  -1  -1  -2  -2  -2  -1
-1  -1  -1
-1  -1  -2  -2  -2  -2  -2  -1  -1  -2  -2  -2  -2  -2  -2  -2  -2  -1
-1  -1  -1
$IF RC >> 0 $SIGNOFF
$EMPTY FAMAOUT
$RUN -OBJ1+DOLIBR 1=QUAD 2=NDRES 4=-MATR 6=FAMAOUT 11=-FAMA 19=-DEB
0  1  0  1  0  0  0
20  11   1
$IF RC >> 0 $SIGNOFF
$EMPTY PADEOUT
$RUN -OBJ2+DOLIBR 2=NDRES 4=-MATR 6=PADEOUT 19=-DEB
0  1  0  1  0  0  1
  1  3.0E-03
 3
-1  -1  -1  -1  -1  -1  -1  -1  -1  -1  -1  -1  -1  -1  -1  -1  -2  -1
-1  -1  -1
-1  -1  -1  -1  -1  -1  -2  -1  -1  -1  -1  -1  -1  -1  -2  -2  -2  -1
-1  -1  -1
-1  -1  -2  -2  -2  -2  -2  -1  -1  -2  -2  -2  -2  -2  -2  -2  -2  -1
-1  -1  -1
$IF RC >> 0 $SIGNOFF
$EMPTY FAMAOUT
$RUN -OBJ1+DOLIBR 1=QUAD 2=NDRES 4=-MATR 6=FAMAOUT 11=-FAMA 19=-DEB
0  1  0  1  0  0  0
20  11  -1
$IF RC >> 0 $SIGNOFF
$EMPTY PADEOUT
$RUN -OBJ2+DOLIBR 2=NDRES 4=-MATR 6=PADEOUT 19=-DEB
0  1  0  1  0  0  1
  1  3.0E-03
 3
-1  -1  -1  -1  -1  -1  -1  -1  -1  -1  -1  -1  -1  -1  -1  -1  -2  -1
-1  -1  -1
-1  -1  -1  -1  -1  -1  -2  -1  -1  -1  -1  -1  -1  -1  -2  -2  -2  -1
-1  -1  -1
```

```
-1  -1  -2  -2  -2  -2  -2  -1  -1  -2  -2  -2  -2  -2  -2  -2  -2  -1
-1  -1  -1
$IF RC >> O $SIGNOFF
$EMPTY FAMAOUT
$RUN -OBJ1+DOLIBR 1=QUAD 2=NDRES 4=-MATR 6=FAMAOUT 11=-FAMA 19=-DEB
O  1  O  1  O  O  O
20  13  -1
$IF RC >> O $SIGNOFF
$EMPTY PADEOUT
$RUN -OBJ2+DOLIBR 2=NDRES 4=-MATR 6=PADEOUT 19=-DEB
O  1  O  1  O  O  1
  1  3.OE-03
 3
-1  -1  -1  -1  -1  -1  -1  -1  -1  -1  -1  -1  -1  -1  -1  -1  -2  -1
-1  -1  -1
-1  -1  -1  -1  -1  -1  -2  -1  -1  -1  -1  -1  -1  -1  -2  -2  -2  -1
-1  -1  -1
-1  -1  -2  -2  -2  -2  -2  -1  -1  -2  -2  -2  -2  -2  -2  -2  -2  -1
-1  -1  -1
$IF RC >> O $SIGNOFF
$EMPTY FAMAOUT
$RUN -OBJ1+DOLIBR 1=QUAD 2=NDRES 4=-MATR 6=FAMAOUT 11=-FAMA 19=-DEB
O  1  O  1  O  O  O
20  13  1
$IF RC >> O $SIGNOFF
$EMPTY PADEOUT
$RUN -OBJ2+DOLIBR 2=NDRES 4=-MATR 6=PADEOUT 19=-DEB
O  1  O  1  O  O  1
  1  3.OE-03
 3
-1  -1  -1  -1  -1  -1  -1  -1  -1  -1  -1  -1  -1  -1  -1  -1  -2  -1
-1  -1  -1
-1  -1  -1  -1  -1  -1  -2  -1  -1  -1  -1  -1  -1  -1  -2  -2  -2  -1
-1  -1  -1
-1  -1  -2  -2  -2  -2  -2  -1  -1  -2  -2  -2  -2  -2  -2  -2  -2  -1
-1  -1  -1
$IF RC >> O $SIGNOFF
$EMPTY FAMAOUT
$RUN -OBJ1+DOLIBR 1=QUAD 2=NDRES 4=-MATR 6=FAMAOUT 11=-FAMA 19=-DEB
O  1  O  1  O  O  O
20  15  1
$IF RC >> O $SIGNOFF
```

```
$EMPTY PADEOUT
$RUN -OBJ2+DOLIBR 2=NDRES 4=-MATR 6=PADEOUT 19=-DEB
0  1  0  1  0  0  1
  1  3.0E-03
 3
-1  -1  -1  -1  -1  -1  -1  -1  -1  -1  -1  -1  -1  -1  -1  -1  -2  -1
-1  -1  -1
-1  -1  -1  -1  -1  -1  -2  -1  -1  -1  -1  -1  -1  -1  -2  -2  -2  -1
-1  -1  -1
-1  -1  -2  -2  -2  -2  -2  -1  -1  -2  -2  -2  -2  -2  -2  -2  -2  -1
-1  -1  -1
$IF RC >> 0 $SIGNOFF
$EMPTY FAMAOUT
$RUN -OBJ1+DOLIBR 1=QUAD 2=NDRES 4=-MATR 6=FAMAOUT 11=-FAMA 19=-DEB
0  1  0  1  0  0  0
20  15  -1
$IF RC >> 0 $SIGNOFF
$EMPTY PADEOUT
$RUN -OBJ2+DOLIBR 2=NDRES 4=-MATR 6=PADEOUT 19=-DEB
0  1  0  1  0  0  1
  1  3.0E-03
 3
-1  -1  -1  -1  -1  -1  -1  -1  -1  -1  -1  -1  -1  -1  -1  -1  -2  -1
-1  -1  -1
-1  -1  -1  -1  -1  -1  -2  -1  -1  -1  -1  -1  -1  -1  -2  -2  -2  -1
-1  -1  -1
-1  -1  -2  -2  -2  -2  -2  -1  -1  -2  -2  -2  -2  -2  -2  -2  -2  -1
-1  -1  -1
$IF RC >> 0 $SIGNOFF
$EMPTY FAMAOUT
$RUN -OBJ1+DOLIBR 1=QUAD 2=NDRES 4=-MATR 6=FAMAOUT 11=-FAMA 19=-DEB
0  1  0  1  0  0  0
24  17  -1
$IF RC >> 0 $SIGNOFF
$EMPTY PADEOUT
$RUN -OBJ2+DOLIBR 2=NDRES 4=-MATR 6=PADEOUT 19=-DEB
0  1  0  1  0  0  1
  1  3.0E-03
 3
-1  -1  -1  -1  -1  -1  -1  -1  -1  -1  -1  -1  -1  -1  -1  -1  -2  -1
-1  -1  -1
-1  -1  -1  -1  -1  -1  -2  -1  -1  -1  -1  -1  -1  -1  -2  -2  -2  -1
```

```
 -1  -1  -1
 -1  -1  -2  -2  -2  -2  -2  -1  -1  -2  -2  -2  -2  -2  -2  -2  -2  -1
 -1  -1  -1
$IF RC >> O $SIGNOFF
$EMPTY FAMAOUT
$RUN -OBJ1+DOLIBR 1=QUAD 2=NDRES 4=-MATR 6=FAMAOUT 11=-FAMA 19=-DEB
O  1  O  1  O  O  O
24  17   1
$IF RC >> O $SIGNOFF
$EMPTY PADEOUT
$RUN -OBJ2+DOLIBR 2=NDRES 4=-MATR 6=PADEOUT 19=-DEB
O  1  O  1  O  O  1
  1  3.OE-03
 3
-1  -1  -1  -1  -1  -1  -1  -1  -1  -1  -1  -1  -1  -1  -1  -1  -2  -1
-1  -1  -1
-1  -1  -1  -1  -1  -1  -2  -1  -1  -1  -1  -1  -1  -1  -2  -2  -2  -1
-1  -1  -1
-1  -1  -2  -2  -2  -2  -2  -1  -1  -2  -2  -2  -2  -2  -2  -2  -2  -1
-1  -1  -1
$IF RC >> O $SIGNOFF
$EMPTY FAMAOUT
$RUN -OBJ1+DOLIBR 1=QUAD 2=NDRES 4=-MATR 6=FAMAOUT 11=-FAMA 19=-DEB
O  1  O  1  O  O  O
24  19   1
$IF RC >> O $SIGNOFF
$EMPTY PADEOUT
$RUN -OBJ2+DOLIBR 2=NDRES 4=-MATR 6=PADEOUT 19=-DEB
O  1  O  1  O  O  1
  1  3.OE-03
 3
-1  -1  -1  -1  -1  -1  -1  -1  -1  -1  -1  -1  -1  -1  -1  -1  -2  -1
-1  -1  -1
-1  -1  -1  -1  -1  -1  -2  -1  -1  -1  -1  -1  -1  -1  -2  -2  -2  -1
-1  -1  -1
-1  -1  -2  -2  -2  -2  -2  -1  -1  -2  -2  -2  -2  -2  -2  -2  -2  -1
-1  -1  -1
$SIGNOFF
```

Control file JOBBRUP

```
$SIGNON CSID PROUTE=PHYS T=1M PRIO=N P=200
PASSWORD
$COPY DOMAST(1138,1325) TO -PRBRUP
$EDIT -PRBRUP
SET VERIFY=OFF
R 61 72
      COMMON /DINAR/TWQ(189),DIM(21),ATQ(84),CIPA(42),TNM(63),
     1              FFIND(21),SJP(160),THQ(183),BOO(21),DTM(80),
     2              EBO(21),Q(21),PV(420),TPFH(2),TPF(42),
     3              BETA(168),GAMMA(210),LAMBDA(84),
     4              CLEB(6),ANGLES(20),SFKV(20),PAA(41),QAA(41),
     5              ACUC(82),ACUL(82)
      COMMON /LDINA/TAU(2100),CFF(8400),BRUP(1647),
     1              TAUM(2583),TM(123),FFLS(5166),
     2              TMBU(1968),HELP(48),COSP(27),
     3              TVV(246),TVT(369),SYMT(246),
     4              KAT(369),PAT(369),QAT(369),
     5              PLP(738),PLQ(11193)
R 92 109
      NTC=3
      DTWQ=9
      NLS=1
      CCN=1
      BD1=1
      GD1=1
      NT=20
      NFP=100
      NTM=80
      TMI=6
      TMF=8
      NXM=41
      MAM=4
      NCHM=61
      EQNM=3
      N1=9
      PLPD=6
      PLQD=91
STOP
$RUN *FORTG SCARDS=-PRBRUP SPRINT=*DUMMY* O=-OBJECT
$EMPTY NNBROUT
```

```
$RUN -OBJECT+DOLIBR 2=YYRES 6=NNBROUT 19=-DEB
0  0  1  0  1  1  0  1  0  0
 1   1
16  24   1
 1  40   2   3   1
 19
 1   2   3   4   5   6   7   8   9  20  21  22  23  14  15  16  17  18
19
 0.0000E+00   1.0000E+00   0.0000E+00   1.0000E+00
$COPY NNBROUT TO *PRINT*
$SIGNOFF
 1   4   7  10  13  16  19  22  25  28  31  34  37  40  43  46  49  52
55
 2   5   8  11  14  17  20  23  26  29  32  35  38  41  44  47  50  53
56
 3   6   9  12  15  18  21  24  27  30  33  36  39  42  45  48  51  54
55
```

e. Test Run

To check whether the program is running correctly on any given system, Doleschall performs a limited calculation for n-D scattering using rank one singlet R-type potentials and a rank one tensor force only. For comparison, he brings the correct results from a calculation on his home computer system.

The test run is carried out in full by the control file JOBTEST which has the form of the JOB- files in the previous section. Output from these is copied into the permanent files QUADOUT, KEREOUT, FAMAOUT and PADEOUT and to *PRINT*.

The run is restricted to one iteration of FAMA/PADE (for $J,\pi=1/2^+$) with no concluding breakup or elastic scattering calculations. Because it is a test run, a larger amount of output is called for than is normally required.

f. Permanent Files

There are a number of permanent files maintained in connection with the running of this program. Table B.1 lists those which have been stored on tape. **data set** refers to the FORTRAN data set reference number, if any, with which the file is associated during execution.

In addition to the basic files of the program package, there are several files which relate specifically to the D(n,nn)p reaction. Files prefixed by JOBS- execute a simplified form of the program using mesh points from SQUAD and a rank one Yamaguchi potential. Otherwise they resemble

NAME	description	data set
DOCODE	complete source listing	
DOLIBR	subprograms in object form	
DOMAST	source listing of main programs	
GAQUAD	raw data for GAUS	2
JOBBRUP	BRUP control file, fixed angles	
JOBELAS	ELAS control file	
JOBFAIT	FAMA+PADE control file, $9/2^+$-$19/2^+$	
JOBFAPA	FAMA+PADE control file, $1/2^+$-$9/2^-$	
JOBFITS	FITI control file	
JOBKERE	KERE control file	
JOBNNFSI	BRUP control file, n-n FSI	
JOBNNQFS	BRUP control file, n-n QFS	
JOBNPFSI	BRUP control file, n-p FSI	
JOBNPQFS	BRUP control file, n-p QFS	
JOBQUAD	QUAD control file	
JOBSCRE	BRUP control file, SCRE' geometry	
JOBTEST	test run control file	
MANUAL	this manual	
NDRES[2]	T-matrices, $2'S_0R$,4T4RA3,P,D interaction	2
QUAD	processed Gaussian quadrature data	1
SQUAD	simplified version of QUAD	1
SRES[3]	T-matrices, $'S_0Y$, ^3S_1Y interaction	2
SSRES1	T-matrices, $'S_0R$, ^3S_1R interaction	2
SSRES2[4]	T-matrices, $'S_0R$, ^3S_1R interaction	2
SSRES3[5]	T-matrices, $'S_0R$, ^3S_1R interaction	2
STRES	T-matrices, $'S_0R$,1T4RA interaction	2
S2SRES	T-matrices, $2'S_0R$, ^3S_1R interaction	2
YYRES	T-matrices, $'S_0Y$, ^3S_1Y interaction	2
YYRES2[3]	T-matrices, $'S_0Y$, ^3S_1Y interaction	2
YYRES3[5]	T-matrices, $2'S_0Y$, $'S_0Y$, ^3S_1Y	2
Y2YRES	T-matrices, $2'S_0Y$, ^3S_1Y interaction	2

[1]Symmetric Constant Relative Energy
[2]special structure (see text)
[3]simplified quadrature (using SQUAD)
[4]modified n-p effective range
[5]modified n-n effective range

Table B.1 Permanent files.

the JOB-files of section d.

Files denoted by -RES- contain three-body T-matrices. These are associated with file 2 of section b. They represent the result of calculations up to the end of the final FAMA-PADE iteration($19/2^+$ in all cases). For the more complicated potentials this involves a considerable amount of computation, making these files well worth retaining. Prefixes and suffixes indicate the potential used.

NDRES contains three sets of T-matrices for each three-body angular momentum and parity: the first for the 2'S R,4T4RA3,P,D interaction, the second omitting D-waves, and the third omitting both P- and D-waves. This was constructed by defining the full potential in QUAD and KERE, and running PADE with TEST(2)=1, FIDI=3 (three calculations). The potential weights (TOFI) were chosen so that P and D waves were omitted as required. The matrices are interleaved because FAMA and PADE iterations must be run in order of increasing angular momentum (JT).

Physical results are produced from -RES- files simply by running BRUP or ELAS with the desired file on data set 2. NDRES must be used with TEST(3)=1, TIND=1,4,7,... for the first set of T-matrices (full calculation), TIND=2,5,8,... for the second set, etc.

g. DOCODE Contents

line		program
1		PRGAUS
44	SUBROUTINE	DREGAU
100	SUBROUTINE	QREGAU
156	SUBROUTINE	HIBA
163	SUBROUTINE	TERMIN
176	SUBROUTINE	MOVE
215	SUBROUTINE	GQPW
228	INTEGER FUNCTION	IEVEN
234	SUBROUTINE	OLIRIN
252	SUBROUTINE	OLIRVA
271	SUBROUTINE	OLIRCO
290	COMPLEX FUNCTION	COMDET
337	LOGICAL FUNCTION	HALIRE
428		PRQUAD
479	SUBROUTINE	DOQUAD
776	SUBROUTINE	DSQPRO
814	SUBROUTINE	WSQPRO
1180	SUBROUTINE	MATPRO
1200	DOUBLE PRECISION FUNCTION	QF0INT
1239	SUBROUTINE	LEG
1258	SUBROUTINE	LEGDER
1283	SUBROUTINE	QFUNS
1372	DOUBLE PRECISION FUNCTION	DYDZ
1380	DOUBLE PRECISION FUNCTION	YTRZ
1388	DOUBLE PRECISION FUNCTION	ZTRY
1406	SUBROUTINE	HAUELI
1439	SUBROUTINE	HAUSOL
1469		PRKERE
1576	SUBROUTINE	DOKERE
2132	SUBROUTINE	HSPRE
2190	SUBROUTINE	PARAM
2317	REAL FUNCTION	FMF
2369	SUBROUTINE	HISC
2649	SUBROUTINE	SLERPQ
2896	LOGICAL FUNCTION	DOLEIG
3331	LOGICAL FUNCTION	HAINRE
3421	REAL FUNCTION	VMV
3431	SUBROUTINE	MATMUL
3442		PRFAMA
3655	SUBROUTINE	DOFAMA
4146	SUBROUTINE	BVNPRO
4207	SUBROUTINE	INGPGW
4218	SUBROUTINE	MAICIK
4543	SUBROUTINE	KERNEL
4997	SUBROUTINE	KERTAU
5347	LOGICAL FUNCTION	FCOM
5463	REAL FUNCTION	VCC0
5487	REAL FUNCTION	SJS
5557		PRPADE

```
5740                SUBROUTINE DOPADE
6066           LOGICAL FUNCTION PADEFI
6363              REAL FUNCTION EAPADE
6453                             PRPADD
6643                SUBROUTINE DOPADD
6975           LOGICAL FUNCTION PADEFD
7307                             PRCOGR
7415                SUBROUTINE DOCOGR
7648           LOGICAL FUNCTION COGRAD
7800                SUBROUTINE CONMAT
7835                SUBROUTINE MAVEMU
7896                             PRCODP
8009                SUBROUTINE DOCODP
8247           LOGICAL FUNCTION COGRDP
8414                SUBROUTINE MAVMDP
8477 DOUBLE PRECISION FUNCTION DREAL
8482 DOUBLE PRECISION FUNCTION DIMAG
8487                             PRELAS
8616                SUBROUTINE DOELAS
9089                SUBROUTINE ELATTM
9213                SUBROUTINE ELAPOL
9662                SUBROUTINE POCSIR
9672                SUBROUTINE ANAPOW
9727              REAL FUNCTION AZIANG
9749                SUBROUTINE CURV
9797           COMPLEX FUNCTION DFUN
9863              REAL FUNCTION ALP
9897              REAL FUNCTION VCC
9961                             PRBRUP
10149               SUBROUTINE DOBRUP
10801               SUBROUTINE BRUPTM
11437          LOGICAL FUNCTION KINEMA
11553          LOGICAL FUNCTION ARLEKI
11814               SUBROUTINE ARCLEN
11855               SUBROUTINE OUTRES
12009               SUBROUTINE ALPFUN
12039             REAL FUNCTION CSTRCO
12069               SUBROUTINE NXTRAN
12091               SUBROUTINE POLARI
12323               SUBROUTINE BRANPO
12392          COMPLEX FUNCTION INTERP
12404               SUBROUTINE VARTRA
12547               SUBROUTINE DECPOL
12569                            PRBOPA
12695               SUBROUTINE DOBOPA
13131               SUBROUTINE BOPARA
13197               SUBROUTINE IDSE
13267             REAL FUNCTION BOFMF
13314               SUBROUTINE BOHISC
13477               SUBROUTINE BOMATR
13748               SUBROUTINE BOKERN
13960          LOGICAL FUNCTION PADEHO
14140                            PRBOPD
14266               SUBROUTINE DOBOPD
```

```
14701          LOGICAL FUNCTION PADEHD
14881                           PRFITI
14997                SUBROUTINE DOFITI
15514          LOGICAL FUNCTION FIT
15726             REAL FUNCTION FGV
16153                SUBROUTINE FISEPQ
16381                SUBROUTINE PROP
16495             REAL FUNCTION FORMF
16547             REAL FUNCTION ARCTG
16559          LOGICAL FUNCTION HALICO
16662                           PRFITE
16779                SUBROUTINE DOFITE
17311             REAL FUNCTION FGVT
17663                SUBROUTINE MLEIGV
17739             REAL FUNCTION HAUDET
17772                SUBROUTINE FTSEPQ
18023                           PRCONV
18242                SUBROUTINE MARK
18256                SUBROUTINE CAFOIN
18294                SUBROUTINE CAFORE
18332                SUBROUTINE CAFOCO
18370                           PRMESH
18446                           PRDORE
18481                           PRINIT
18491                           PRFACO
18533                           PRCDC
18604                           SOLAFI
19512                           NMESRCH: PROC OPTIONS(MAIN);
19572                           PRGEBO
19686                SUBROUTINE DOGEBO
19913                SUBROUTINE GEMATR
20278                SUBROUTINE GEKERN
20498                SUBROUTINE BSFUNC
20620          COMPLEX FUNCTION GEFMF
```

APPENDIX C PARAMETERS OF THE TWO-BODY INTERACTIONS

Refer to table IV.2 for effective range parameters (S-wave only).

The separable potential in the k,s(spin) partial wave has the form

$$V^{k\,s}(p,p')=\Sigma_{y\,z}g_y^{k\,s}(p)\lambda_{y\,z}g_z^{k\,s}(p') \qquad \text{C.1}$$

where the summation is up to the rank of the potential. λ_{yz} is diagonal for all potentials except the 4T4RA3.

Y-type $g^{k\,s}(p)=[p^k\Sigma_{\gamma=0}^{m}\gamma_\gamma p^{2\gamma}]/[\Pi_{\beta=0}^{k}\Sigma_{\beta=0}^{m}(1+\beta_\gamma p^2)]$

partial wave	m	β	γ	λ
nn $^1S_0$	0	1.890 -2	1.0	-1.585 -1
nn $^1\tilde{S}_0$	0	1.615 -2	1.0	-1.476 -1
nn 2^1S_0	0	1.887 -2	1.0	-1.584 -1
	1	2.923 -3	1.0	1.293 -1
		2.481 -3	-1.852 -2	
nn $2^1\tilde{S}_0$	0	1.614 -2	1.0	-1.476 -1
	1	3.641 -3	1.0	1.128 -1
		3.097 -3	-1.967 -2	

partial wave	m	β	γ	λ
np $^1S_0$	0	1.542 -2	1.0	-1.481 -1
		1.423 -2	5.406 -3	
np 2^1S_0	0	1.537 -2	1.0	-1.479 -1
	1	2.790 -3	1.0	9.554 -2
		2.267 -3	-1.619 -2	
np $^3S_1$	0	1.246 -2	1.0	-1.934 -1
np $^1P_1$	2	5.000 -2	1.0	1.152 -2
		2.445 -2	-6.557 -3	
		5.201 -3	9.907 -4	
		5.201 -3		
2^3P_0	2	1.069 -2	1.0	-4.054 -3
		1.069 -2	4.072 -3	
		1.069 -2	1.226 -4	
		1.069 -2		
	1	5.315 -3	1.0	2.519 -3
		5.315 -3	-1.752 -2	
		5.315 -3		
$^3P_1$	2	1.560 -2	1.0	5.763 -3
		1.423 -2	5.406 -3	
		6.113 -3	2.605 -4	
		6.113 -3		
$^3P_2$	1	1.186 -2	1.0	-6.409 -4
		1.191 -3	2.919 -3	
		1.191 -3		

R-type $g^{k\,s}(p)=[p^k/(1+\beta p^2)^k]\Sigma_{i=1}^{m}[\gamma_i/(1+\beta p^2)^i]$

partial wave	m	β	γ	λ
nn $^1S_0$	5	3.689 -3	1.290 -1 -5.108 1.377 +1 -1.239 +1 4.599	-1.739000 -1
nn $^1\tilde{S}_0$	5	3.245 -3	4.000 -2 -5.750 1.560 +1 -1.360 +1 4.710	-1.552000 -1
nn 2^1S_0	5	4.605 -3	1.555 -1 -6.500 1.913 +1 -1.797 +1 6.185	-2.788200 -1
	5	1.409 -2	-3.749 -1 1.015 +1 -3.189 -4.846 2.634	1.275000 -1
np $^1S_0$	5	5.345 -3	1.100 -1 -5.320 1.958 +1 -1.812 +1 5.750	-1.693600 -1
np $^1\tilde{S}_0$	5	5.171 -3	6.200 -2 -6.297 1.908 +1 -1.760 +1 5.755	-1.744200 -1

partial wave	m	β	γ	λ
np 2^1S_0	5	4.923 -3	2.140 -1 -8.801 2.650 +1 -2.467 +1 7.757	-3.206300 -1
	5	9.814 -3	-3.970 -1 1.077 +1 -3.305 -5.375 2.880	1.828000 -1
np $^3S_1$	5	4.473 -3	4.770 -1 -7.707 1.842 +1 -1.249 +1 2.300	-2.349877 -1
$^1D_2$	4	6.775 -3	3.198 -6.900 4.116 5.860 -1	-3.232000 -5
np $^3D_2$	4	8.625 -3	2.562 -5.036 2.889 5.850 -1	-1.427000 -4
np $^3D_3$	4	9.988 -3	1.542 +1 -2.833 +1 1.374 +1 1.700 -1	-1.053000 -6

The potential for coupling between k,s and m,t partial wave states has the general form:

$$\langle p,ks|V|p',mt\rangle=\Sigma_{y,z} g_y^{k,s}(p)\lambda_{y,z} g_z^{m,t}(p') \qquad C.2$$

Thus the tensor interaction has two form factors ($^3S_1$ and $^3D_1$) for each channel.

partial wave	m	β	γ	λ
1T4RA	5	4.860 -3	4.710000 -1	-2.034986 -1
			-8.185000	
		$^3S_1$	2.146000 +1	
			-1.747000 +1	
			4.724000	
		4.988 -3	7.633816 -1	-2.034986 -1
			-4.591094 -2	
		$^3D_1$	2.661634 -2	
			0.0	
			0.0	

The 1X1+3X3 form of λ in the 4T4RA3 interaction facilitates fitting the deuteron properties to the first channel exclusively.

partial wave	m	β	γ	λ
4T4RA3	5	4.860 -3	4.710000 -1	next page
			-8.185000	
		$^3S_1$	2.146000 +1	
			-1.747000 +1	
			4.724000	
		4.988 -3	7.633816 -1	
			-4.591094 -2	
		$^3D_1$	2.661634 -2	
			0.0	
			0.0	
	5	5.868 -3	2.979000	
			-4.688000	
		$^3S_1$	-1.396000	
			4.293000	
			-1.880000 -1	
		8.062 -3	5.947873 -2	
			-3.544604 -2	
		$^3D_1$	-5.049303 -2	
			-2.136605 -3	
			0.0	
	5	1.483 -2	8.472000 -1	
			-2.396000	
		$^3S_1$	2.928000 -1	
			2.307000	
			-5.100000 -2	
		9.960 -3	-1.088496 -3	
			5.548746 -2	
		$^3D_1$	-1.101823 -5	
			-4.560621 -4	
			0.0	
	5	8.243 -3	2.388000	
			-1.295000	
		$^3S_1$	-3.045000 -1	
			-1.798000 -1	
			0.0	
		9.430 -3	6.263965 -2	
			3.418646 -2	
		$^3D_1$	-2.175946 -2	
			4.105694 -4	
			0.0	

λ_{yz}

z \ y	1	2	3	4
1	-2.034986 -1	0.0	0.0	0.0
2	0.0	2.982 -1	4.834 -2	-1.952 -2
3	0.0	4.834 -2	6.277 -2	6.498 -3
4	0.0	-1.952 -2	6.498 -3	-3.532 -2